# A RANDOM-EFFECTS ANALYSIS OF NEAR-SOURCE GROUND MOTION FOR THE DIABLO CANYON POWER PLANT SITE, SAN LUIS OBISPO COUNTY, CALIFORNIA

JOB NO. 10805-603-166
JULY 25, 1991

EVERGREEN, COLORADO

# A RANDOM-EFFECTS ANALYSIS OF NEAR-SOURCE GROUND MOTION FOR THE DIABLO CANYON POWER PLANT SITE, SAN LUIS OBISPO COUNTY, CALIFORNIA

by

Kenneth W. Campbell

Prepared for

Lawrence Livermore National Laboratory

Dames & Moore

Evergreen, Colorado

July 25, 1991

## INTRODUCTION

As requested by the U.S. Nuclear Regulatory Commission (NRC), I repeated my previous analysis of near-source ground motion (Campbell, 1990) using a random-effects model similar to that proposed by Brillinger and Preisler (1984, 1985). The strong-motion parameters of interest in this study were peak horizontal acceleration (PHA), peak vertical acceleration (PVA), and horizontal and vertical components of 5%-damped pseudorelative velocity response (PSV). The results of this analysis are presented below.

## GROUND-MOTION MODEL

There was a minor addition to the ground-motion model used previously (Campbell, 1990). N. Abrahamson (written communication, 1991) found that there were significant differences in the long-period horizontal components of pseudorelative velocity on soil and soft rock. This prompted the addition of an additional site term. The revised ground-motion model is given by an expression of the form

$$\begin{aligned}\ln Y = {} & \beta_1 + \beta_2 M + \beta_3 \ln[R + \beta_4 \exp(\beta_5 M)] + \beta_6 F + \beta_7 \tanh[\beta_8 (M + \beta_9)] \\ & + \beta_{10} \tanh(\beta_{11} D) + \beta_{12} S + \sum_{k=1}^{3} \beta_{k+12} B_k + \epsilon,\end{aligned} \tag{1}$$

where $Y$ is the strong-motion parameter of interest; $M$ is earthquake magnitude ($M_L$ for $M < 6.0$ and $M_s$ for $M \geq 6.0$); $R$ is distance to seismogenic rupture in kilometers (hereafter referred to as seismogenic distance); $F$ is a parameter representing style of faulting [$F = 0$ for strike-slip faults, $F = 1$ for reverse, reverse-oblique, thrust, and thrust-oblique faults (collectively referred to as reverse faults)]; $D$ is depth to basement rock (sediment depth) in kilometers; $S$ is a parameter characterizing site geology ($S = 0$ for soil sites, $S = 1$ for soft-rock sites); $B_k$ is a parameter representing building effects ($B_1 = 1$ for embedded buildings 3-11 stories in height, $B_2 = 1$ for embedded buildings greater than 11 stories in height, $B_3 = 1$ for nonembedded buildings greater than 2 stories in height, $B_1 = B_2 = B_3 = 0$ for all other recording sites); $\epsilon$ is a random error term; $\tanh(*)$ is the hyperbolic tangent function; and $\beta_1, \ldots, \beta_{15}$ are parameters to be determined from the analysis. A thorough discussion of this model is presented by Campbell (1990).

## REGRESSION ANALYSES

The regression coefficients $\beta_1, \ldots, \beta_{15}$ were estimated from a nonlinear random-effects regression analysis. Unlike the nonlinear weighted least-squares analysis used previously, the random-effects analysis includes both within-strata and between-strata variances in its estimation procedure. The random-effects model used in the present analysis was based on a maximum-likelihood technique proposed by PG&E (1990) and N. Abrahamson (written communication, 1991). It is similar to the random-effects model proposed by Brillinger and Preisler (1984, 1985) with two modifications: (1) recordings were grouped by earthquake and distance (hereafter referred to as strata) in order to reduce the bias associated with the

uneven distribution of recordings with respect to distance and magnitude, as recommended by Campbell (1981, 1990), and (2) the variances associated with the random-error terms were assumed to be magnitude dependent, as suggested by Youngs *et al.* (1990).

The random-effects model used to estimate the regression coefficients in Equation (1) is given by the expression

$$y_{ij} = \mu_{ij}(\beta) + \eta_i + \epsilon_{ij}, \tag{2}$$

where

$$\mu_{ij} = \beta_1 + \beta_2 m_i + \beta_3 \ln[r_{ij} + \beta_4 \exp(\beta_5 m_i)] + \beta_6 f_i + \beta_7 \tanh[\beta_8(m_i + \beta_9)]$$
$$+ \beta_{10} \tanh(\beta_{11} d_{ij}) + \beta_{12} s_{ij} + \sum_{k=1}^{3} \beta_{k+12} b_{ijk},$$

$y_{ij}$ represents the $j$th observed value of $\ln Y$ in the $i$th stratum, all lower-case variables represent observed values of the upper-case parameters in Equation (1), and $\eta_i$ and $\epsilon_{ij}$ are independent normal variates with zero mean and within-strata and between-strata variances of $\sigma^2(m_i)$ and $\tau^2(m_i)$, respectively. The error term $\eta_i$ is a random-effects term common to all recordings of the $i$th stratum.

The regression coefficients and variances represented by Equation (2) were estimated by maximizing the log-likelihood function

$$\ln \mathrm{L}[y_{ij} \mid \beta, \sigma, \tau] = -\frac{1}{2} N \ln(2\pi) - \frac{1}{2} \sum_{i=1}^{I} (J_i - 1) \ln[\sigma^2(m_i)]$$
$$- \frac{1}{2} \sum_{i=1}^{I} \ln[\sigma^2(m_i) + J_i \tau^2(m_i)] - \frac{1}{2} \sum_{i=1}^{I} \frac{J_i \overline{y}_i^{\,2}}{\sigma^2(m_i) + J_i \tau^2(m_i)} \tag{3}$$
$$- \frac{1}{2} \sum_{i=1}^{I} \sum_{j=1}^{J_i} \frac{(y_{ij} - \mu_{ij}(\beta) - \overline{y}_i)^2}{\sigma^2(m_i)},$$

where

$$\overline{y}_i = \frac{1}{J_i} \sum_{j=1}^{J_i} y_{ij} - \mu_{ij}(\beta),$$

$$\sigma(m_i) = \begin{cases} \sigma_1, & \text{if } m_i < 6.2; \\ \sigma_2, & \text{if } m_i \geq 6.2, \end{cases}$$

$$\tau(m_i) = \begin{cases} \tau_1, & \text{if } m_i < 6.2; \\ \tau_2, & \text{if } m_i \geq 6.2, \end{cases}$$

$N$ is the total number of recordings, $I$ is the number of strata, and $J_i$ is the number of recordings in the $i$th stratum.

Youngs *et al.* (1990), using a much larger data set, assumed $\sigma(m_i)$ and $\tau(m_i)$ to be continuous functions of magnitude. Due to the smaller number of recordings and limited magnitude range in the present study, I chose to model these parameters as discrete functions of magnitude by separating the earthquakes into two magnitude intervals, $m_i < 6.2$ and $m_i \geq 6.2$, with each interval having roughly the same number of events.

The maximum-liklihood estimation was performed on a PC using NONLIN, a generalized nonlinear regression algorithm developed by SYSTAT, Inc. I first tried to simultaneously fit both the regression coefficients and the variances from Equations (2) and (3) using NONLIN. However, convergence was so slow using this method that I decided instead to implement an alternative procedure suggested by N. Abrahamson (personal communication). Abrahamson's technique, which separates the estimation of the variances from that of the regression coefficients, uses an iterative procedure to speed-up the convergence process. The steps involved in this procedure are as follows:

1. Use Equation (2) to estimate $\beta_1, \ldots, \beta_{15}$ by nonlinear least squares.

2. Calculate $\mu_{ij}(\beta)$ from the expression in Equation (2).

3. Calculate $\overline{y}_i$ from the expression in Equation (3).

4. Estimate $\sigma^2(m_i)$ and $\tau^2(m_i)$ from the expressions

$$\sigma_l{}^2 = \frac{1}{N_l - 1} \sum_{i=1}^{I_l} \sum_{j=1}^{J_i} (y_{ij} - \mu_{ij}(\beta) - \overline{y}_i)^2,$$

and

$$\tau_l{}^2 = \frac{1}{I_l - 1} \sum_{j=1}^{I_l} \overline{y}_i{}^2,$$

where

$$N_l = \sum_{i=1}^{I_l} J_i$$

and $I_l$ is the number of strata in the $l$th magnitude interval.

5. Holding $\mu_{ij}(\beta)$ constant, use Equation (3) to estimate new values for $\sigma^2(m_i)$ and $\tau^2(m_i)$ by maximum likelihood.

6. Calculate $\eta_i$ from the expression

$$\eta_i = \frac{\tau^2(m_i)}{\sigma^2(m_i) + J_i \tau^2(m_i)} \sum_{j=1}^{J_i} y_{ij} - \mu_{ij}(\beta).$$

7. Calculate a new set of observations $x_{ij}$ from the expression

$$x_{ij} = y_{ij} - \eta_i.$$

8. Use $x_{ij}$ together with Equation (2) to estimate new values for $\beta_1, \ldots, \beta_{15}$ by nonlinear least squares.

9. Calculate new values for $\overline{y}_{ij}$ and $\mu_{ij}(\beta)$ and repeat Steps 5 through 9 to convergence.

For purposes of the present analysis, the iterative process was terminated when differences between successive estimates of both the regression coefficients and variances were found to be less than 0.0001. Usually this criterion was met in about 20 to 50 iterations. However, in those instances where two or more of the regression parameters were highly correlated, it took as many as 100 iterations to meet this criterion.

As before, the regression analyses of the response-spectral ordinates were performed on the logarithm of the ratio of pseudorelative velocity to peak acceleration (PSV/PGA). Due to the memory limitations inherent in NONLIN, it was not possible to fit $\beta_8$ and $\beta_{11}$ (formerly $f_2$ and $g_2$) for more than one spectral component at a time. Therefore, unlike the previous analysis, these regression coefficients were derived independently of one another. As I will show later, this constraint caused the predicted spectra from the present analysis to exhibit more period-to-period variability than similar spectra developed by Campbell (1990).

Prior to running the random-effects model, I used an iterative nonlinear least-squares analysis to determine which regression coefficients were expected to be statistically significant at the 90% confidence level. Those coefficients found to be statistically significant were then included in a subsequent random-effects regression analysis. This was done as a reasonable alternative to the extremely time-consuming process of using an iterative random-effects analysis to select the regression coefficients, which was beyond the scope of this study.

As before, the attenuation relationships for ln PSV were derived by combining the regression models for ln PGA and ln(PSV/PGA) using the relationship

$$\ln \text{PSV} = \ln \text{PGA} + \ln(\text{PSV/PGA}). \tag{4}$$

As a result, the variances derived from the random-effects regression analyses could not be used as estimates of the variances associated with ln PSV. Instead, magnitude-dependent estimates of within-strata and between-strata variances were computed from the residuals derived from the observed and predicted values of ln PSV. A similar procedure was used to estimate the within-strata and between-strata variances for the entire data set ($M = 4.7$–$7.8$).

The results of the regression analyses are summarized in Tables 1–3. Those regression coefficients enclosed in parentheses, although believed to be statistically significant, were found to exhibit unusually large variability as indicated by their asymptotic standard errors and, as a result, were held constant during the analyses. The total standard errors given by the $\sigma_t$ in Tables 4 and 5 were derived from the within-strata and between-strata variances ${\sigma_l}^2$ and ${\tau_l}^2$ from the relationship

$$\sigma_t = \sqrt{{\sigma_l}^2 + {\tau_l}^2}, \tag{5}$$

assuming statistical independence of $\eta_i$ and $\epsilon_{ij}$.

## DISCUSSION OF RESULTS

Figures 1–6 compare the results of the random-effects regression analyses with those derived previously using a weighted least-squares (variance-weighted) analysis (Campbell, 1990). As these figures show, the differences in the two sets of predicted ground motions are generally less than 10%. The only ground motions that exhibit larger variations are horizontal spectral velocities at periods exceeding 0.5 sec (Figs. 3–5), where the ramdom-effects predictions are as much as 20% to 40% less than the corresponding variance-weighted predictions. These differences appear to have been caused by differences in the regression coefficients associated with the magnitude and sediment-depth terms in Equations (1) and (2).

## GROUND-MOTION ESTIMATES FOR DIABLO CANYON

The attenuation relationships developed in the present study were used to derive site-specific estimates of free-field ground motion for the Diablo Canyon site. The earthquake scenario used to develop these estimates was the Long Term Seismic Program (LTSP) analysis earthquake proposed by PG&E (1988). This earthquake is a moment magnitude ($M_w$) 7.2 earthquake hypothesized to occur about 4.5 km offshore on the Hosgri fault.

PG&E's choice of a faulting scenario for the proposed LTSP event was complicated by uncertainty concerning the actual location and geometry of the Hosgri fault. Based on an interpretation of available geological and geophysical data obtained near the site, PG&E (1988) eventually proposed three possible faulting scenarios for this event: strike-slip displacement on a vertical fault, reverse-oblique displacement on a steeply dipping fault, and thrust displacement on a shallow-dipping fault. Based on a depth section and crustal velocity model provided by PG&E (1990), seismogenic distances to the Diablo Canyon site were estimated to be 4.7, 4.9, and 5.1 km for the proposed reverse-oblique, strike-slip, and thrust scenarios, respectively.

Seismic velocity profiles near the site (PG&E, 1988, Figs. 2-9, 4-13, and 5-5) indicate that there is a relatively strong velocity gradient within the top 4 km of the crust beneath the site. Although rocks of the Franciscan Complex—usually considered to be basement rock—underlay the site at a depth of about 1 to 2 km, the inferred velocity gradient in

the upper 4 km is more representative of sedimentary rock rather than basement rock (R. Wheeler and K. Campbell, unpublished data). As a result, depth to basement rock was conservatively estimated to be 4 km for purposes of predicting site-specific ground motions at the Diablo Canyon site.

Estimates of peak acceleration for PG&E's proposed LTSP analysis earthquake are presented in Table 6. For these and subsequent estimates, $M_s$ was assumed to be equal to $M_w$, as suggested by Hanks and Kanamori (1979), and the standard error of estimate was assumed to be equal to $\sigma_t$. For convenience, the estimates have been segregated by style of faulting and uncertainty level. Estimates for the reverse-oblique and thrust-faulting scenarios were calculated from Equation (1) assuming $F = 1$, since by definition both are reverse-faulting earthquakes.

Five-percent damped pseudoabsolute acceleration (PSA) spectra for PG&E's proposed LTSP analysis earthquake for each of the three proposed faulting scenarios are presented in Figures 7–18 along with the variance-weighted spectra developed by Campbell (1990). A comparison of these two spectra indicates that the spectra derived from the random-effects analysis have generally smaller amplitudes than those derived from the weighted least-squares analysis. The smaller amplitudes associated with the random-effects estimates can be attributed to one or more of the following: (1) lower predicted peak accelerations, (2) smaller variances, or (3) lower predicted spectral accelerations at moderate-to-long periods.

## REFERENCES


Brillinger, D.R., and H.K. Preisler (1984). An exploratory analysis of the Joyner-Boore attenuation data, *Bull. Seism. Soc. Am.*, v. 74, p. 1441–1450.

Brillinger, D.R., and H.K. Preisler (1985). Further analysis of the Joyner-Boore Attenuation Data, *Bull. Seism. Soc. Am.*, v. 75, p. 611–614.

Campbell, K.W. (1981). Near-source attenuation of peak horizontal acceleration, *Bull. Seism. Soc. Am.*, v. 71, p. 2039–2070.

Campbell, K.W. (1990). Empirical prediction of near-source soil and soft-rock ground motion for the Diablo Canyon power plant site, San Luis Obispo County, California, Dames & Moore report to Lawrence Livermore National Laboratory, September, 1990, Evergreen, Colorado.

Hanks, T.C., and H. Kanamori (1979). A moment magnitude scale, *J. Geophys. Res.*, v. 84, p. 2348–2350.

PG&E (1988). Final report of the Diablo Canyon long term seismic program for the Diablo Canyon power plant, Pacific Gas and Electric Company report to the U. S. Nuclear Regulatory Commission, Docket Nos. 50-275 and 50-323, July 31, 1988, San Francisco, California.

PG&E (1990). Response to ground-motion questions LP 1 and LP 9, and workshop questions 1 through 6, Pacific Gas and Electric Company report to the U.S. Nulcear Regulatory Commission, Docket Nos. 50-275 and 50-323, August, 1990, San Francisco, California.

Youngs, R.R., F. Makdisi, and K. Sadigh (1990). The case for magnitude dependent dispersion in peak ground acceleration [Abs.], *Seismological Research Letters*, v. 61, p. 30.

## TABLE 1

### Regression Coefficients: Horizontal Components

| Parameter, $Y$ | Period (sec) | No. Eq. | No. Rec. | $c_1$ | $c_2$ | $c_3$ | $c_4$ | $c_5$ | $c_6$ | $c_7$ | $c_8$ | $c_9$ | $c_{10}$ | $c_{11}$ | $c_{12}$ |
|---|---|---|---|---|---|---|---|---|---|---|---|---|---|---|---|
| PHA, $g$ | — | 26 | 244 | -1.774 | 1.50 | -2.55 | 0.604 | 0.590 | 0.277 | — | — | — | — | — | — |
| PSV, cm/sec | 0.04 | 16 | 99 | 0.041 | 1.50 | -2.55 | 0.604 | 0.590 | 0.277 | — | — | — | — | — | — |
| | 0.05 | 21 | 164 | 0.338 | 1.50 | -2.55 | 0.604 | 0.590 | 0.277 | — | — | — | — | — | — |
| | 0.075 | 21 | 167 | 1.019 | 1.50 | -2.55 | 0.604 | 0.590 | 0.277 | — | — | — | — | — | — |
| | 0.10 | 21 | 167 | 1.508 | 1.50 | -2.55 | 0.604 | 0.590 | 0.277 | — | — | — | — | — | — |
| | 0.15 | 21 | 167 | 2.101 | 1.50 | -2.55 | 0.604 | 0.590 | 0.277 | — | — | — | — | — | — |
| | 0.20 | 21 | 167 | 2.470 | 1.50 | -2.55 | 0.604 | 0.590 | 0.277 | — | — | — | — | — | — |
| | 0.30 | 21 | 167 | 2.840 | 1.50 | -2.55 | 0.604 | 0.590 | 0.277 | — | — | — | — | — | — |
| | 0.40 | 21 | 167 | 2.453 | 1.50 | -2.55 | 0.604 | 0.590 | 0.277 | 0.641 | 0.951 | -4.7 | — | — | — |
| | 0.50 | 21 | 167 | 2.275 | 1.50 | -2.55 | 0.604 | 0.590 | 0.277 | 0.915 | (1.06) | -4.7 | — | — | — |
| | 0.75 | 21 | 167 | 1.739 | 1.50 | -2.55 | 0.604 | 0.590 | 0.277 | 1.41 | 1.17 | -4.7 | 0.175 | 4.57 | — |
| | 1.0 | 21 | 167 | 1.313 | 1.50 | -2.55 | 0.604 | 0.590 | 0.277 | 1.72 | 0.888 | -4.7 | 0.430 | 5.75 | — |
| | 1.5 | 21 | 167 | 0.789 | 1.50 | -2.55 | 0.604 | 0.590 | 0.277 | 2.31 | 0.628 | -4.7 | 0.647 | 6.41 | -0.131 |
| | 2.0 | 21 | 167 | 0.557 | 1.50 | -2.55 | 0.604 | 0.590 | 0.277 | 2.73 | 0.530 | -4.7 | 0.637 | 5.29 | -0.236 |
| | 3.0 | 20 | 155 | 0.069 | 1.50 | -2.55 | 0.604 | 0.590 | 0.277 | 2.84 | 0.531 | -4.7 | 0.916 | 3.09 | -0.232 |
| | 4.0 | 19 | 147 | -0.306 | 1.50 | -2.55 | 0.604 | 0.590 | 0.277 | 2.68 | 0.584 | -4.7 | 1.26 | (3.09) | -0.375 |

## TABLE 2

### Regression Coefficients: Vertical Components

| Parameter, $Y$ | Period (sec) | No. Eq. | No. Rec. | $c_1$ | $c_2$ | $c_3$ | $c_4$ | $c_5$ | $c_6$ | $c_7$ | $c_8$ | $c_9$ | $c_{10}$ | $c_{11}$ | $c_{12}$ |
|---|---|---|---|---|---|---|---|---|---|---|---|---|---|---|---|
| PVA, $g$ | — | 25 | 239 | -3.888 | 1.11 | -1.61 | 0.101 | 0.687 | 0.090 | — | — | — | — | — | — |
| PSV, cm/sec | 0.04 | 16 | 98 | -2.014 | 1.11 | -1.61 | 0.101 | 0.687 | 0.090 | — | — | — | — | — | — |
| | 0.05 | 21 | 162 | -1.573 | 1.11 | -1.61 | 0.101 | 0.687 | 0.090 | — | — | — | — | — | — |
| | 0.075 | 21 | 164 | -0.823 | 1.11 | -1.61 | 0.101 | 0.687 | 0.090 | — | — | — | — | — | — |
| | 0.10 | 21 | 164 | -0.377 | 1.11 | -1.61 | 0.101 | 0.687 | 0.090 | — | — | — | — | — | — |
| | 0.15 | 21 | 164 | -0.004 | 1.11 | -1.61 | 0.101 | 0.687 | 0.090 | — | — | — | — | — | — |
| | 0.20 | 21 | 164 | 0.146 | 1.11 | -1.61 | 0.101 | 0.687 | 0.090 | — | — | — | — | — | — |
| | 0.30 | 21 | 164 | 0.202 | 1.11 | -1.61 | 0.101 | 0.687 | 0.090 | — | — | — | — | — | — |
| | 0.40 | 21 | 164 | 0.034 | 1.11 | -1.61 | 0.101 | 0.687 | 0.090 | 0.263 | 1.05 | -4.7 | — | — | — |
| | 0.50 | 21 | 164 | -0.222 | 1.11 | -1.61 | 0.101 | 0.687 | 0.090 | 0.537 | (1.05) | -4.7 | — | — | — |
| | 0.75 | 21 | 164 | -0.359 | 1.11 | -1.61 | 0.101 | 0.687 | 0.090 | 0.814 | (1.05) | -4.7 | — | — | — |
| | 1.0 | 21 | 164 | -0.808 | 1.11 | -1.61 | 0.101 | 0.687 | 0.090 | 1.27 | 0.973 | -4.7 | 0.113 | 4.03 | — |
| | 1.5 | 21 | 163 | -1.595 | 1.11 | -1.61 | 0.101 | 0.687 | 0.090 | 1.89 | 0.828 | -4.7 | 0.469 | 3.61 | — |
| | 2.0 | 21 | 163 | -1.528 | 1.11 | -1.61 | 0.101 | 0.687 | 0.090 | 2.10 | 0.493 | -4.7 | 0.516 | 4.06 | — |
| | 3.0 | 20 | 146 | -1.306 | 1.11 | -1.61 | 0.101 | 0.687 | 0.090 | 1.36 | (0.493) | -4.7 | 0.828 | 0.547 | — |
| | 4.0 | 17 | 142 | -1.393 | 1.11 | -1.61 | 0.101 | 0.687 | 0.090 | 1.23 | (0.493) | -4.7 | 1.07 | 0.463 | — |

## TABLE 3

### Regression Coefficients: Building Effects

| Horizontal Components | | | | | Vertical Components | | | | |
|---|---|---|---|---|---|---|---|---|---|
| Parameter, $Y$ | Period (sec) | $c_{13}$ | $c_{14}$ | $c_{15}$ | Parameter, $Y$ | Period (sec) | $c_{13}$ | $c_{14}$ | $c_{15}$ |
| PHA, $g$ | — | -0.173 | -0.344 | — | PVA, $g$ | — | -0.274 | -0.401 | — |
| PSV, cm/sec | 0.04 | -0.173 | -0.344 | — | PSV, cm/sec | 0.04 | -0.274 | -0.401 | — |
| | 0.05 | -0.233 | -0.391 | -0.062 | | 0.05 | -0.398 | -0.533 | -0.134 |
| | 0.075 | -0.294 | -0.432 | -0.113 | | 0.075 | -0.355 | -0.531 | -0.191 |
| | 0.10 | -0.296 | -0.344 | -0.080 | | 0.10 | -0.401 | -0.573 | -0.242 |
| | 0.15 | -0.173 | -0.344 | — | | 0.15 | -0.274 | -0.401 | — |
| | 0.20 | -0.173 | -0.344 | — | | 0.20 | -0.056 | -0.198 | 0.136 |
| | 0.30 | -0.173 | -0.344 | — | | 0.30 | 0.138 | -0.007 | 0.435 |
| | 0.40 | -0.173 | -0.344 | — | | 0.40 | 0.145 | -0.037 | 0.262 |
| | 0.50 | -0.173 | -0.344 | — | | 0.50 | 0.205 | 0.028 | 0.289 |
| | 0.75 | -0.173 | -0.344 | — | | 0.75 | 0.037 | -0.022 | 0.261 |
| | 1.0 | 0.066 | -0.008 | — | | 1.0 | 0.078 | 0.163 | 0.406 |
| | 1.5 | 0.016 | 0.182 | — | | 1.5 | 0.210 | 0.486 | 0.584 |
| | 2.0 | 0.123 | 0.175 | — | | 2.0 | 0.410 | 0.540 | 0.656 |
| | 3.0 | 0.409 | 0.545 | 0.497 | | 3.0 | 0.699 | 0.793 | 0.839 |
| | 4.0 | 0.594 | 0.717 | 0.639 | | 4.0 | 0.668 | 0.869 | 0.959 |

## TABLE 4

### Standard Errors: Horizontal Components

| | | Magnitude Range | | | | | | | | | | | | | | |
|---|---|---|---|---|---|---|---|---|---|---|---|---|---|---|---|---|
| | | 4.7–7.8 | | | | | 4.7–6.1 | | | | | 6.2–7.8 | | | | |
| Parameter, $Y$ | Period (sec) | No. Eq. | No. Rec. | $\sigma_t$ | $\tau$ | $\sigma$ | No. Eq. | No. Rec. | $\sigma_t$ | $\tau_1$ | $\sigma_1$ | No. Eq. | No. Rec. | $\sigma_t$ | $\tau_2$ | $\sigma_2$ |
| PHA, $g$ | — | 26 | 244 | 0.436 | 0.206 | 0.384 | 14 | 122 | 0.474 | 0.263 | 0.394 | 12 | 122 | 0.385 | 0.153 | 0.353 |
| PSV, cm/sec | 0.04 | 16 | 99 | 0.419 | 0.239 | 0.344 | 7 | 34 | 0.528 | 0.339 | 0.405 | 9 | 65 | 0.349 | 0.161 | 0.310 |
| | 0.05 | 21 | 164 | 0.475 | 0.277 | 0.386 | 10 | 62 | 0.539 | 0.319 | 0.434 | 11 | 102 | 0.439 | 0.246 | 0.362 |
| | 0.075 | 21 | 167 | 0.489 | 0.271 | 0.407 | 10 | 62 | 0.602 | 0.376 | 0.470 | 11 | 105 | 0.416 | 0.179 | 0.376 |
| | 0.10 | 21 | 167 | 0.508 | 0.282 | 0.423 | 10 | 62 | 0.625 | 0.401 | 0.479 | 11 | 105 | 0.431 | 0.177 | 0.393 |
| | 0.15 | 21 | 167 | 0.532 | 0.267 | 0.461 | 10 | 62 | 0.655 | 0.375 | 0.537 | 11 | 105 | 0.447 | 0.177 | 0.411 |
| | 0.20 | 21 | 167 | 0.516 | 0.229 | 0.462 | 10 | 62 | 0.642 | 0.311 | 0.562 | 11 | 105 | 0.427 | 0.164 | 0.394 |
| | 0.30 | 21 | 167 | 0.444 | 0.201 | 0.396 | 10 | 62 | 0.511 | 0.228 | 0.457 | 11 | 105 | 0.399 | 0.178 | 0.357 |
| | 0.40 | 21 | 167 | 0.429 | 0.192 | 0.383 | 10 | 62 | 0.505 | 0.239 | 0.445 | 11 | 105 | 0.382 | 0.157 | 0.348 |
| | 0.50 | 21 | 167 | 0.419 | 0.181 | 0.378 | 10 | 62 | 0.499 | 0.253 | 0.431 | 11 | 105 | 0.372 | 0.124 | 0.350 |
| | 0.75 | 21 | 167 | 0.483 | 0.240 | 0.419 | 10 | 62 | 0.547 | 0.306 | 0.453 | 11 | 105 | 0.456 | 0.201 | 0.409 |
| | 1.0 | 21 | 167 | 0.468 | 0.241 | 0.402 | 10 | 62 | 0.540 | 0.267 | 0.469 | 11 | 105 | 0.440 | 0.231 | 0.374 |
| | 1.5 | 21 | 167 | 0.428 | 0.203 | 0.378 | 10 | 62 | 0.472 | 0.228 | 0.411 | 11 | 105 | 0.422 | 0.195 | 0.374 |
| | 2.0 | 21 | 167 | 0.419 | 0.192 | 0.373 | 10 | 62 | 0.432 | 0.225 | 0.369 | 11 | 105 | 0.428 | 0.178 | 0.389 |
| | 3.0 | 20 | 155 | 0.493 | 0.200 | 0.451 | 9 | 50 | 0.447 | 0.209 | 0.396 | 11 | 105 | 0.527 | 0.189 | 0.492 |
| | 4.0 | 19 | 147 | 0.541 | 0.253 | 0.478 | 8 | 42 | 0.516 | 0.249 | 0.452 | 11 | 105 | 0.541 | 0.186 | 0.508 |

## TABLE 5

### Standard Errors: Vertical Components

| Parameter, $Y$ | Period (sec) | Magnitude Range: 4.7–7.8 No. Eq. | No. Rec. | $\sigma_t$ | $\tau$ | $\sigma$ | 4.7–6.1 No. Eq. | No. Rec. | $\sigma_t$ | $\tau_1$ | $\sigma_1$ | 6.2–7.8 No. Eq. | No. Rec. | $\sigma_t$ | $\tau_2$ | $\sigma_2$ |
|---|---|---|---|---|---|---|---|---|---|---|---|---|---|---|---|---|
| PVA, $g$ | — | 25 | 239 | 0.609 | 0.283 | 0.539 | 13 | 119 | 0.670 | 0.281 | 0.608 | 12 | 120 | 0.557 | 0.327 | 0.451 |
| PSV, cm/sec | 0.04 | 16 | 98 | 0.536 | 0.410 | 0.345 | 7 | 33 | 0.602 | 0.399 | 0.451 | 9 | 65 | 0.501 | 0.415 | 0.281 |
| | 0.05 | 21 | 162 | 0.656 | 0.368 | 0.542 | 10 | 61 | 0.815 | 0.423 | 0.696 | 11 | 101 | 0.554 | 0.335 | 0.441 |
| | 0.075 | 21 | 164 | 0.648 | 0.314 | 0.567 | 10 | 61 | 0.779 | 0.381 | 0.679 | 11 | 103 | 0.572 | 0.271 | 0.503 |
| | 0.10 | 21 | 164 | 0.633 | 0.291 | 0.562 | 10 | 61 | 0.782 | 0.376 | 0.685 | 11 | 103 | 0.541 | 0.230 | 0.490 |
| | 0.15 | 21 | 164 | 0.613 | 0.306 | 0.531 | 10 | 61 | 0.716 | 0.340 | 0.630 | 11 | 103 | 0.544 | 0.281 | 0.465 |
| | 0.20 | 21 | 164 | 0.580 | 0.313 | 0.488 | 10 | 61 | 0.647 | 0.286 | 0.580 | 11 | 103 | 0.546 | 0.327 | 0.437 |
| | 0.30 | 21 | 164 | 0.569 | 0.333 | 0.461 | 10 | 61 | 0.607 | 0.334 | 0.507 | 11 | 103 | 0.552 | 0.328 | 0.443 |
| | 0.40 | 21 | 164 | 0.590 | 0.378 | 0.454 | 10 | 61 | 0.625 | 0.349 | 0.519 | 11 | 103 | 0.588 | 0.403 | 0.427 |
| | 0.50 | 21 | 164 | 0.538 | 0.359 | 0.402 | 10 | 61 | 0.611 | 0.400 | 0.462 | 11 | 103 | 0.507 | 0.339 | 0.376 |
| | 0.75 | 21 | 164 | 0.569 | 0.407 | 0.398 | 10 | 61 | 0.573 | 0.418 | 0.393 | 11 | 103 | 0.580 | 0.406 | 0.413 |
| | 1.0 | 21 | 164 | 0.585 | 0.384 | 0.441 | 10 | 61 | 0.572 | 0.398 | 0.411 | 11 | 103 | 0.615 | 0.391 | 0.475 |
| | 1.5 | 21 | 163 | 0.600 | 0.384 | 0.461 | 10 | 60 | 0.599 | 0.451 | 0.393 | 11 | 103 | 0.623 | 0.355 | 0.512 |
| | 2.0 | 21 | 163 | 0.588 | 0.340 | 0.480 | 10 | 60 | 0.533 | 0.340 | 0.410 | 11 | 103 | 0.639 | 0.354 | 0.532 |
| | 3.0 | 20 | 146 | 0.609 | 0.299 | 0.525 | 9 | 43 | 0.613 | 0.295 | 0.538 | 11 | 103 | 0.622 | 0.305 | 0.542 |
| | 4.0 | 17 | 138 | 0.693 | 0.278 | 0.635 | 6 | 35 | 0.478 | 0.100 | 0.468 | 11 | 103 | 0.748 | 0.264 | 0.699 |

## TABLE 6

### Site-Specific Estimates of Peak Acceleration: Diablo Canyon Site, California ($M_s = 7.2$, $R = 4.7$–$5.1$ km, $D = 4$ km)

| Parameter, $Y$ | Strike Slip $R$ | Median | Median+1$\sigma_t$ | Reverse Oblique $R$ | Median | Median+1$\sigma_t$ | Thrust $R$ | Median | Median+1$\sigma_t$ |
|---|---|---|---|---|---|---|---|---|---|
| PHA, $g$ | 4.9 | 0.46 | 0.68 | 4.7 | 0.61 | 0.90 | 5.1 | 0.60 | 0.88 |
| PVA, $g$ | 4.9 | 0.51 | 0.90 | 4.7 | 0.57 | 1.00 | 5.1 | 0.55 | 0.97 |

# PEAK HORIZONTAL ACCELERATION

## Strike-Slip Faults: M = 5.0, 6.5, 8.0

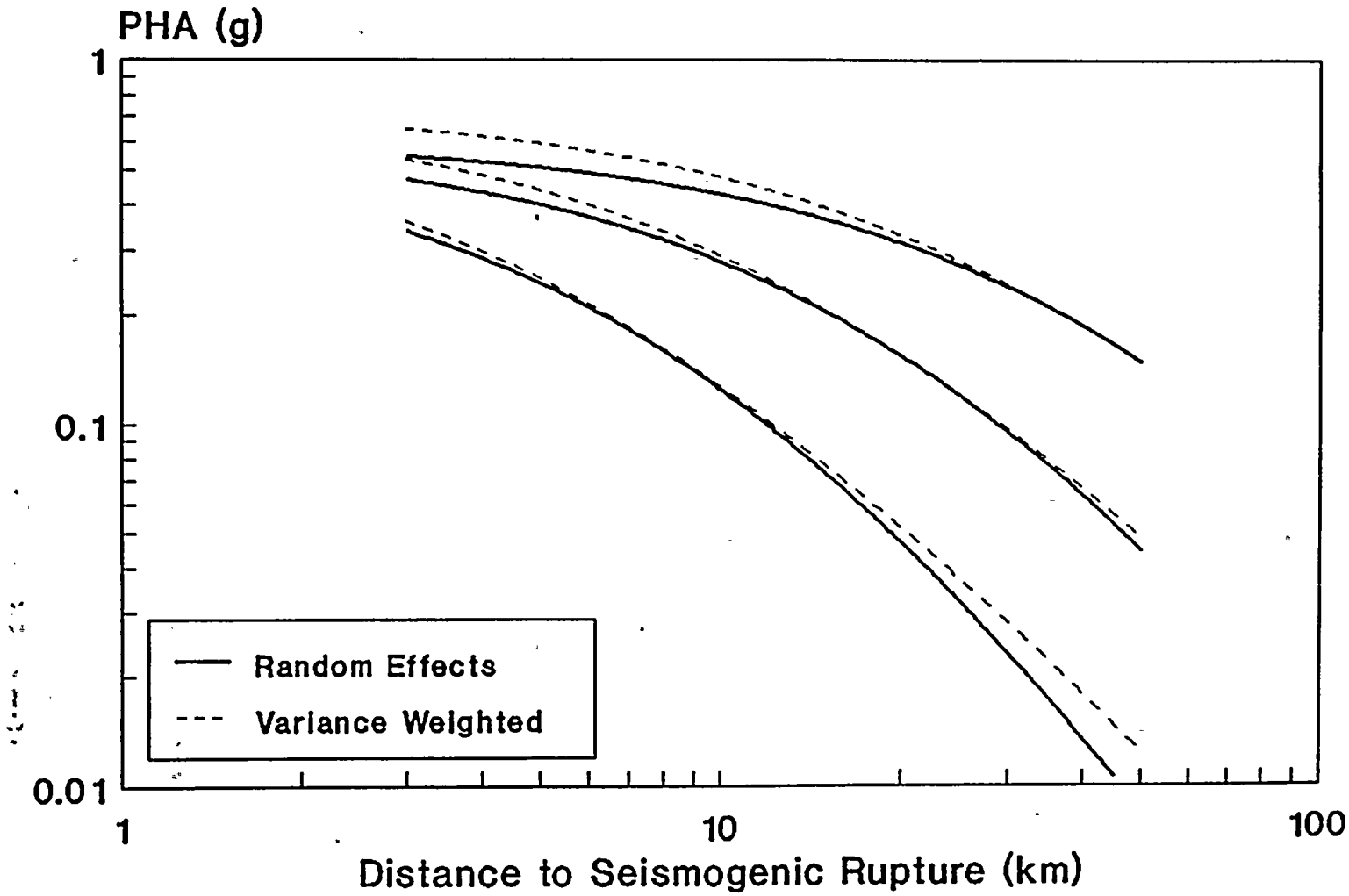


Figure 1

# PEAK VERTICAL ACCELERATION
## Strike-Slip Faults: M = 5.0, 6.5, 8.0

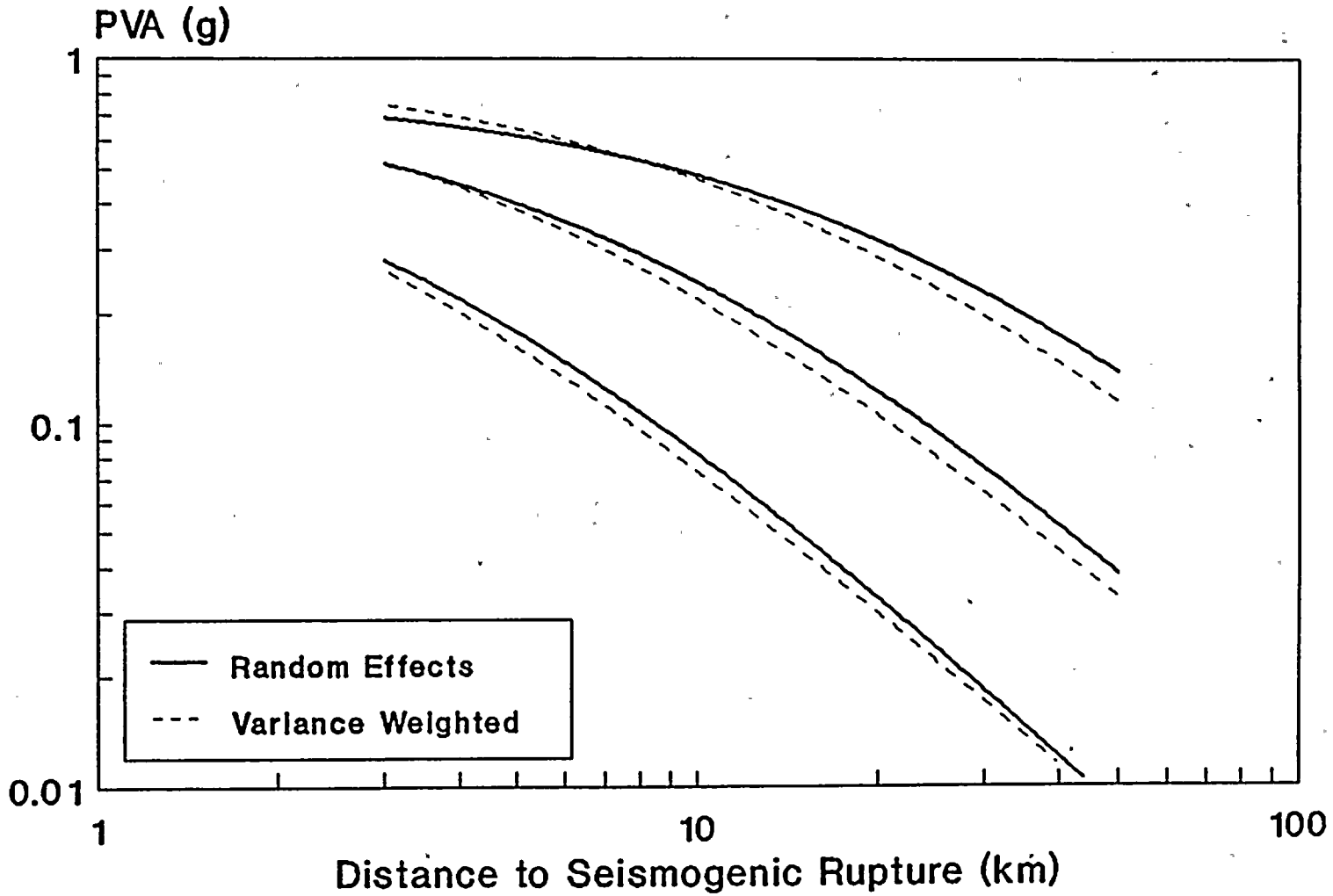


Figure 2

# HORIZONTAL VELOCITY SPECTRA
## Strike-Slip Faults: M = 5.0, 6.5, 8.0
## R = 10, D = 0

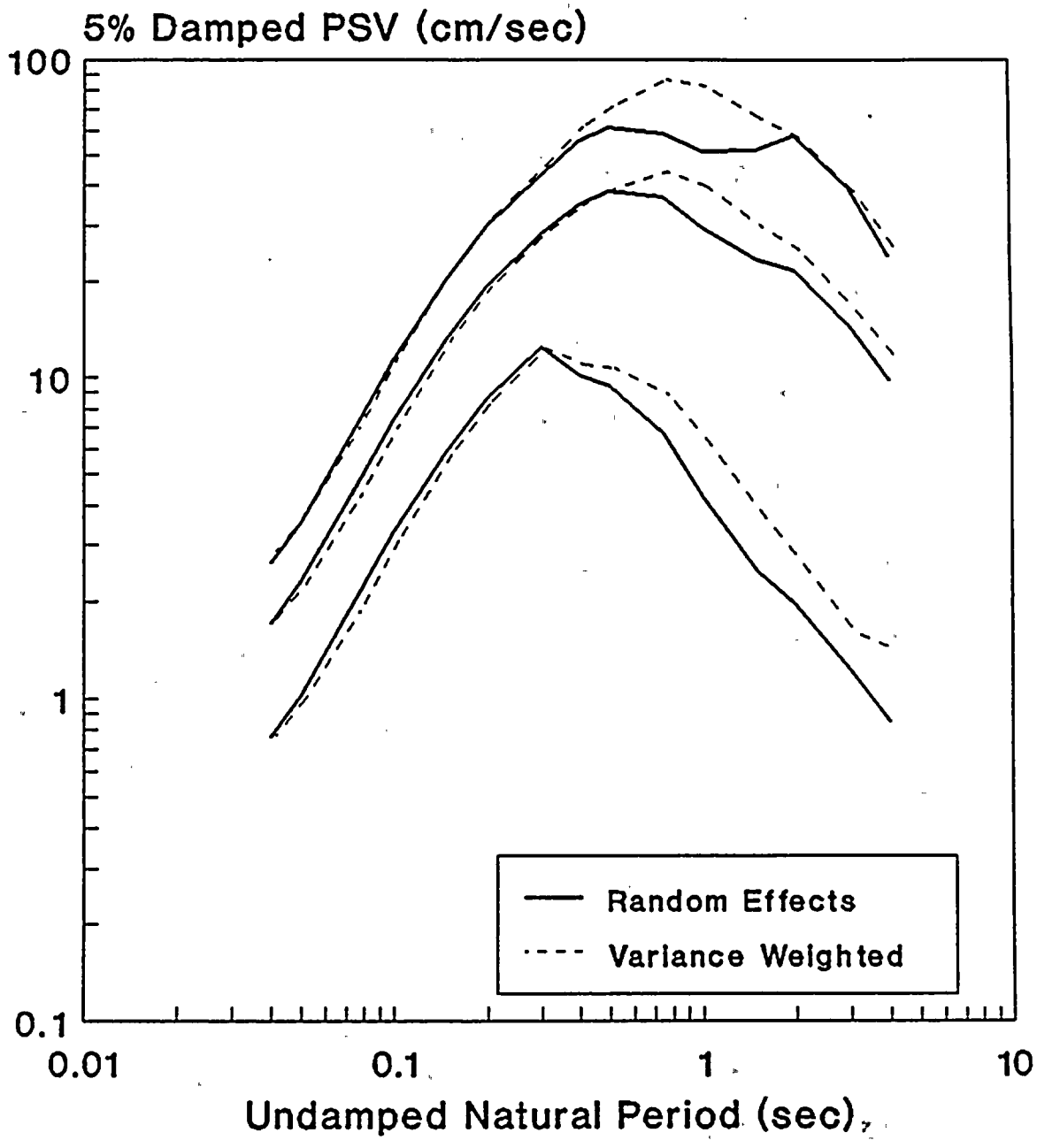


Figure 3

# HORIZONTAL VELOCITY SPECTRA

## Strike-Slip Faults: R = 10, 25, 50
## M = 6.5, D = 0

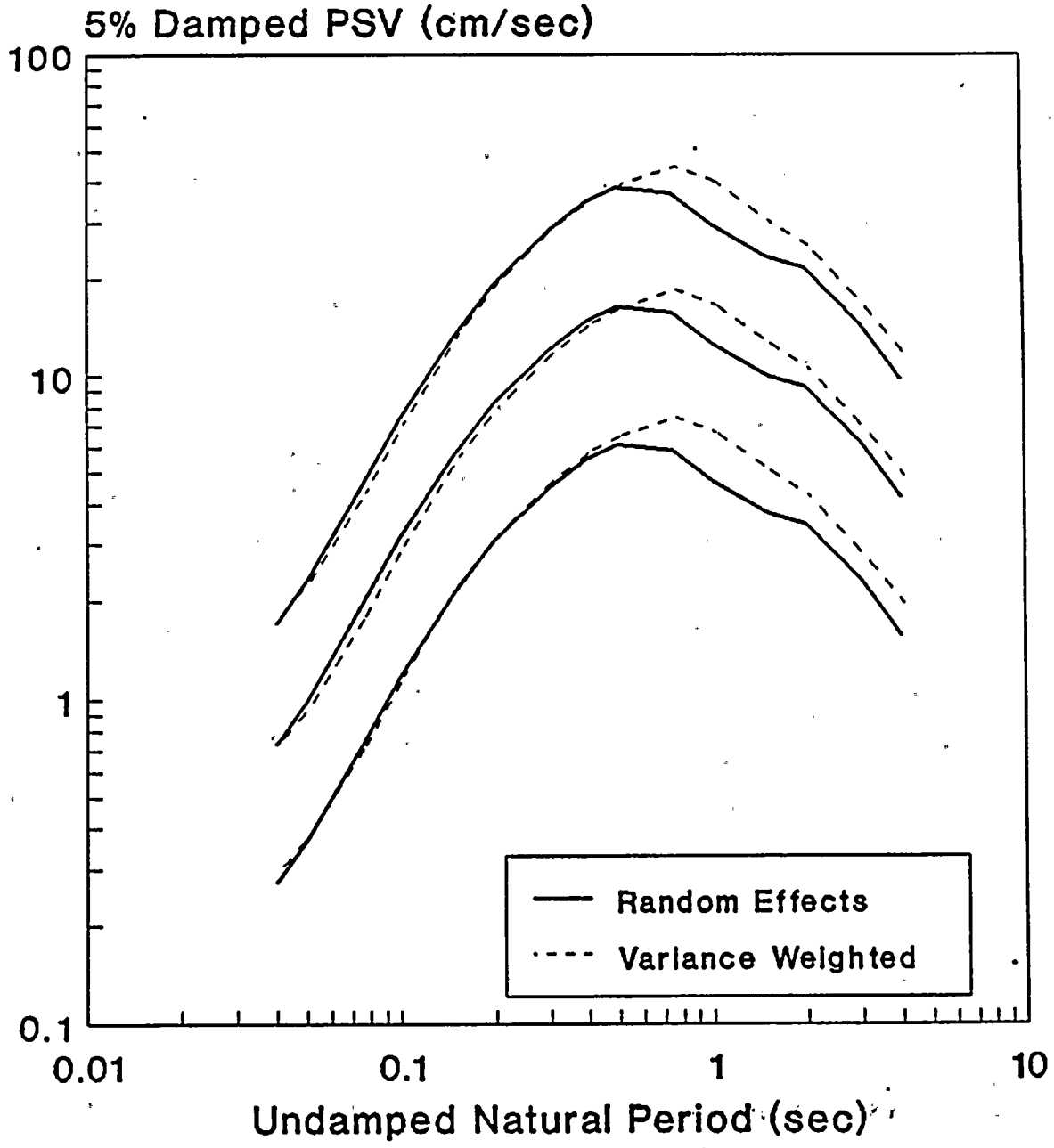


Figure 4

# VERTICAL VELOCITY SPECTRA
## Strike-Slip Faults: M = 5.0, 6.5, 8.0
## R = 10, D = 0

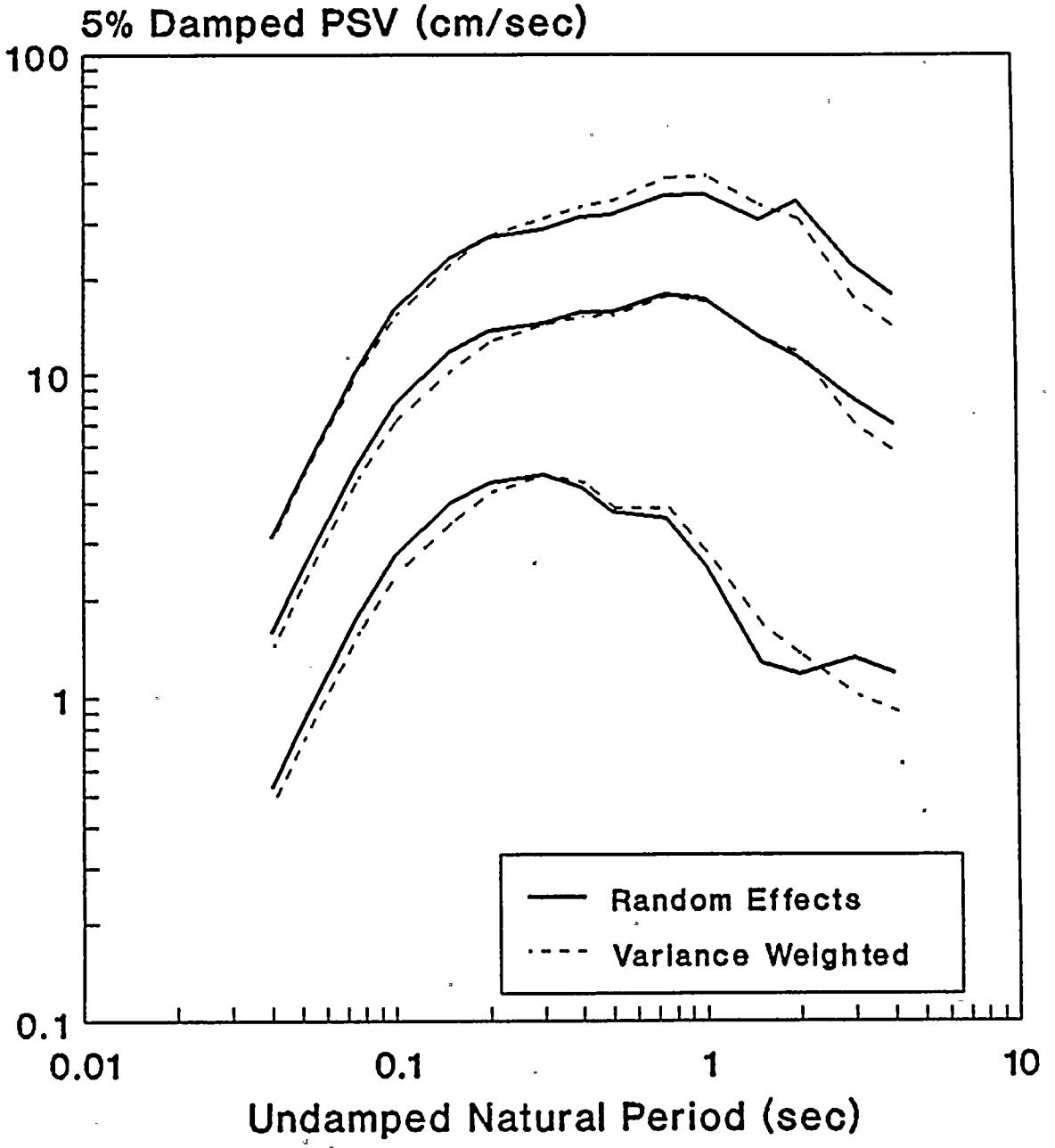


Figure 6

# VERTICAL VELOCITY SPECTRA
## Strike-Slip Faults: R = 10, 25, 50
## M = 6.5, D = 0

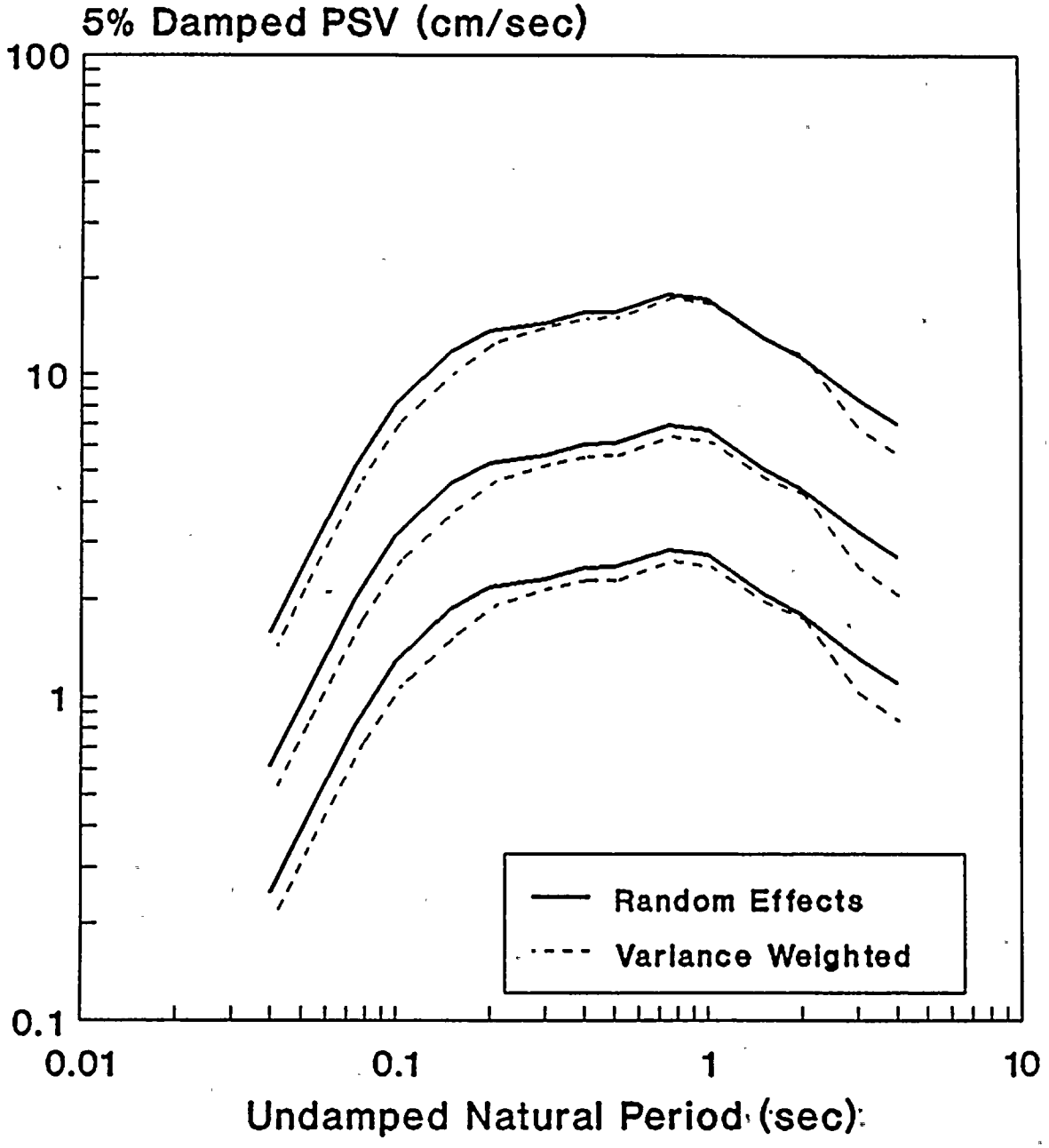


Figure 6

# HORIZONTAL ACCELERATION SPECTRA
## Strike-Slip Fault: M = 7.2, R = 4.9
## D = 4.0

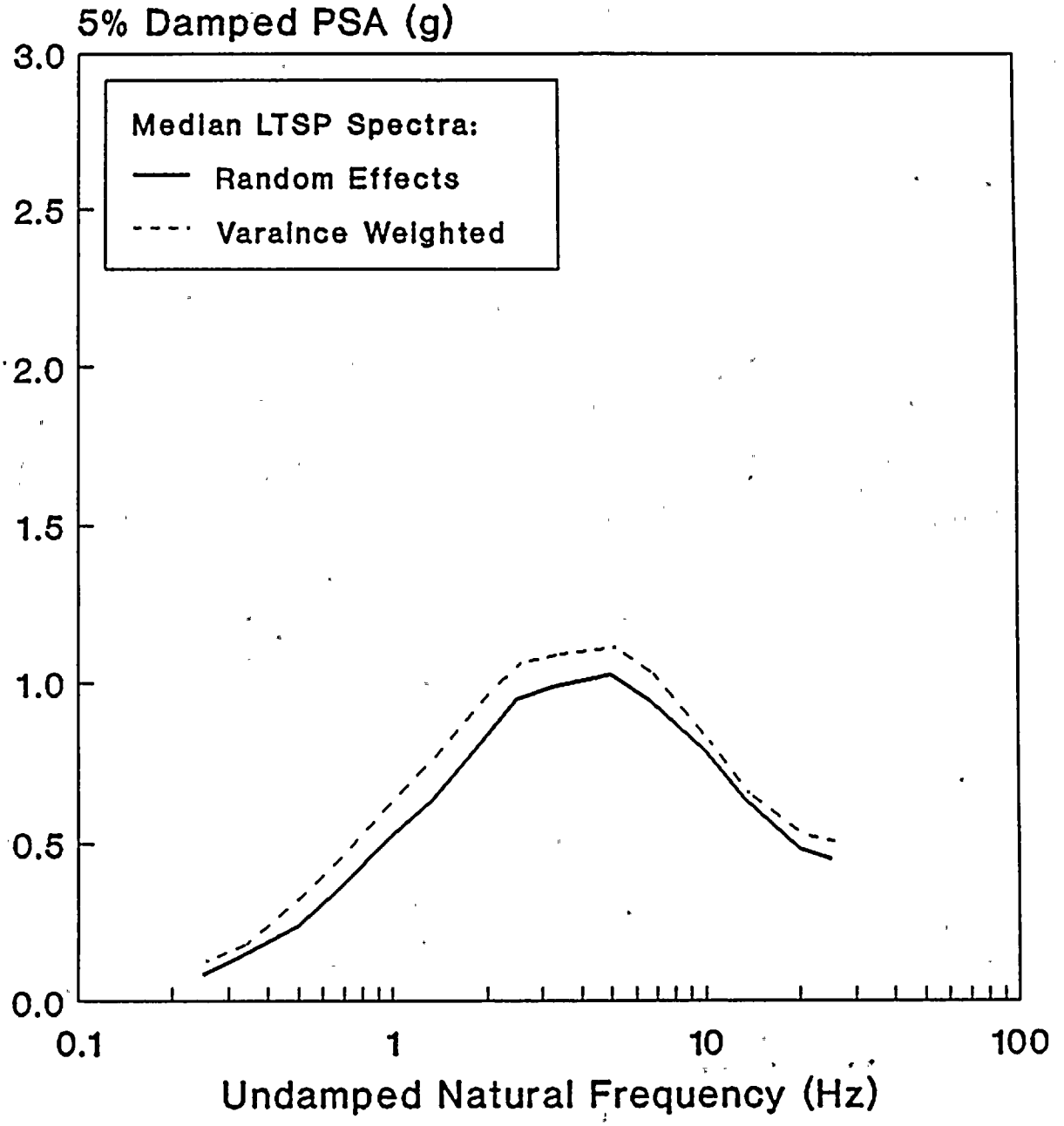


Figure 7

# HORIZONTAL ACCELERATION SPECTRA
## Strike-Slip Fault: M = 7.2, R = 4.9
## D = 4.0

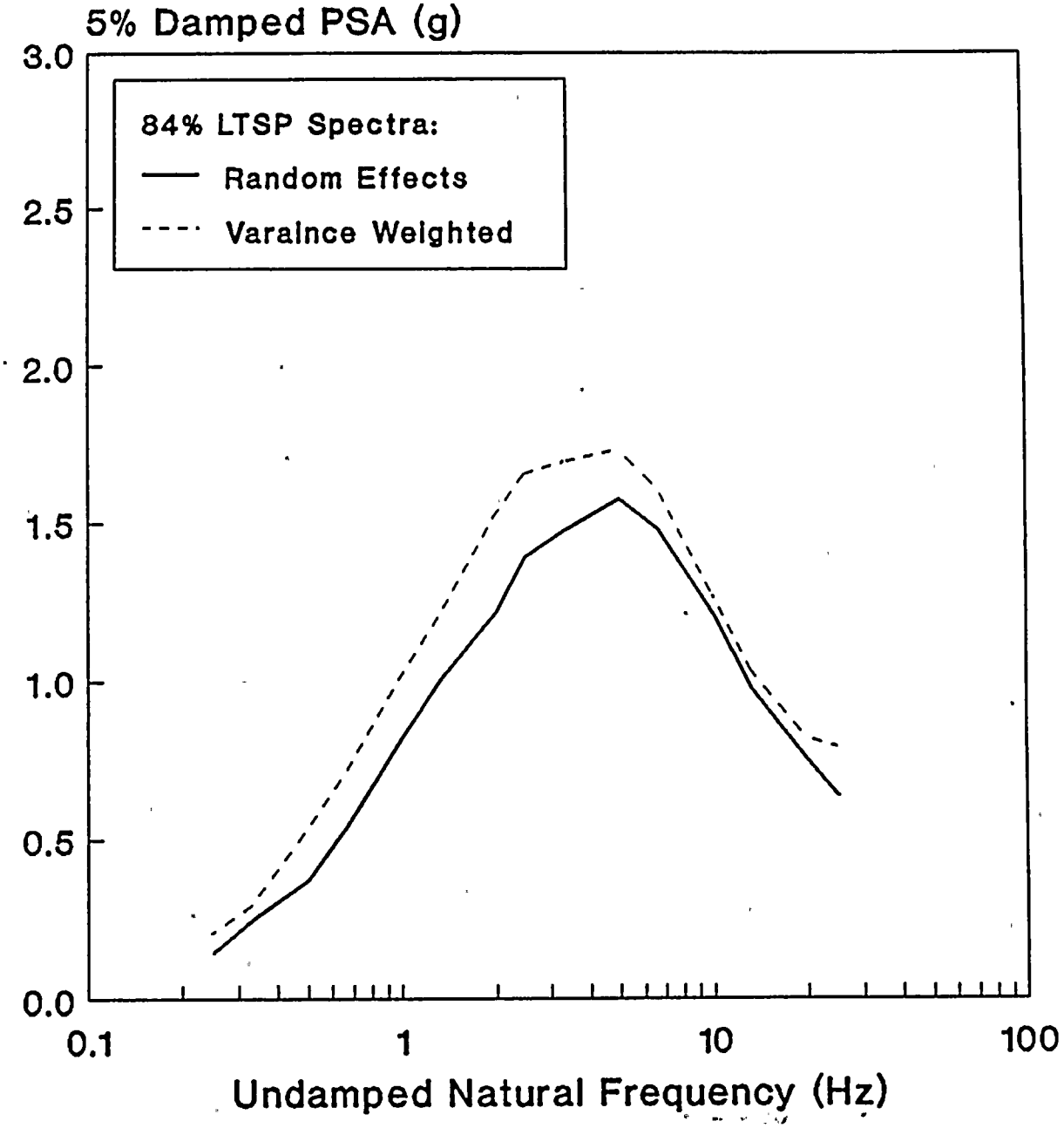


Figure 8

# HORIZONTAL ACCELERATION SPECTRA
## Reverse-Oblique Fault: M = 7.2, R = 4.7
## D = 4.0

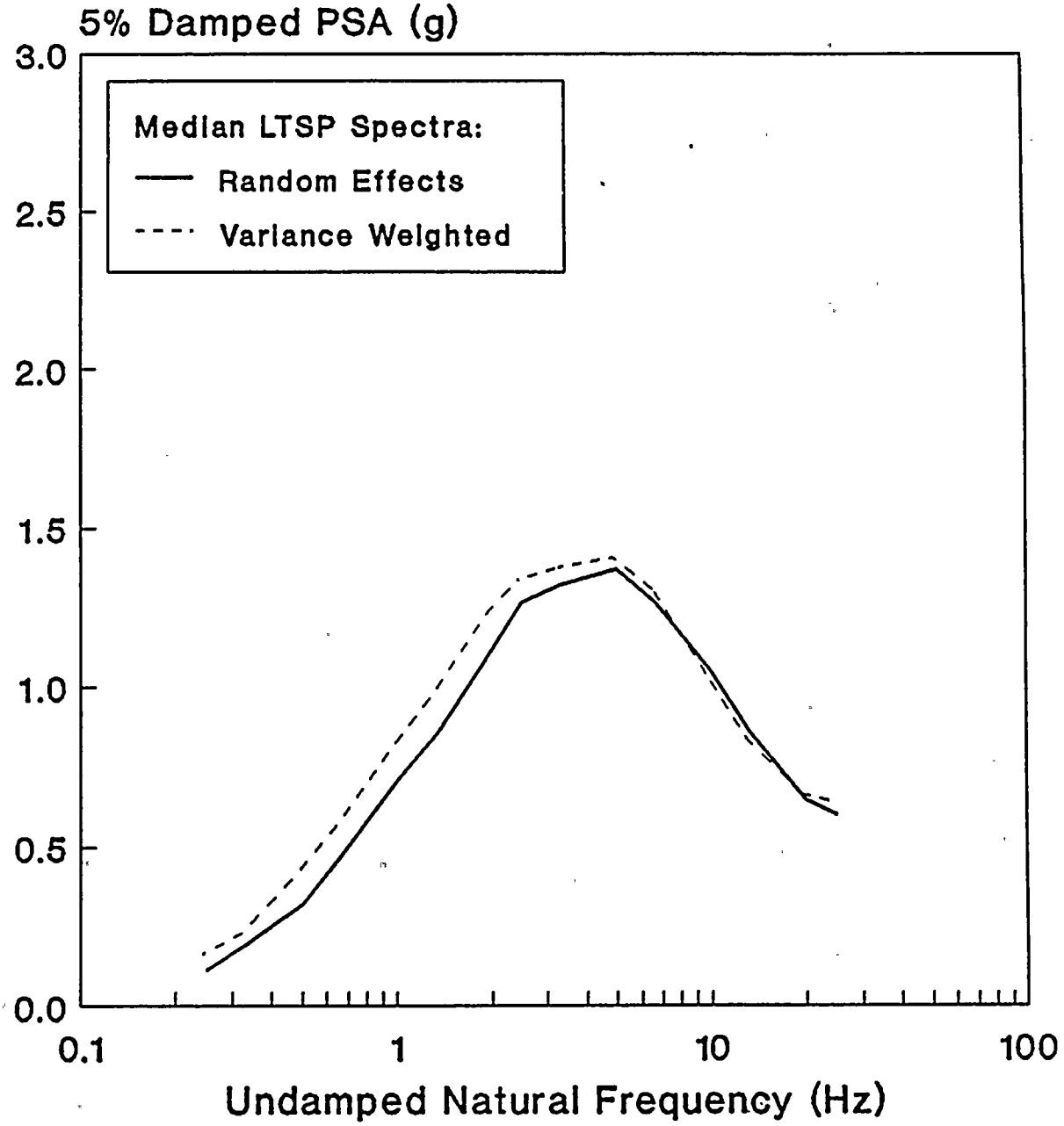


Figure 9

# HORIZONTAL ACCELERATION SPECTRA
## Reverse-Oblique Fault: M = 7.2, R = 4.7
## D = 4.0

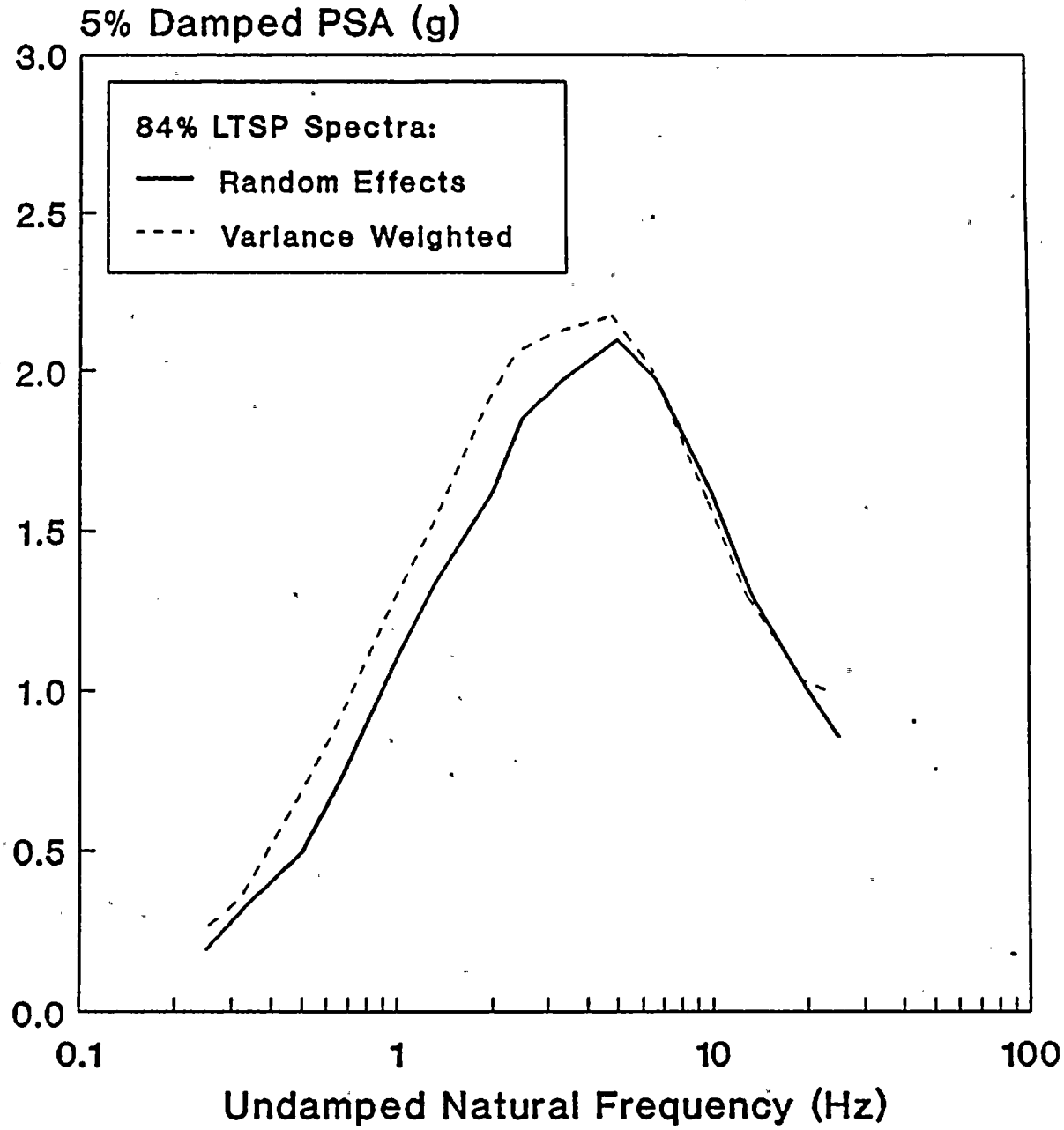


Figure 10

# HORIZONTAL ACCELERATION SPECTRA
## Thrust Fault: M = 7.2, R = 5.1
## D = 4.0

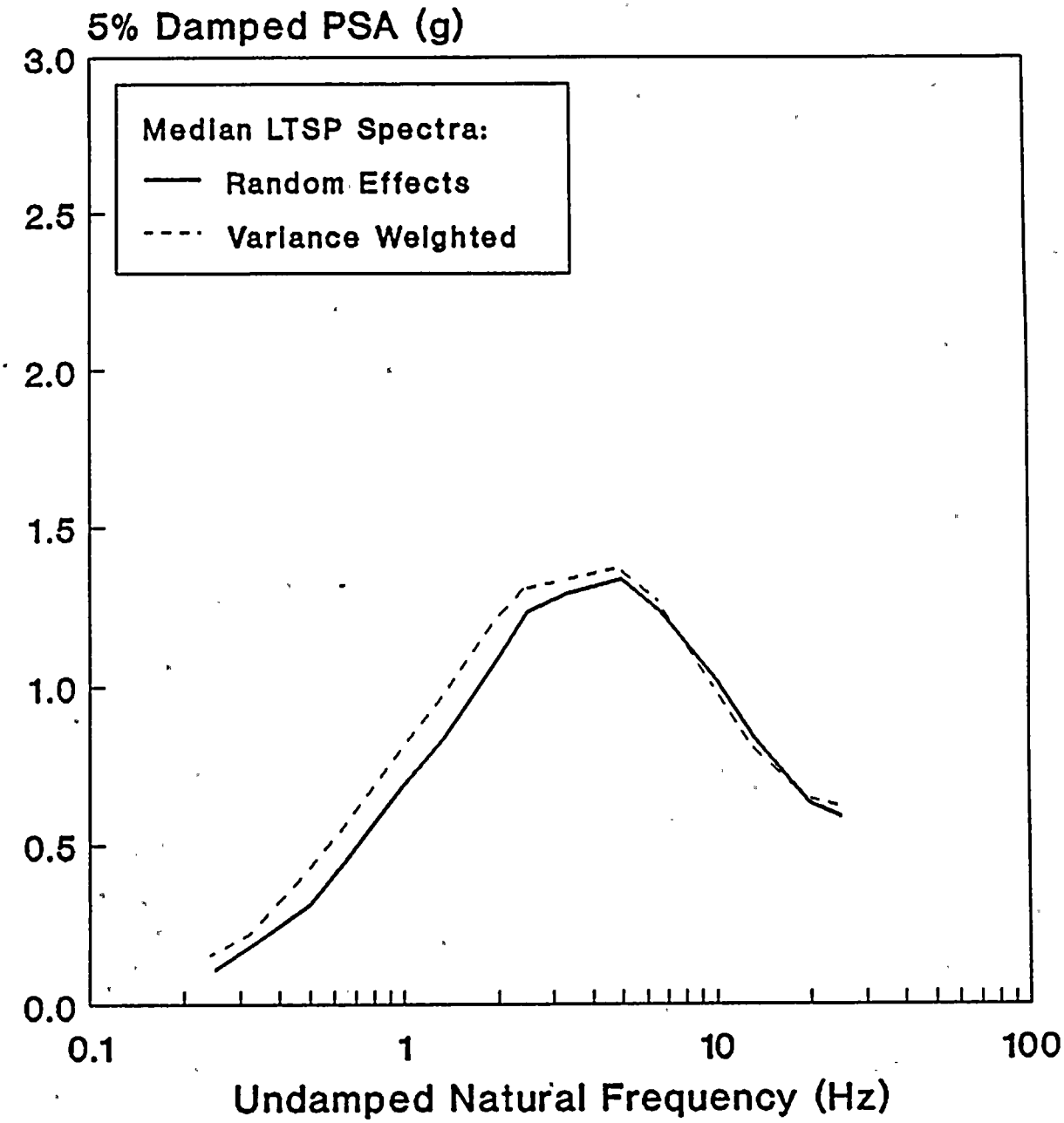


Figure 11

# HORIZONTAL ACCELERATION SPECTRA
## Thrust Fault: M = 7.2, R = 5.1
## D = 4.0

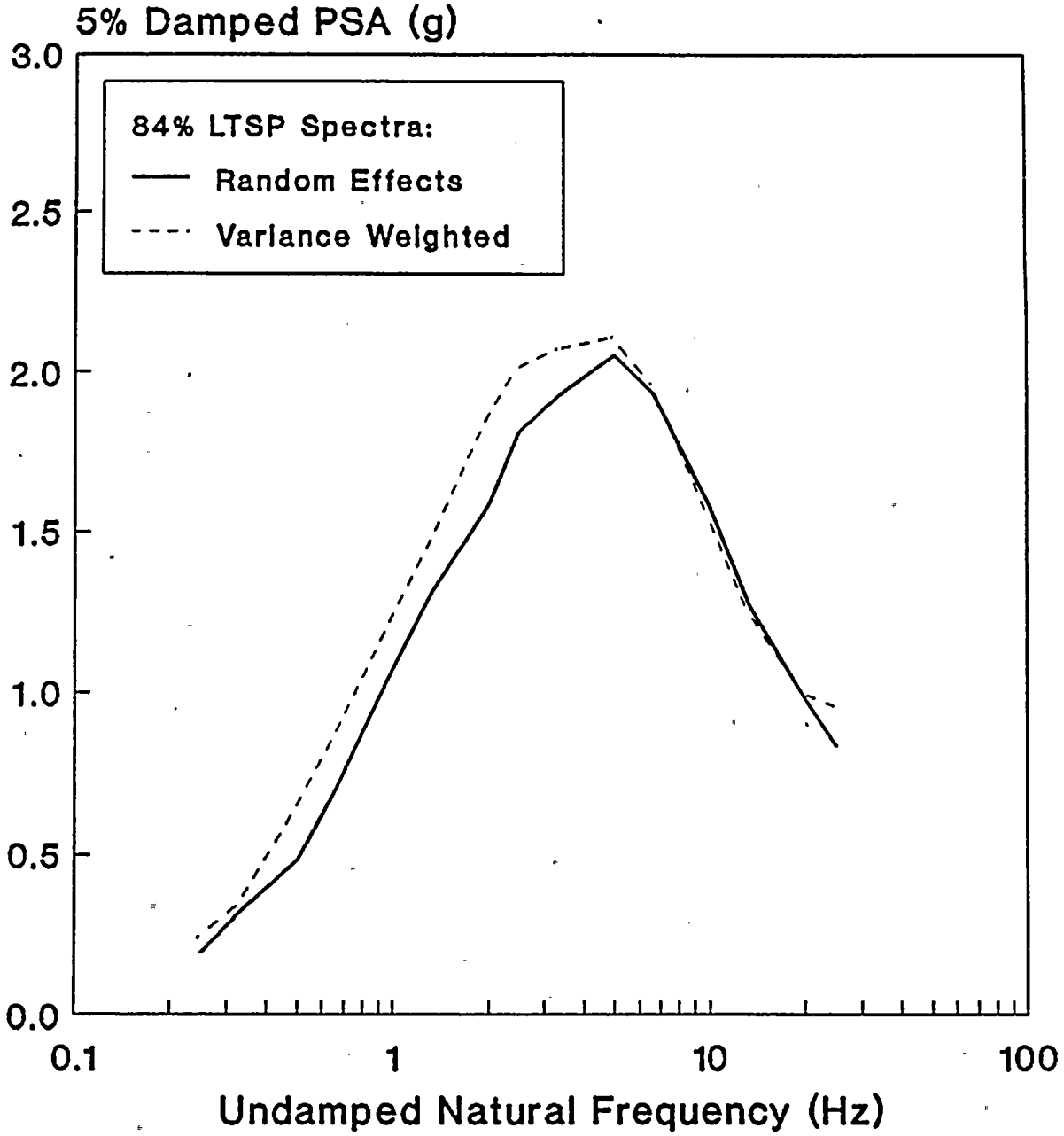


Figure 12

# VERTICAL ACCELERATION SPECTRA
## Strike-Slip Fault: M = 7.2, R = 4.9
## D = 4.0

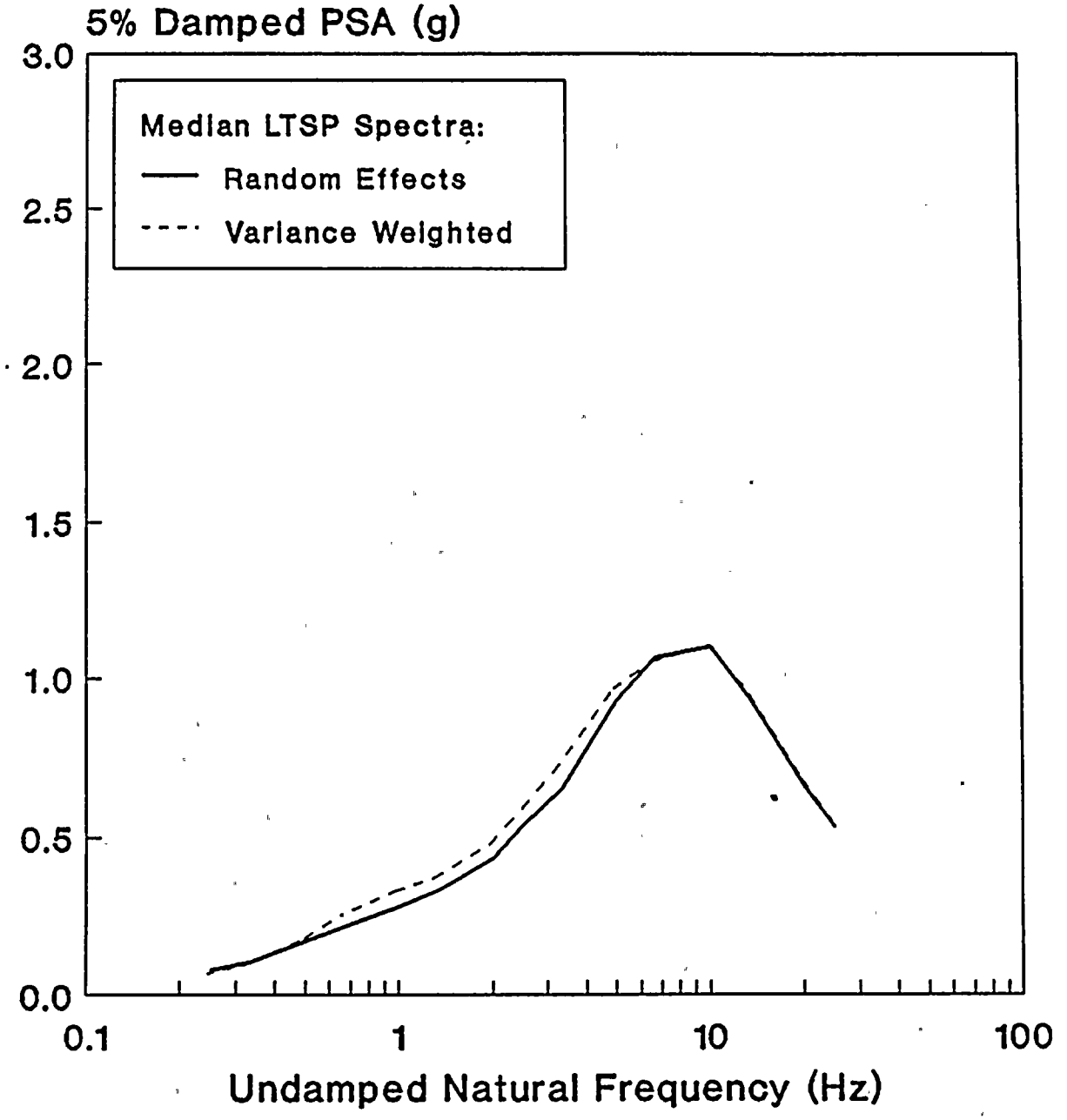


Figure 13

# VERTICAL ACCELERATION SPECTRA
## Strike-Slip Fault: M = 7.2, R = 4.9
## D = 4.0

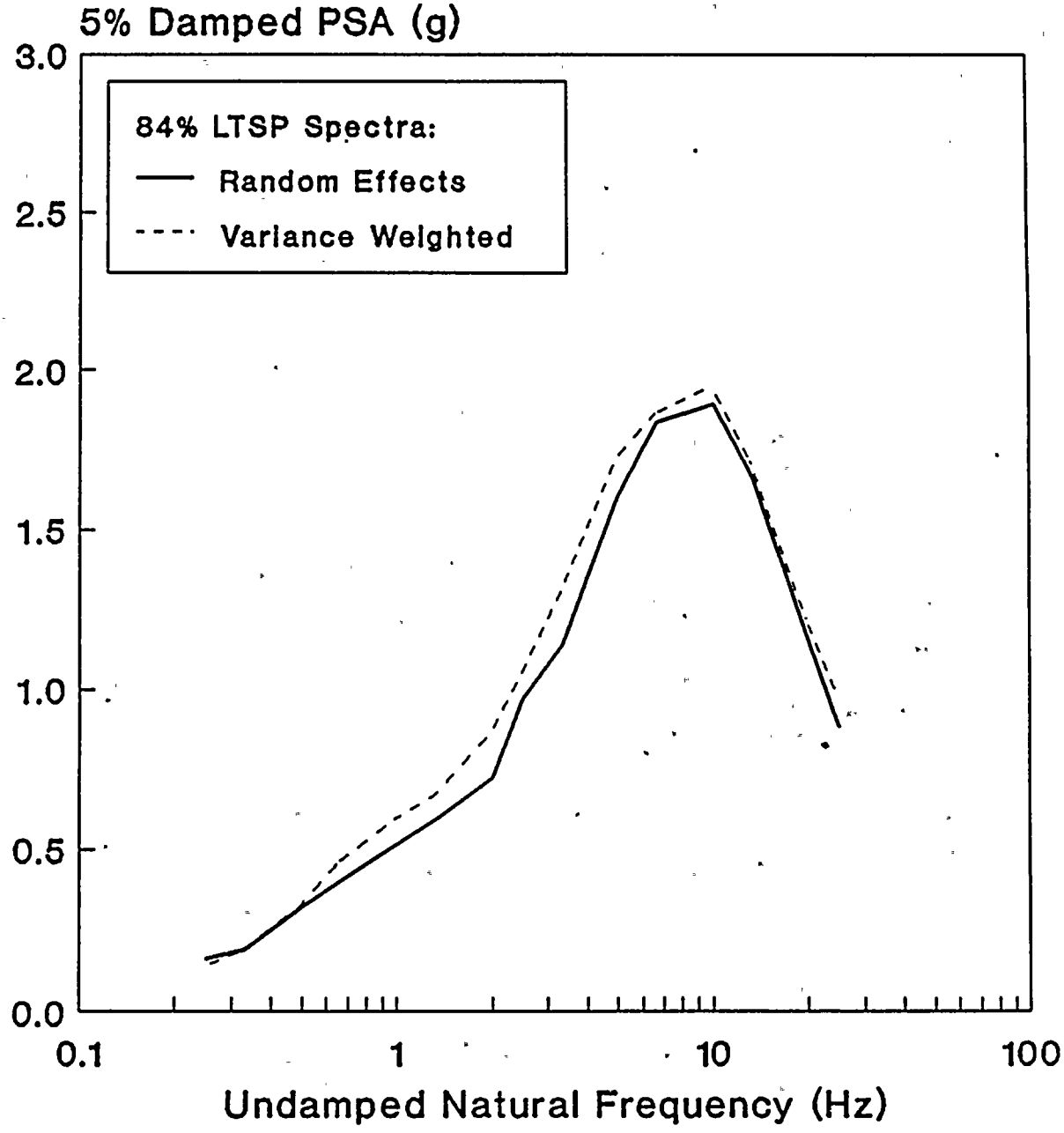


Figure 14

# VERTICAL ACCELERATION SPECTRA
## Reverse-Oblique Fault: M = 7.2, R = 4.7
## D = 4.0

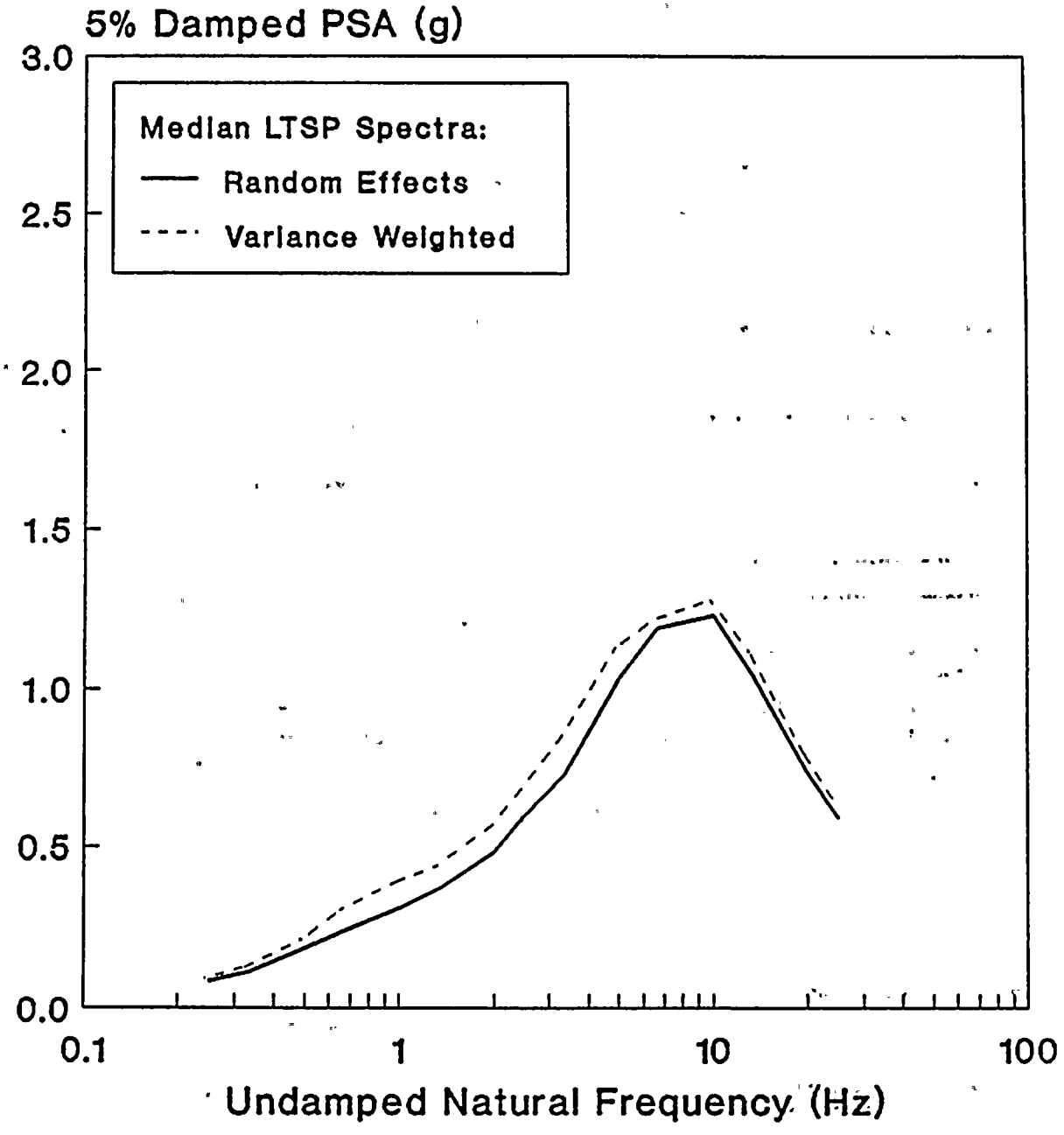


Figure 16

# VERTICAL ACCELERATION SPECTRA
## Reverse-Oblique Fault: M = 7.2, R = 4.7
## D = 4.0

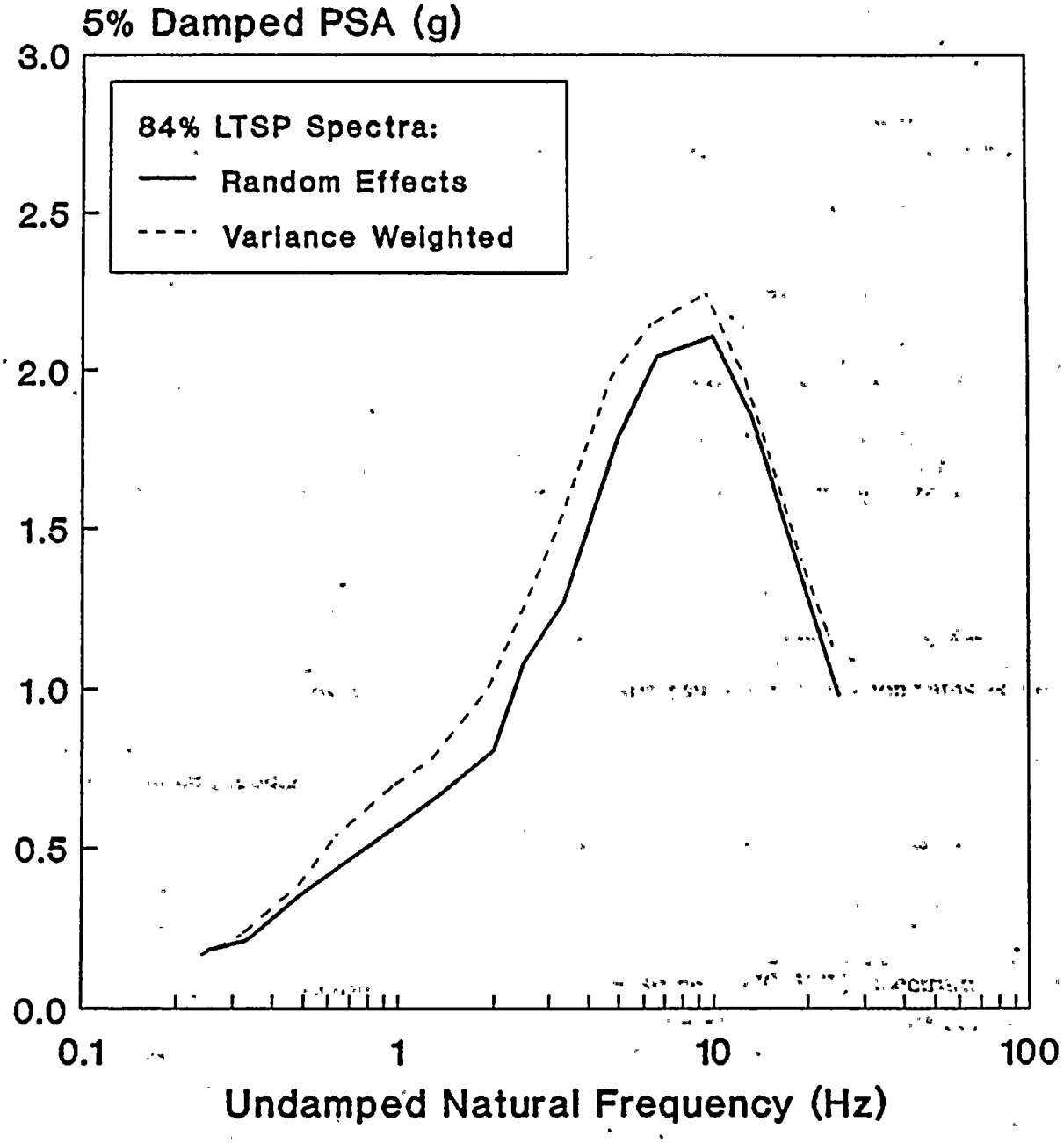


Figure 16

# VERTICAL ACCELERATION SPECTRA
## Thrust Fault: M = 7.2, R = 5.1
## D = 4.0

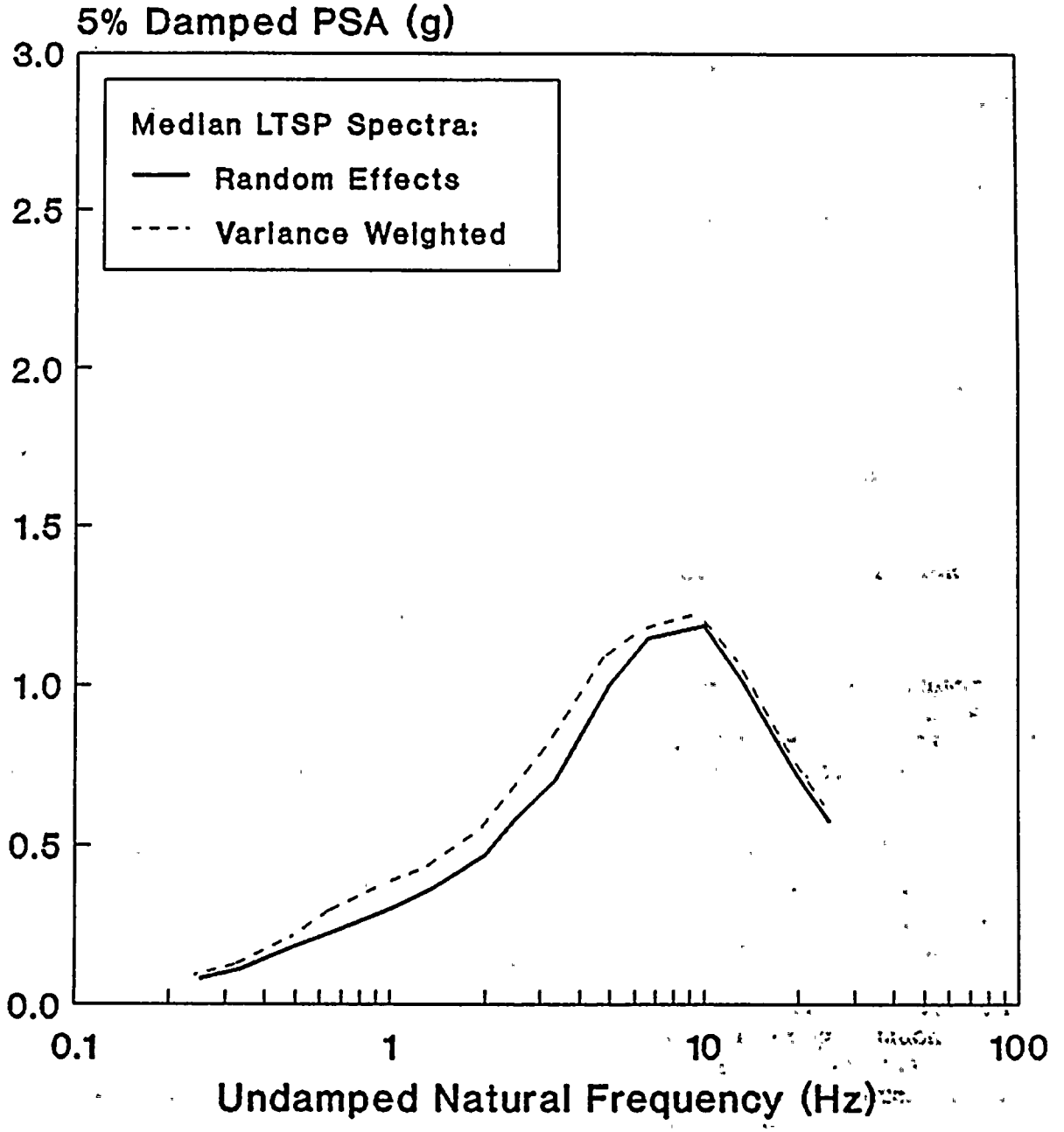


Figure 17

# VERTICAL ACCELERATION SPECTRA
## Thrust Fault: M = 7.2, R = 5.1
## D = 4.0

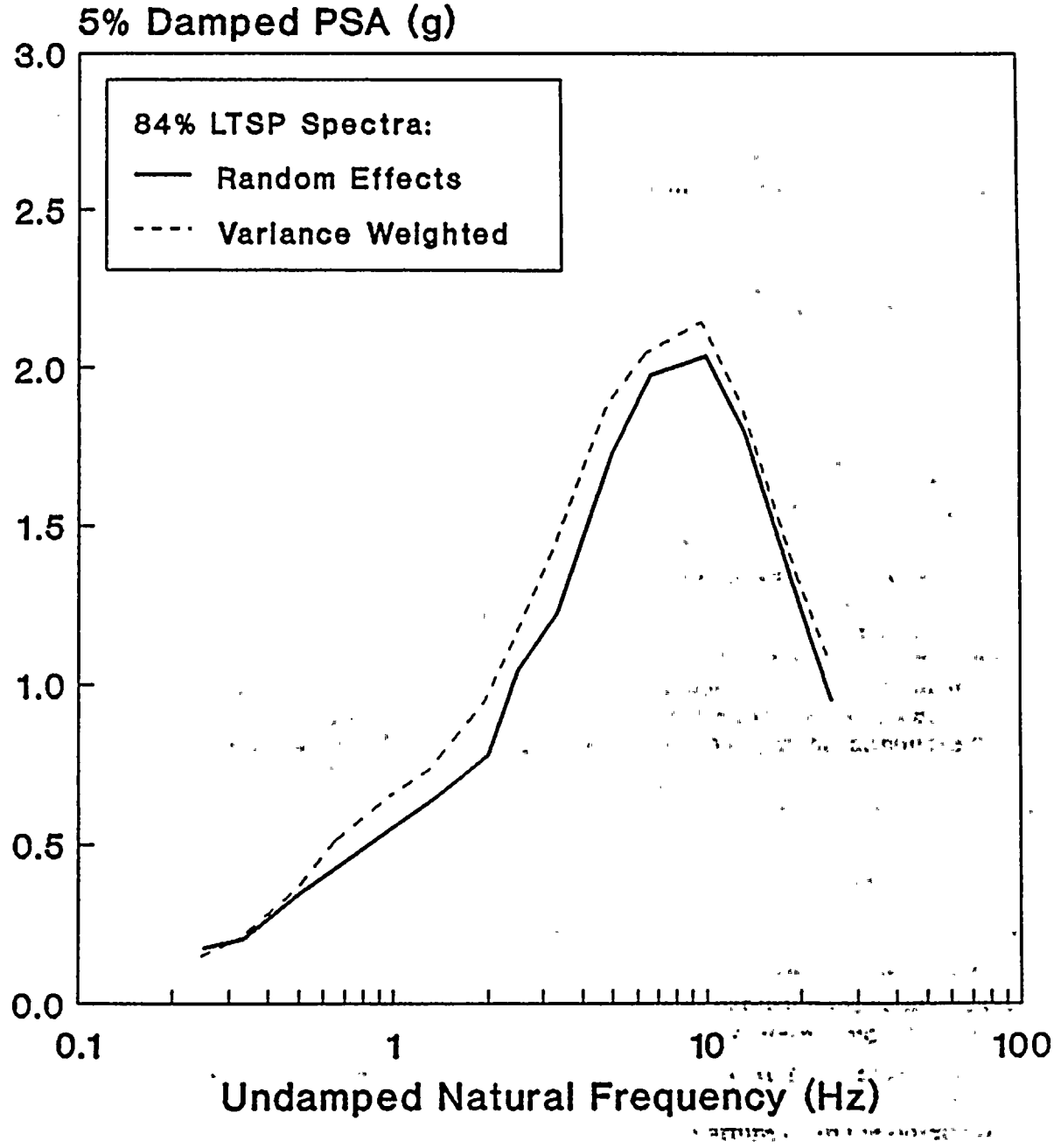


Figure 18

DEPARTMENT OF GEOLOGICAL SCIENCES
TELEPHONE: (213) 740-6106
FAX (213) 740-8801

July 30, 1991

Dr. Jean Savy
Mail Stop L-196
Lawrence Livermore Laboratory
P. O. Box 808
Livermore, CA 94550

Dear Jean:

The purpose of the present letter is to modify the content of my letter mailed to you on September 10, 1990 with regard to the Diablo Canyon Long Term Seismic Program ground-motion evaluations. The modification has become necessary because the P.G.&E told me that Fig. 4.11 of Final Report was mislabeled.

The curve labeled as Imperial Valley aftershock in the original Fig. 4.11 showed a significantly lower (by about a factor of 2) amplitude in the frequency range higher than 5 Hz than other events including those at the Diablo Canyon site. I interpreted this difference to the local site effect, because I thought that soft sediments in Imperial Valley may attenuate waves of higher frequencies more strongly than rock sites.

According to P.G.&E. the above labeling of the curve was incorrect. The curve originally labeled as Imperial Valley is for the Diablo Canyon site, and the curve originally labeled as DCPP is for Imperial Valley aftershock. This change, in fact, is in harmony with the recent results on sire amplification factors determined for many stations in central and southern California including the Imperial Valley. We found (e.g. Su et al., EOS, 71, 1475, 1990, see Fig. 8 in the attached review paper by Aki and Irikura (1991), to be published in the Proc. of 4th International Conference on Seismic Zonation, August 25-29, 1991) that the weak-motion amplification factor is greater for younger sediments than older rocks even at 12 Hz. This observation is well established for central and southern California including the Imperial Valley. In other words, even at frequencies as high as 12 Hz, the amplification due to lower impedance dominates over the attenuation due to higher absorption at sediment sites relative to rock sites. I can, therefore, readily accept the statement of P.G.&E. that Fig. 4.11 was mislabeled.

The above change eliminates my earlier concern expressed in my September 10, 1990 letter that the use of Imperial Valley event as the empirical source-function might have caused underestimation of the ground motion at the Diablo Canyon site by about a factor of 2 at frequencies higher than 5 Hz.

Sincerely yours,

Keiiti Aki

KA:st
Enclosure
cc: R. L. Rothman

# CHARACTERIZATION AND MAPPING OF EARTHQUAKE SHAKING FOR SEISMIC ZONATION

Keiiti Aki[I] and Kojiro Irikura[II]

## ABSTRACT

This is a review of the current state of the art in characterization and mapping of earthquake shaking for seismic zonation. We start with the characterization of ground motion and describe recent advances and unresolved issues in the following areas: (1) deterministic kinematic source models, (2) stochastic source models, (3) limitation of the ω–squared model, (4) strong motion prediction for a large earthquake using observed seismograms of small earthquakes, (5) empirical attenuation relationships for various regions, (6) effects of local geology using broad classification of site conditions, (7) applicability of weak-motion amplification factor to strong motion, (8) non-linearity of site response, (9) relation between site-specific weak-motion amplification factor and intensity, and (10) numerical simulation of ground motion time history. We then review the current status of the data base, mapping of ground motion and intensity for microzonation in both U.S. and Japan, and propose future directions of research and its implementation based on the current state-of-the-art in ground motion characterization.

## A. CHARACTERIZATION OF EARTHQUAKE GROUND MOTION

### Deterministic Kinematic Source Models

The ground motion caused by an earthquake can be expressed as a space-time convolution of the slip function on the fault with Green's function which represents the earth's medium response (e.g., Aki and Richards, 1980). This mathematical framework has been used extensively for determining the space-time slip distribution on a fault plane from the observed seismograms using Green's functions calculated for realistic models of the earth (e.g., Kikuchi and Kanamori, 1982; Ruff and Kanamori, 1983; Archuleta, 1984; Hartzell and Heaton, 1985, 1986; Takeo, 1987; Kikuchi and Fukao, 1987; Fukuyama and Irikura, 1988; Beroza and Spudich, 1988; Iwata and Irikura, 1989; Hartzell and Iida, 1990; Gariel et al., 1991).

The data used in the above inversion studies came from a variety of sources including teleseismic body waves and surface waves recorded by observatory seismographs and near-source velocities and displacements recorded by strong motion seismographs. The frequency range covered in the inversion is usually lower than 1 Hz although some of the recent studies mentioned above attempted to extend the frequency range to a few Hz. The difficulty of deterministic modeling for high frequency waves is due to the increased details and complexities of earth structure affecting Green's function with the increasing frequency.

---

[I]W. M. Keck Foundation Professor of Geological Sciences, Department of Geological Sciences, University of Southern California, Los Angeles, CA 90089-0740

[II]Professor, Disaster Prevention Research Institute, Kyoto University, Uji, Kyoto, 611, Japan

Despite the limited frequency window, the above inversion studies have brought out spatial and temporal behaviors of earthquake faults which are rich in complexity and heterogeneity. The part of the fault plane with large slip was called "asperity" by Lay and Kanamori (1981), who studied the relation between the asperity distribution and the tectonic setting for circum-Pacific subduction zones. They classified the subduction zones into several types according to the size of asperities, from the Chile-type with the largest asperity, to the Mariana type where major asperities are absent.

Hartzell and Heaton (1985) also examined source time functions of the 63 largest shallow earthquakes from circum-Pacific subduction zones in the period range from 2.5 to 50 sec., and found that some of the properties of source function such as roughness and multiplicity appear to be characteristic of each subduction zone.

The significance of the asperity distribution estimated from low-frequency motion to the generation of high-frequency motion relevant to earthquake engineering application is not straightforward. For example, according to the numerical simulation of spontaneous rupture propagation over a heterogeneous fault by Das and Aki (1977), a smooth fault which generates large slip (i.e. asperity) tends to be relatively deficient of high-frequency excitation than a rough fault. In fact, in the case of the Izu-Hanto-Toho-Oki earthquake of 1980, the area of large slip determined by Takeo (1987) from records of the displacement meters did not coincide with the region of high slip velocity obtained by Iwata and Irikura (1989) using the near-source accelerograms by tomographic imaging.

Another issue with the engineering application of asperity is their repeatability in earthquakes recurring from a given fault segment. It will take a long time to answer this question because of the long recurrence interval for any earthquake associated with a particular fault segment.. In the meantime, the statistical aspects of asperity pattern characteristic to a seismic region may be included in the probabilistic seismic hazard analysis as discussed later.

As mentioned above, the deterministic modeling is limited in the applicable frequency range. To overcome this limitation, two lines of research have been pursued in strong motion seismology. One is the introduction of stochastic element in the source model thereby reducing the number of parameters describing details of the source, and the other is the use of the records of small earthquakes sharing similar propagation paths as the target earthquake in place of Green's function.

## Stochastic Source Models

A stochastic source model called "ω-squared model" proposed by Hanks and McGuire (1981) has gained broad support from the seismological community as a means to predict the amplitude spectra or peak values of strong ground motion for practical engineering applications. In this model, earthquake accelerations are considered to be band-limited random noise in the band between the corner frequency $f_0$ and the high-cut frequency $f_{max}$, and the spectral shape is given by the Brune (1970, 1971) spectrum specified by the seismic moment Mo and the stress parameter $\Delta\sigma$. $\Delta\sigma$ is related to the corner frequency by

$$f_o = 4.9 \times 10^6 \beta(\Delta\sigma/Mo)^{1/3} \qquad (1)$$

where $\beta$ is shear wave velocity in km/s, and $\Delta\sigma$ is in bar, and $M_o$ is in dyne cm. The physical meaning of $\Delta\sigma$ has become somewhat unclear by the stochastic extension of the original Brune model. For engineering application, however, we may accept the above equation as a definition of $\Delta\sigma$ in terms of seismic moment and corner frequency, following Boore and Atkinson (1987) who stated "this parameter is known by several names; we prefer to refer to it simply as the stress parameter and thereby not attach any physical significance in terms of fault models".

Since Joyner and Boore (1988) made an extensive review of the development and application of the $\omega$-squared model in the context of alternative models, we shall focus here on regional and tectonic dependence of the model parameters and the limitation in the frequency and magnitude range of its applicability. Let us first consider the regional variation of the stress parameter $\Delta\sigma$ and its dependence on magnitude, fault type, focal depth, etc. Originally, Hanks and McGuire (1981) found that a constant $\Delta\sigma$ of about 100 bar can explain the root mean squared and peak acceleration of all California earthquakes within a factor of 2. Later, Boore (1986) revised the estimate of $\Delta\sigma$ at 50 bar by taking into account the average amplification factor at the site of strong motion seismograph.

According to Boore and Atkinson (1987, 1989), the stress parameter for earthquakes in the eastern U.S. is also constantly independent of magnitude, and at about 100 bar, twice as high as that in the western U.S.. Sommerville et al. (1987) also support the constant stress parameter independent of magnitude. On the other hand, Nuttli (1983) and Nuttli et al. (1987) proposed the stress parameter which increases with magnitude. Recent works by Chael (1987) and Chun et al. (1989) also support the magnitude dependent stress parameter. In any case the absolute level of stress parameter estimated by Nuttli et al. (1987) ranges from 60 bar for M=5 to 160 bar for M=7, which are not too far from 100 bar obtained by Boore and Atkinson (1987).

The applicability of the $\omega$-squared model to strong ground motion from earthquakes in Japan has been confirmed by Irikura (1983, 1986) and Takemura and Ikeura (1988) for $M_{JMA} < 7$.

Possible effects of fault type, focal depth and repeat time on the stress parameter were also carefully reviewed by Joyner and Boore (1988). The difficulty in separating various factors affecting the strong ground motion prevented definitive conclusions on their effects. No new study since 1988 seems to give more definitive conclusions.

Another parameter of the $\omega$-squared model, $f_{max}$, shows a strong regional variation. According to Atkinson and Boore (1990), $f_{max}$ at rock sites is always higher than about 40 Hz in the eastern U.S. as compared to 10 to 15 Hz in the western U.S.. Hanks (1982), Anderson and Hough (1984) and others found that $f_{max}$ depends on the geologic condition of the recording site. On the other hand, Aki and Papageorgiou (1989) found the $f_{max}$ effect remained after eliminating the site effect from the acceleration spectrum. More recently, Kinoshita (1990, 1991) found that $f_{max}$ observed at the bottom of deep boreholes (about 3km) in bedrock in central Japan showed strong variation depending on the location of the earthquake source. $f_{max}$ varied from lower than 10 Hz to higher than 30 Hz, depending on the plate-tectonic setting of the seismic source. ($f_{max}$ is less than 10 Hz for intraplate shallow earthquakes in Izu and Yamanashi, as well as for those occurring at depth around 70 km where the Pacific plate touches the Philippine sea plate, while it is higher than 30 Hz for shallow subduction zone earthquakes, and 10 to 20

Hz for earthquakes deeper than about 100 km.) Thus, we must conclude that both site and source effects influence $f_{max}$ in the frequency range of engineering interest.

A weak but significant increase of $f_{max}$ with decreasing magnitude was observed by Papageorgiou and Aki (1983) for California earthquakes and by Irikura and Yokoi (1984) and Umeda et al (1984) for Japanese earthquakes, rendering another support for the source effect on $f_{max}$.

Thus, the issue of $f_{max}$ is not whether it is categorically due to site effect or source effect but what their contributions are for individual cases.

Limitation of the ω-squared model

The most fundamental limitation of the ω-squared model comes from its failure to explain the observed seismic spectrum for the whole seismic frequency range. For example, as shown by Boore (1986), the ω-squared model with the stress parameter adequate for explaining the strong motion data cannot explain the observed $M_S$-moment relation. In fact, the ω-squared model proposed by Aki (1967) to explain the observed spectral ratios for the period range longer than 1 sec had the stress parameter of only 0.5 bar, a hundred times less than that required to explain strong ground motion data. A more recent global compilation of empirical relations among various magnitude scales by Gusev (1983) also indicates a low stress parameter of about 7 bar which corresponds to the lower one of his two corner frequencies. Both Aki (1967) and Gusev (1983) explain the observed $M_S$-moment relation better than the ω-squared model as shown by Boore (1986) and Papageorgiou (1988). In view of the recent interest in long period motion in the Earthquake Engineering community, the failure of the ω-squared model in explaining observed $M_S$, which is related to seismic motions at period 20 seconds, may be a serious problem. A similar departure of observed spectrum from the ω-squared model for a broad frequency range has been presented also for the intraplate earthquakes in Japan by Umeda (1981), and for the subduction zone earthquakes in Japan by Izutani (1984). For the same reason, Papageorgiou and Aki (1983) distinguished two stress drops in their specific barrier model of heterogeneous earthquake fault, the local stress drop for high frequency excitation, and the global stress drop for low frequency excitation. A recent summary of source parameters for California earthquakes in terms of the specific barrier model can be found in Chin and Aki (1991), who applied the model to the Loma Prieta earthquake of 1989.

A similar departure from the ω-squared model was recognized for the subduction zone earthquakes in Mexico by Singh et al (1990), who found that the ω-squared model is inadequate to explain the observed source spectra in a broad frequency range; they resemble spectra given by Gusev (1985) with some difference.

On the other hand, Houston and Kanamori (1986) concluded a broad applicability of the ω-squared model with a constant stress parameter of 30 bar using the short-period records of P waves from earthquakes with $M_W$ from 6.5 to 9.5 at teleseismic distances. The same data were also analyzed by Boore (1986), who concluded that the $\omega^2$ model with the stress parameter 50 bars explain observed amplitude within a factor of 2 to 3 for magnitudes up to 9.5, although we recognize a systematic departure from the observed $M_S$ - moment relation for $M > 7$.

Another limitation of the ω-squared model is the simple assumption used to account for the propagation path effect by the following expression:

$$\frac{1}{R}\exp\left(\frac{-\pi f R}{\beta Q(f)}\right) \qquad (2)$$

where f is frequency, Q(f) is the quality factor ($Q=(2h)^{-1}$, h being the damping constant) and R is a properly chosen distance between the earthquake source and recording site. The above formula implies that the earthquake source is effectively a point in space, and the amplitude of seismic waves attenuate with distance as if they were in a homogeneous unbounded medium.

The effects of fault rupture propagation (a departure from the point source assumption) on high-frequency radiation relevant to strong motion seismology has been demonstrated observationally by Boatwright and Boore (1982), and theoretically by Boore and Joyner (1978), Koyama (1985) and Koyama and Izutani (1990). This directivity effect as well as the effect of asperities discussed earlier are not included explicitly in the ω-squared model, although some attempts have been made to modify the ω-squared model to incorporate the effect of directivity (Boore and Joyner, 1989, Koyama and Izutani, 1990). These and other effects of spatial-temporal pattern of slip function as well as the propagation path effects of more realistic crustal structures, however, can be included directly in the deterministic kinematic modeling described earlier. Furthermore, the long-period range, in which the ω-squared model has difficulty, is easier to work with using deterministic modeling.

Thus, it is natural to look for effective hybrid approaches combining the deterministic and stochastic modeling. One approach may be to start with the ω-squared model and distribute them in space and time to simulate a complex rupture process for a large earthquake. This approach may be able to include some of the effect missing in a single source of the ω-squared model, but will not be able to produce long-period motion accurately. Another approach may be to start with a simplified deterministic model and introduce random variations for some model parameters such as rupture speed, amount of slip, rise time, etc. This approach requires a new statistical characterization of source process which must be validated through comparison with observation as well as by a sound physical basis.

Strong Motion Prediction for Large Earthquakes Using Observed Seismograms of Small Earthquakes

A promising approach toward developing an effective hybrid method is the use of observed seismograms of small earthquakes for predicting seismic motions for a large earthquake, sometimes called the empirical Green's function method. This method was originated by Hartzell (1978), and has become popular among many seismologists as reviewed by Joyner and Boore (1988).

The advantage of this method is not only to exploit the common propagation path and local site effects shared by subevents and the target earthquake, but also the possibility to introduce randomness for high frequency waves while keeping the coherent deterministic property for low frequency waves. Joyner and Boore (1986, 1988) describes a method for summing subevents in order to meet the condition for moment at the low frequency end and

the asymptotic decay at the high frequency end, but recognizes the deficiency in the intermediate frequency range.

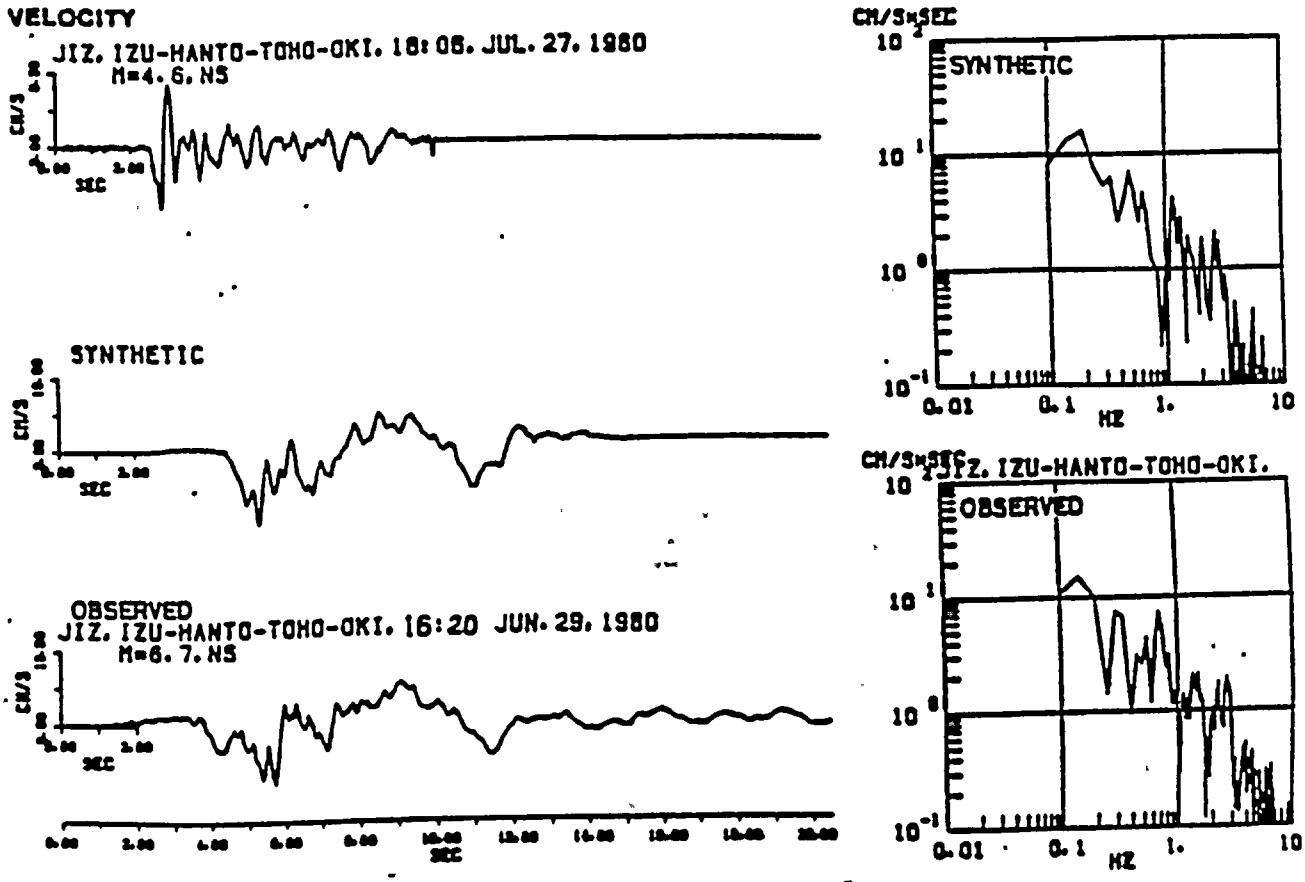


FIGURE 1. An example of synthetic velocity seismogram using the empirical Green's function method based on equation (3). The record of subevent (M=4.6), the synthetic and observed record of the target earthquake (M=6.7) are shown at the top, middle and bottom, respectively. The Fourier spectra of synthetic and observed records are compared on the right. The recording site is on rock.

Here, we shall describe a procedure from Irikura and Aki (1985) for constructing a seismogram for a large earthquake by summing subevent seismograms, following the ω-squared scaling law with a constant stress parameter.

Let the moment of the target earthquake be $N^3$ times that of the subevent. We divide the fault plane into NxN elements. The seismogram A(t) for the target earthquake is expressed in terms of the seismogram a(t) of the subevent as follows:

$$A(t) = \sum_{i=1}^{N^2} (r/r_i)\, F_i(t) * a(t),$$

$$F_i(t) = \delta(t-t_i) + \frac{1}{n''} \sum_{j=1}^{(N-1)n'} \cdots \delta\,(t-t_i - (j-1)\,\tau/(N-1)n'), \qquad (3)$$

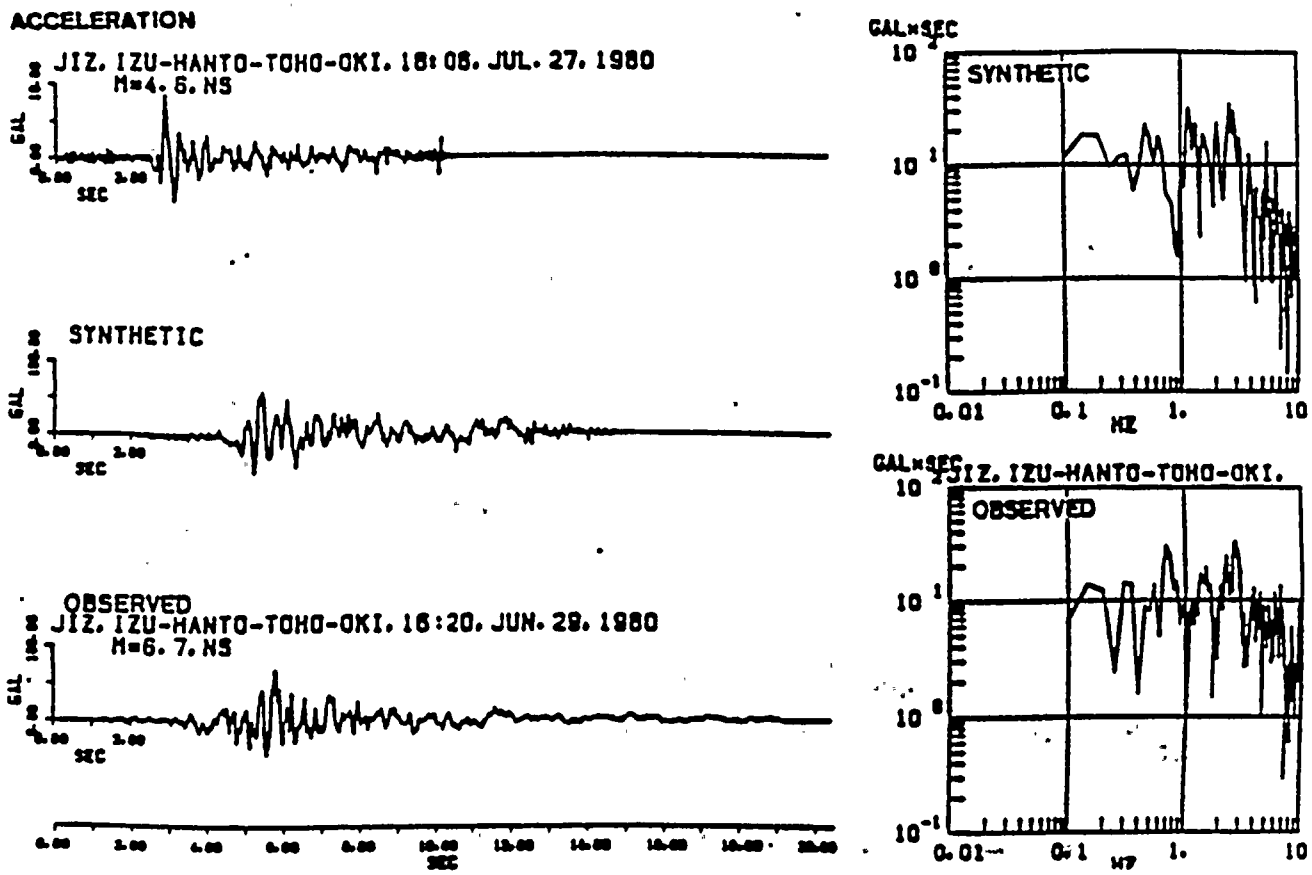


FIGURE 2. An example of synthetic acceleration seismogram using the empirical Green's function method based on equation (3). The record of subevent (M=4.6), the synthetic and observed record of the target earthquake (M=6.7) are shown at the top, middle and bottom, respectively. The Fourier spectra of synthetic and observed records are compared on the right. The recording site is on rock.

and $t_i = r_i/V_c + \xi_i/V_R,$

where r is the hypocentral distance from the observation point to the subevent, $r_i$ is the distance from the observation point to the ith fault element, $\xi_i$ is the distance from the rupture nucleation point to the ith fault element, $v_R$ is the rupture speed, $v_c$ is the velocity of seismic waves under consideration, $\tau$ is the rise time of the target earthquake, n' is an appropriate integer to eliminate spurious periodicity (Irikura, 1983), and * represents the convolution. The above formula will sum the low frequency end of the spectrum coherently to $N^3$ times that of the subevent, assuring the correct moment. The high frequency end, on the other hand, will be summed incoherently and become proportional to

the square root of the number $N^2$ of summation. Thus, the amplitude of the high frequency end will be proportional to the cube root of that at the low frequency end, meeting the condition for the ω-squared scaling law. Unlike the procedure of Joyner and Boore (1986), this procedure does not introduce any deficiency in the intermediate frequency range. The time-domain filter $F_i(t)$ described in the above equation is equivalent to the frequency-domain filter used by Boatwright (1988) for the same purpose. Physically, the filter mimics a case of rupture process over a heterogeneous fault simulated by Das and Aki (1977), in which a barrier on the fault plane eventually breaks slowly after momentarily stopping the rupture.

Figure 1 and Figure 2 show examples of synthetic ground velocity and acceleration, respectively, calculated by the above method (equation (3)) assuming that both the target earthquake and the subevent obey the ω-squared model. The target earthquake is the Izu-Hanto-Toho-Oki earthquake (M=6.7) of 1980, and the subevent is an aftershock with M=4.6. The actual records of the subevent and the target earthquake are shown at the top and bottom of each figure, respectively. The Fourier spectra of synthetic and observed records of the target earthquake are shown at the right side of each figure. Both waveforms and spectra show a very good agreement between the synthetic and observed records.

Empirical Attenuation Relationships for Various Regions.

There have been numerous empirical formulas published on the dependence of ground motion parameters on distance from the earthquake source and earthquake magnitude. An extensive in-depth review was given by Joyner and Boore (1988) on the formulas for peak ground motions and response spectra. For the western United States, they found that more recent formulas show good agreement among themselves except for the magnitude and distance ranges where the data are scanty.

Figure 3, reproduced from Joyner and Boore (1988), compares different relationships for peak horizontal acceleration at magnitude 6.5 (a) and 7.5 (b). DB, from Donovan and Bornstein (1978), I, from Idriss (1987) for deep soil sites; JB, from Joyner and Boore (1982), reduced by 13% so as to approximate the value for the randomly oriented horizontal component; C, the constrained relationship of Campbell (1987) for a strike-slip earthquake recorded at a free-field site with soil more than 10m deep and no allowance made for directivity. The distance plotted is the closest distance to the vertical projection of the rupture on the surface of the earth. The curves of Donovan and Bornstein and those of Campbell are adjusted assuming a source depth of 5 km. Figure 3a shows that for M=6.5 the different relationships agree to within a fraction of the uncertainty of an individual prediction as given by any of the authors, suggesting that the short-distance prediction at M=6.5 are controlled by the data. For M=7.5, the agreement at short distances, where it matters most, is not as good as at M=6.5, reflecting the scarcity of data points.

With regard to the pseudo velocity response, Joyner and Boore (1988) found that the differences among several recently published curves are somewhat larger than for peak horizontal acceleration. They emphasize, however, that all of the curves of pseudo velocity response spectrum at 1 Hz for 5% damping reviewed by them give higher values, by factors of 1.5 to 3 than the highest value of the ATC-3 spectrum for firm ground at short distances.

Recent development of ground motion relationships for the eastern United States was reviewed by Atkinson and Boore (1990). Recent trends in the comparative study of

eastern versus western U.S. appear to deemphasize the difference found by Nuttli (1981) with regard to the scaling law of the source spectra and the frequency dependent Q(f)

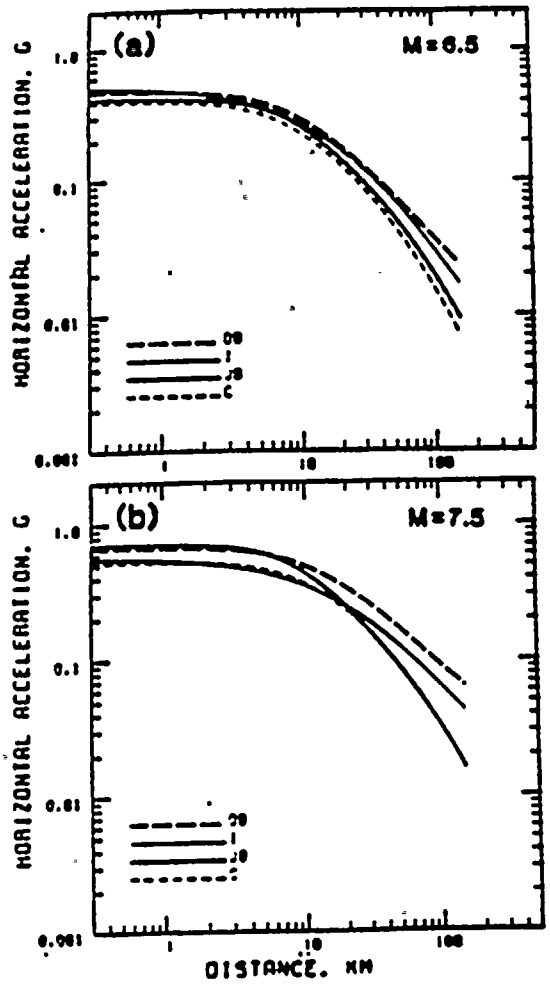


FIGURE 3. Empirical attenuation relations for horizontal peak accelerations due to earthquakes with M=6.5 and M=7.5 in the western U.S. reproduced from Joyner and Boore (1988). DB stands for Donovan and Bornstein (1978), I for Idriss (1987), JB for Joyner and Boore (1982), and C for Campbell (1987).

defined in equation (2). Atkinson and Boore (1990), however, still find significant difference between eastern and western U.S. in the value of $f_{max}$ as mentioned earlier, and in the attenuation with distance. A comparison of pseudovelocity response for eastern U.S. with western U.S. at frequencies 0.1, 1, 5 and 20 Hz is reproduced in Figure 4 from Atkinson and Boore (1990). The difference is negligible at 0.2 Hz, but the attenuation is significantly slower for EUS than WUS at higher frequencies, and amplitude is considerably higher for EUS than WUS at all distances for 20 Hz.

The study of empirical attenuation relationships for Japan has been summarized in a data book published by the Architectural Institute of Japan in 1987, which lists about 20 empirical formulas for peak ground motions and response spectra applicable to Japanese earthquakes. The range of Japanese representative attenuation relationships deviates

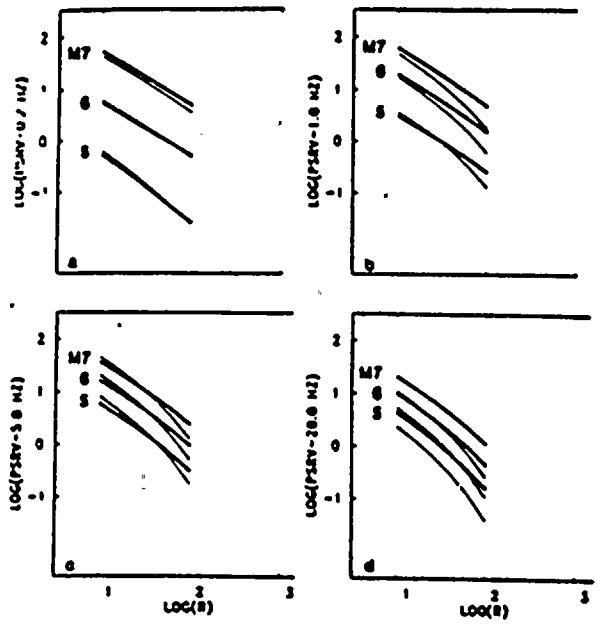


FIGURE 4. Empirical attenuation relations for pseudovelocity response spectra at 0.2, 1.0, 5.0 and 20 Hz reproduced from Atkinson and Boore (1990). Thick curves are for the eastern U.S. and thin ones are for the western U.S.

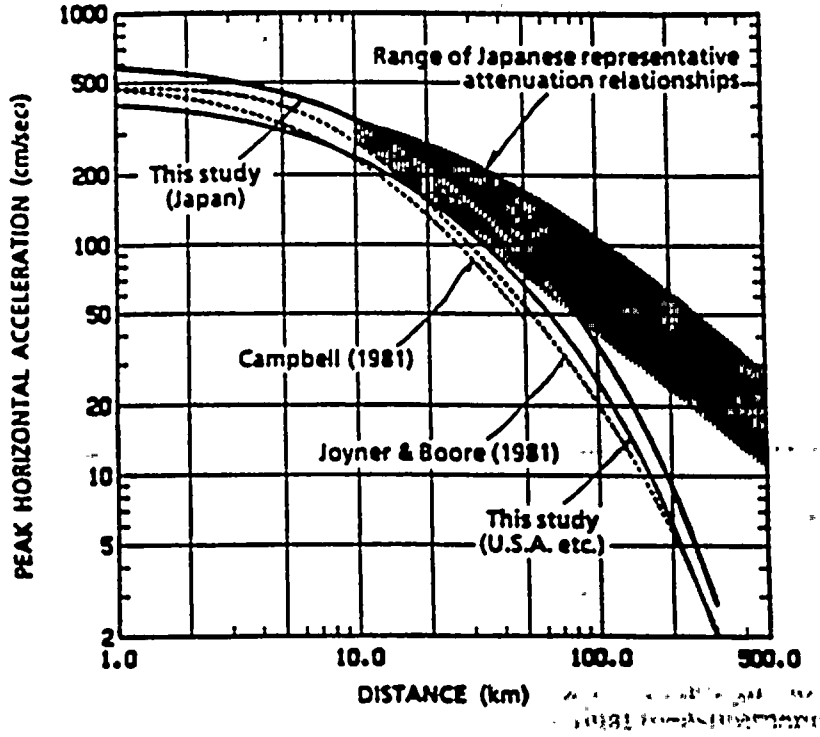


FIGURE 5. Empirical attenuation relations for peak horizontal acceleration normalized to M=6.5 reproduced from Fukushima and Tanaka (1990). The discrepancy between the representative relationships for Japan and those for the western U.S. has been virtually eliminated by a new analysis based on the two-step regression method of Joyner and Boore (1981).

significantly from that for U.S., as shown in Figure 5 reproduced from Fukushima and Tanaka (1990), who attributed the discrepancy to the difference in the procedure for data analysis. They concluded that Japanese old results were biased due to the strong correlation between magnitude and distances in their data set, and applied the two-stage method (Joyner and Boore, 1981, 1982) to avoid the bias. The new result for Japan is very close to that for the U.S., shown by thick line in Figure 5. A part of the curve at distances shorter than about 20km, however, is constrained not by Japanese data but by the data from California, because of the lack of data from Japan.

Joyner and Boore (1988) compared the attenuation relations for peak horizontal acceleration and velocity between Italy (Sabetta and Pugliese (1987)) and western U.S. and found that for distances less than 100km the agreement is within a fraction of the standard deviation of an individual prediction for either study.

The attenuation relations for Mexico have attracted the attention of many researchers (Anderson et al (1986), Bard et al (1988), Ordaz and Singh (1991) among others) because of the severe damage in Mexico city during the Michoacan earthquake of 1985. Figure 6, reproduced from Ordaz and Singh, shows the spectral amplitude plotted as a function of distance up to 400km for frequencies from 0.2 to 5.0 Hz. The stations at the coastal sites (open circle) are distinguished from those inland. Inland sites are marked by solid circles for distances up to 200 km, and by triangles for distances beyond 200 km. Triangles with letter T, with letter C and without any letter indicate sites in Teacalco, Cuernavaca and hillsites in Mexico city, respectively. It is clear from the figure that no systematic difference exists between inland and coastal sites for distances up to 200 km, while inland sites show greater amplitude than coastal sites at all frequencies, except for 5 Hz, for distances between 200 and 400 km. These large differences are not due to the amplification effect of the soft lake sediments in Mexico city, because those sites on the lake sediment are not included in these figures. This large amplitude may be due to the interaction between incident waves and deep sediments as discussed by Bard et al. (1988) and Kawase and Aki (1989).

## Effects of Local Geology

The ground shaking and the associated damage on engineered structures can be strongly influenced by geology and topography in their vicinities, and any attempt at seismic zonation must take into account the local site conditions. However, the characterization of ground shaking in terms of local site conditions is not an easy task because of the diverse geologic materials and irregularly shaped earth structures formed by weathering, erosion, deposition and other geological processes near the surface of the earth. Let us first review the results obtained by the broad classification of site conditions into soil and rock sites.

## Broad Classification of Site Conditions

Remarkably consistent results have emerged, from empirical studies of strong ground motion data based on the broad classification of site conditions, about the local site effect on peak ground acceleration, peak ground velocity, response spectra and other ground motion parameters from the works both in Japan (Hayashi et al. (1971); Kuribayashi et al. (1972); Katayama et al. (1978); Kawashima et al. (1986); among others) and in U.S. (Seed et al. (1976); Mohraz (1976); Trifunac (1976a, b); Boore et al. (1980); Joyner and Boore (1981); among others). Aki (1988) summarized these results in the following observations: The site amplification factor on response spectra depends on the

frequency of ground motion. Soil sites show higher amplification than rock sites by a factor of 2 to 3 for periods longer than about 0.2 seconds, while the relation is reversed for

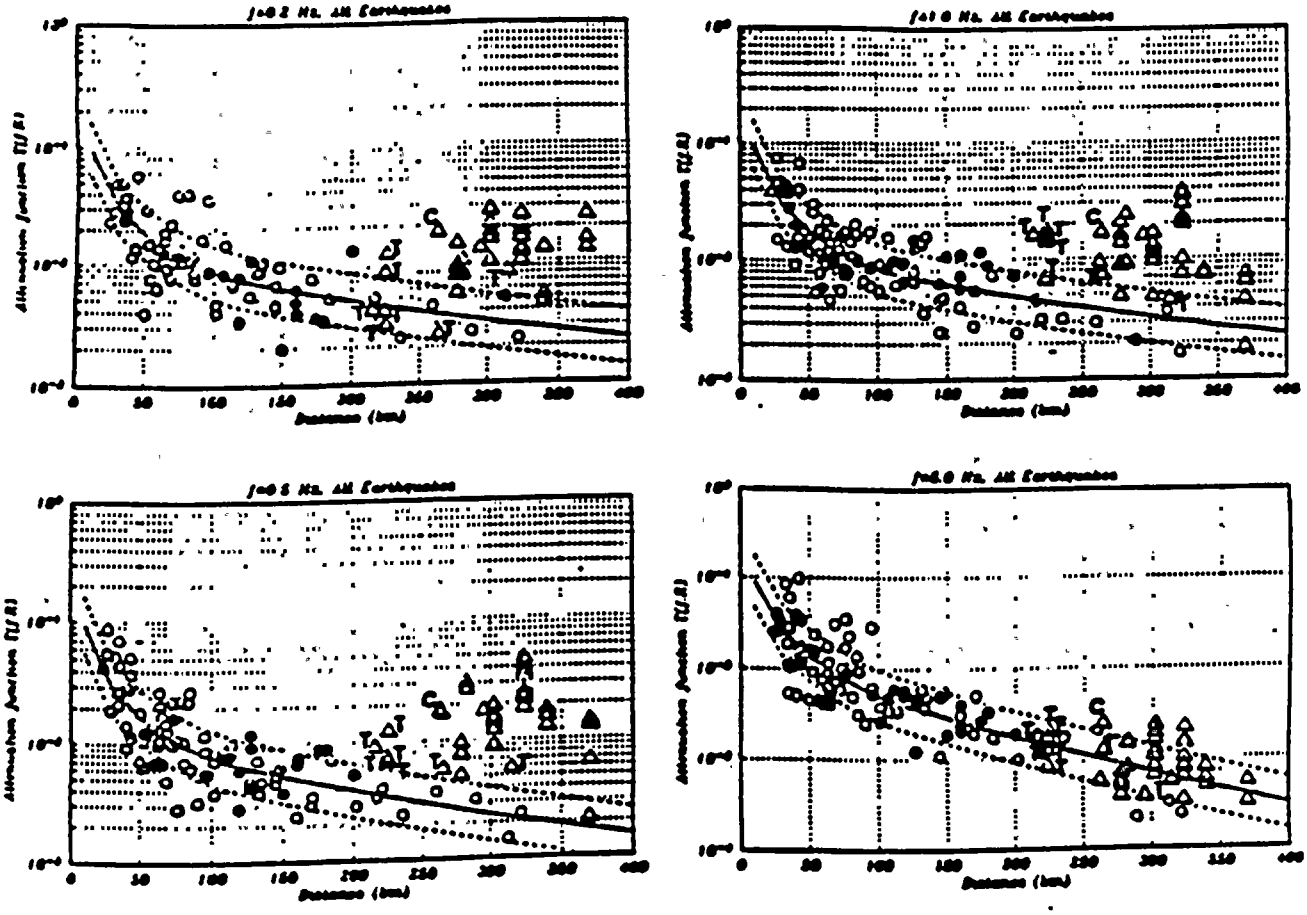

FIGURE 6. Attenuation relations observed for the Michoacan earthquake of 1985 reproduced from Ordaz and Singh (1991). Open circles indicate stations at the coastal sites, while inland sites are marked by solid circles for distances up ro 200 km, and by triangles beyond 200 km. Letter T and C refer to Teacalco and Cuernavaca, respectively. Triangles without letters indicate hill sites in Mexico City.

periods shorter than about 0.2 seconds. This frequency dependence is reflected in the site dependence of peak ground motions. Peak ground velocity and displacement as well as the Arias intensity show higher amplifications for soil sites than rock sites, while peak ground acceleration is roughly independent of the site classification.

The relative independence of peak ground acceleration on whether the recording site is on rocks or soils was again confirmed for the epicentral area of the Loma Prieta earthquake of 1989 (Boore et al., 1989). For epicentral distances greater than about 50 km, however, peak acceleration was strongly influenced by surface geology, lowest acceleration on rock sites, intermediate on alluvium sites and highest on artificial fill and bay mud. According to EERI (1990), the observed differences in horizontal acceleration between sites on hard rock, bay mud, and artificial fill were 100% to 200% in the San Fra··:isco and Oakland areas.

What is the reason for this difference in site effect between inside the epicentral area and outside? The answer to this question requires a systematic study of the earthquake source, propagation path and local site effects on the observed strong ground motion. For example, an anomalously strong reflection from the Moho discontinuity can cause high amplitude at epicentral distances around 100 km (Sommerville and Yoshimura, 1990), and combined effects of source directivity and radiation pattern may cause azimuthal variation in ground motion (Joyner and Boore, 1988). Another possibility is the non-linear amplification effect at soil sites, which will make the difference in amplification between soil and rock sites to diminish with the increase in ground shaking (Idriss, 1990).

In order to find what the correct answer is, let us first review the recent results on the amplification factor for weak motions, and compare their dependence on site conditions with that for strong motions. Recently, Su et al. (1990) extended the work of Phillips and Aki (1986) to a greater amount of better calibrated data from the USGS Central California network, and calculated the site amplification factors for coda waves. The similarity of coda amplification factor to that of direct S waves has been confirmed since Tsujiura (1978), who showed that the logarithmic average of amplification factor for S waves over various directions of wave approach is very close to the amplification factor for coda waves. The applicability of the coda amplification factor to the peak ground motion is verified by the comparison with the station residual for magnitude recently determined by Eaton (1990) for the same network. Figure 7 shows the coda amplification factor A

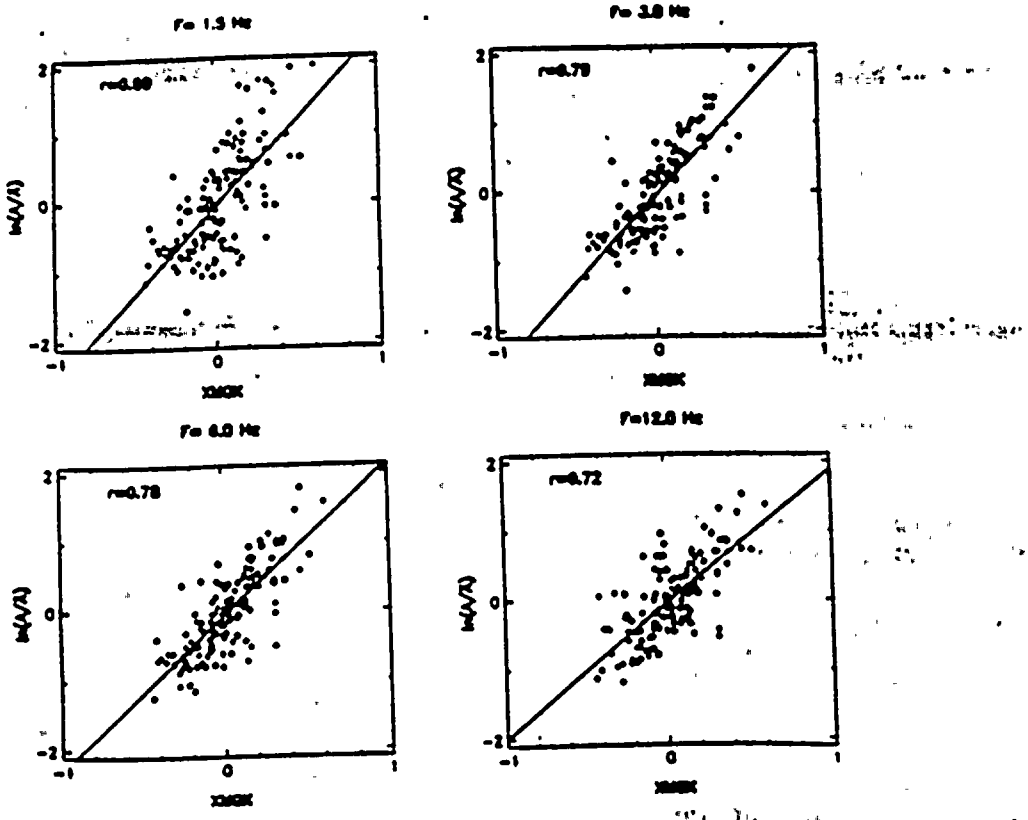

FIGURE 7. The site-specific, weak-motion amplification factor at central California U.S.G.S. network stations for frequency bands centered at 1.5, 3, 6 and 12 Hz plotted against the station residual for magnitude based on the peak amplitude measurement obtained by Eaton (1990). The amplification factor was determined by Su et al. (1990) using the coda method of Phillips and Aki (1986).

relative to the logarithmic mean for $\overline{A}$ over all stations plotted against the station residual for magnitude based on the peak amplitude measurement. The least squares fit for several frequency bands shows that the coda amplification factor scales approximately linearly with the site amplification factor for the peak amplitude. The correlation is highest at 3 to 6 Hz, implying that the predominant frequencies of peak motions used for magnitude measurements lie in this frequency range. The coda amplification factor appears to vary slightly faster than the linear scaling at 1.5 Hz, and slower at 12 Hz relative to the peak amplitude.

In order to find the relation between the coda amplification factor and the site condition, the surface geology of the station site was classified into 5 geologic ages, namely, (1) Quaternary, (2) Pliocene, (3) Miocene to Cretaceous sediments, (4) Franciscan formation and Mesozoic granitic rocks, and (5) Pre-Cretaceous metamorphic rocks. The site amplification factors for stations in each group are logarithmically averaged and plotted in Figure 8 against the median age, together with the standard errors of individual measurements and that of their mean. Figure 8 shows a remarkably smooth power law relation between the amplification factor (relative to the logarithmic mean over all stations) and the age of the site geologic formation. The amplification factor varies more strongly with the age at lower frequencies, proportional to $(age)^{0.36}$ at 1.5 Hz and $(age)^{0.22}$ at 12 Hz. The relation between the age and amplification factor is very significant on the average as indicated by the small standard error (10-15%) of mean shown in Figure 8, but the standard error is large (about a factor of 1.6) with regard to the individual measurement.

The above frequency dependence is similar to that obtained from strong motion data in that the site effect is stronger for lower frequencies. It does not, however, show the reversal at the cross-over frequency at about 5 Hz as the analysis of strong motion data consistently showed. As shown in Figure 8, the younger sediment site shows higher amplification than the older rock site at all frequencies up to 12 Hz. When Aki (1988) reviewed the result of Phillips and Aki (1986), he recognized the frequency dependent reversal in the coda amplification factor between the granite site and the fault-zone sediment site, although not between the Franciscan rock site and the non-fault-zone sediment site, and attributed the reversal to the domination of absorption effect over low impedance effect at frequencies higher than 5 Hz. With the increased number of better calibrated stations (from 35 in Phillips and Aki (1986) to 133), however, the reversal is eliminated as an average effect on weak motion. We now conclude that the amplification due to low impedance of younger sediments still dominates over the deamplification due to high absorption at least up to 12 Hz on the average for central California, as far as the weak-motion is concerned.

If the weak motion amplification factor applies to the strong motion, we should observe higher peak acceleration for soil sites than rock sites because peak accelerations in most strong motion records are associated with frequencies lower than 12 Hz. As mentioned earlier, strong motion peak acceleration does not show such a systematic site dependence.

Applicability of Weak-Motion Amplification Factor to Strong Motion

The effect of a soft, low impedance, surface layer on seismic motion has been well recognized in Japan since the early 1930's through pioneering observational studies by Ishimoto and theoretical studies by Sezawa. Takahashi and Hirano (1941) was probably the first to interpret the observed difference in actual earthquake records at different sites

quantitatively by a linear elasticity theory. Early results on strong site effects on ground motion in Japan were summarized by Kanai et al. (1956).

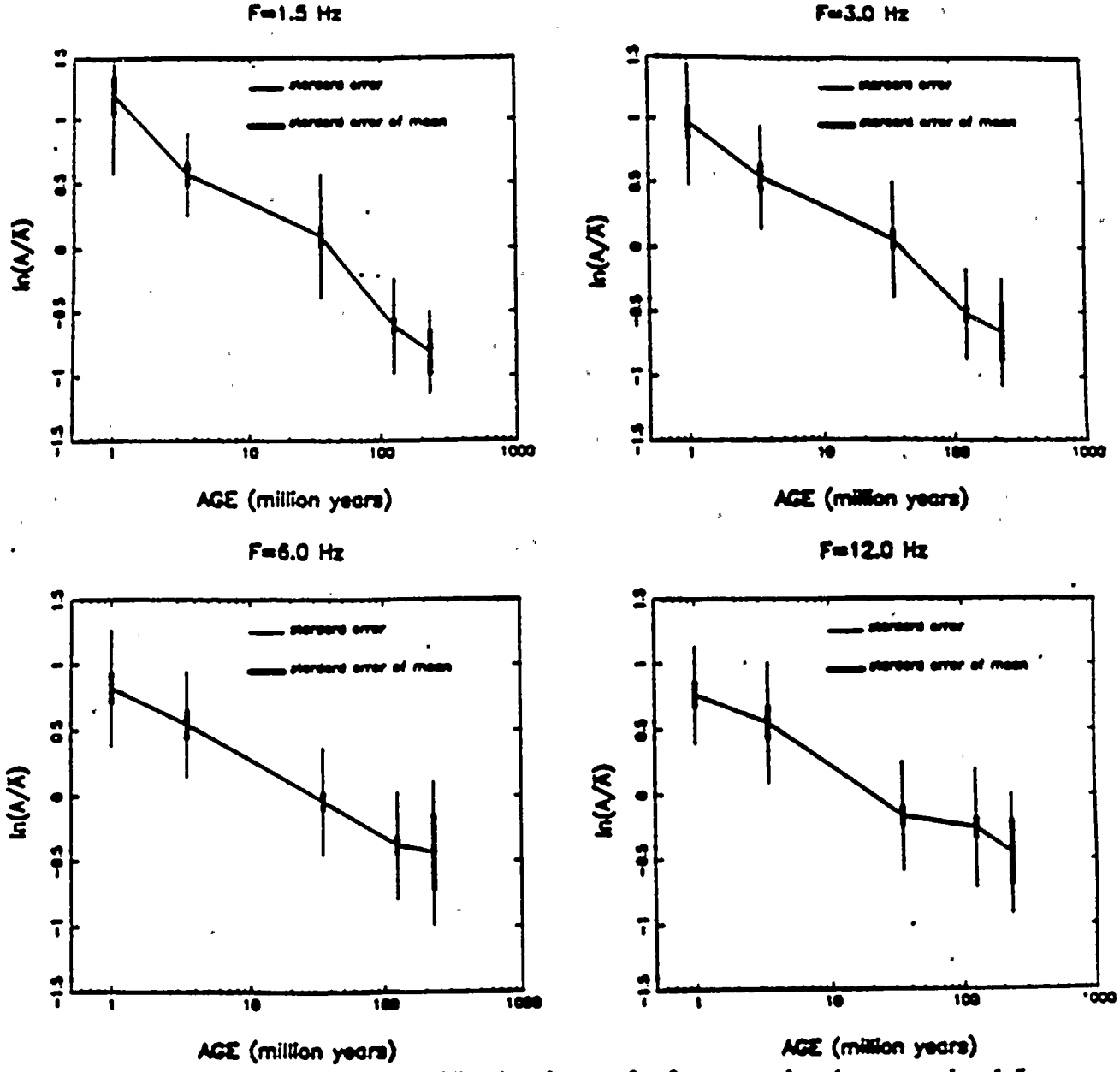


FIGURE 8. The weak-motion amplification factors for frequency bands centered at 1.5, 3, 6, and 12 Hz are plotted against the geologic age of the sediment reproduced from Su et al. (1990). The amplification is greater at younger sites for all frequencies on the average. The standard error of mean is small (10 to 15%) indicating the strong age dependence, although the standard error is large (about a factor of 1.6) for individual measurements.

In the United States, the first study of site amplification was made by Gutenberg (1957) for the Pasadena area. Hudson (1972) compared the amplification factor obtained by Gutenberg with the observed ground motion during the San Fernando earthquake of

1971, and concluded that Gutenberg's prediction did not apply to the strong ground motion. We shall come back to this discrepancy later in the present section. A more systematic comparison of site effects on weak motion and strong motion was made by Borcherdt (1970) who studied seismic signals recorded in the San Francisco Bay area from the underground explosions in the Nevada Test Site. He measured the amplification factor in the frequency range 0.5 to 2.5 Hz, and found that it correlates very well with the site dependent part of intensity variation during the 1906 San Francisco earthquake as well as the amplification factor observed during the 1957 San Francisco earthquake. His work was used in the predictive intensity mapping for seismic zonation by Evernden et al. (1981, 1985), as discussed later. Records of strong ground motions obtained in the San Francisco Bay area during the Loma Prieta earthquake of 1989, in general, supports the applicability of weak-motion amplification factor to strong motion in this particular area (Borcherdt, 1990).

A similar study was extended to the Los Angeles basin by Rogers et al. (1984, 1985) who recorded NTS signals at 28 sites at which strong ground motions were also recorded during the 1971 San Fernando earthquake. They also found that the amplification factor shows a good correlation between the weak motion (NTS) and strong motion (San Fernando) data for the frequency range from 0.1 to 5 Hz..

A similar agreement of the amplification factor between weak and strong motion was observed by Tucker and King (1984) for a sediment-filled valley in Garm, USSR. They could not find any significant difference in the spectral ratio of the edge to the middle of the valley between weak ($10^{-9}$-$10^{-3}$g) and strong (.04-0.2g) acceleration in the frequency range 0 to 50 Hz..

The most spectacular demonstration of the applicability of linear theory is the case of Mexico City during the Michoacan earthquake of 1985. According to Singh et al. (1988), the ground motion at the lake bed is amplified 8-50 times relative to the hill-zone site with very little evidence for non-linearity up to the strain as much as 0.2%. The linearity of the lake bed is also supported by the approximate equivalence of predominant period between microtremor and strong motion (Kobayashi and Midorikawa, 1986). The study of Liege, Belgium earthquake (M=4.9) of 1983 by Jongmans and Campillo (1990) also supports the applicability of linear theory to the strong motion site amplification. The study of the Coalinga earthquake by Jarpe et al. (1988), however, gave a mixed result. The amplification factors for frequencies lower than 10 Hz were the same for weak and strong motions up to 0.7 g, but those for frequencies above 10 Hz are significantly reduced for the strong motion as compared to the weak motion. Other mixed results were reported by Jarpe et al. (1989) shortly after the Loma Prieta earthquake. They computed spectral ratios of strong- and weak-motion recordings for two pairs of rock and soil sites, one near the Lawrence Livermore National Laboratory, and the other in Treasure Island (fill) and Yerba Buena Island (rock) in San Francisco near the Bay Bridge. For the first pair, the weak motion spectral ratios agree with the strong motion amplification for frequencies 3 to 12 Hz, while for the second pair, the strong-motion spectral ratio is much lower than the weak motion spectral ratio for frequencies 1 to 7 Hz.

The difficulty for seismologists to demonstrate the non-linear site effect has been due, as Esteva (1977) stated, to the effect being overshadowed by the overall patterns of shock generation and propagation. In other words, the seismological detection of the non-linear site effect requires a simultaneous understanding of effects of earthquake source, propagation path and local geological site conditions.

The Loma Prieta earthquake of 1989 presents the first case in which such a simultaneous understanding may be achieved because of numerous works currently in progress on various aspects of the strong ground motion during the earthquake. We shall describe in some detail the preliminary result obtained by Chin and Aki (1991), who found a pervasive non-linear site effect at sediment sites in the epicentral area by the simultaneous consideration of the above three effects.

Chin and Aki (1991) estimated the weak motion amplification factor at each site of the strong motion seismographs operated by the California Division of Mines and Geology (CDMG) from the coda amplification factor determined by Phillips and Aki (1986) and Su et al. (1990) using the USGS Central California Network data as mentioned earlier. The estimated site amplification factor was used to eliminate the site effect from the Fourier amplitude spectra of observed accelerograms of the Loma Prieta earthquake. The propagation path effect was examined first by calculating synthetic seismograms for point dislocation sources in an 11-layer crustal model simulating the seismic motion from the Loma Prieta earthquake toward San Francisco at various distances to confirm the approximate validity of the 1/R law of geometrical spreading to this case. Then, they proceeded to determine the attenuation factor $Q^{-1}(f)$ and the source spectrum S(f) for the frequency range from f=1 to 25 Hz. The source spectrum was interpreted in terms of the specific barrier model of Papageorgiou and Aki (1983a,b), and it was found that both source and attenuation parameters fit nicely with those obtained earlier from the data on other major California earthquakes.

Chin and Aki (1991), then synthesized time history of ground acceleration at each CDMG station by applying the method of Boore (1983) to the source, path and site parameters determined above. Examples of synthetic and observed accelerograms are shown in Figure 9. The agreement between the synthetic and observed accelerograms was good for duration and spectral content, but a strong systematic discrepancy was found for the absolute value of acceleration. For epicentral distances less than 50 km, the predicted peak acceleration considerably overestimates that observed for sediment sites and underestimates it for the Franciscan formation site as shown in Figure 10. It appears that the strong difference in the amplification factor between the Franciscan and the sediment observed for weak motion disappears at acceleration levels higher than about 0.1-0.3g. Take, for example, Capitola and Santa Cruz, the two stations closely located in the epicentral area. The amplification factor estimated by the coda method is 2 to 5 times higher at Capitola (Pleistocene sediment) than Santa Cruz (Pre-Cretaceous metasedimentary rock) in the frequency range from 1.5 to 25 Hz. On the other hand, the horizontal mean peak acceleration during the Loma Prieta earthquake is nearly the same (about 0.4g) at both sites despite the fact that Capitola is closer to the hypocenter. Interestingly, during the Morgan Hill earthquake of 1984, the peak value was 0.15g at Capitola and 0.07g at Santa Cruz; the relative amplification is intermediate between the weak motion and the Loma Prieta case.

Since the above apparently non-linear effect shows up at all stations on sediment sites within about 50 km from the epicenter (Gilroy #3, Saratoga, Corralitos, Agnew, Hollister, Capitola, Salinas and Watsonville as shown in Figures 10 and 12) it is unlikely that the effect is due to the radiation pattern, near-source structure, or topography.

The above discrepancy in the amplification factor between weak and strong motions reminds us of the similar discrepancy pointed out by Hudson (1972) for the Pasadena area between the amplification factor obtained by Gutenberg (1957) using relatively weak motion and that observed during the San Fernando earthquake of 1971. For example, the

amplification factor at the CIT campus relative to the Seismological Laboratory is greater than 1 for the frequency range from 0.1 to 10 Hz, and is peaked (about a factor of 5) at 1 Hz. On the other hand, during the San Fernando earthquake, the peak horizontal acceleration in the campus was slightly greater at the Milikan Library, but significantly smaller at the Athenaeum than at the Seismological Laboratory where the peak acceleration

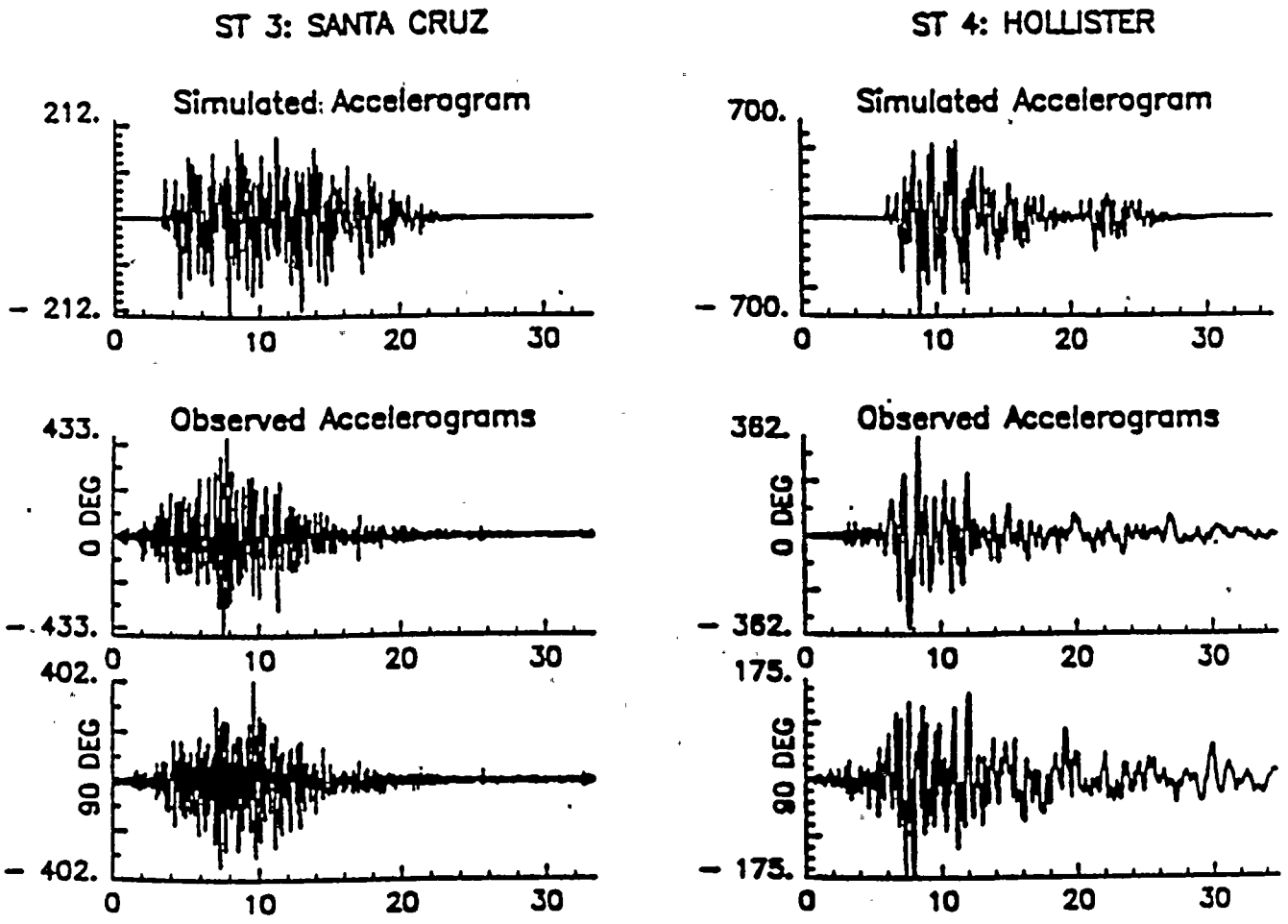


FIGURE 9. Comparison between the observed and synthetic accelerograms at Santa Cruz (left) and Hollister (right) for the Loma Prieta earthquake of 1989, reproduced from Chin and Aki (1991).

was 0.18g. In general, the strong systematic dependence of amplification factor on the site condition found by Gutenberg for the Pasadena area seems to have disappeared in Hudson's result. The site dependence, however, showed up in both the 1971 San Fernando earthquake data and the distant underground explosion data studied by Rogers et al. (1984), as mentioned earlier, although the amplification factor inferred from the strong motion appeared to be less than that inferred from the weak motion data.

Non-linearity of Site Response

The non-linear site response during the Loma Prieta earthquake detected by Chin and Aki (1991) appears to be in the range expected for typical sediment sites from geotechnical engineering studies. A large body of literature exist on the laboratory and

theoretical studies of non-linear dynamic behavior of the soil. There have also been some field studies of the non-linear effect using the actual strong motion records (e.g. Abdel-Ghaffer and Scott , 1979; Tokimatsu and Midorikawa,1981; and Kamiyama, 1989). These studies usually document the strain dependent shear modulus G and damping factor

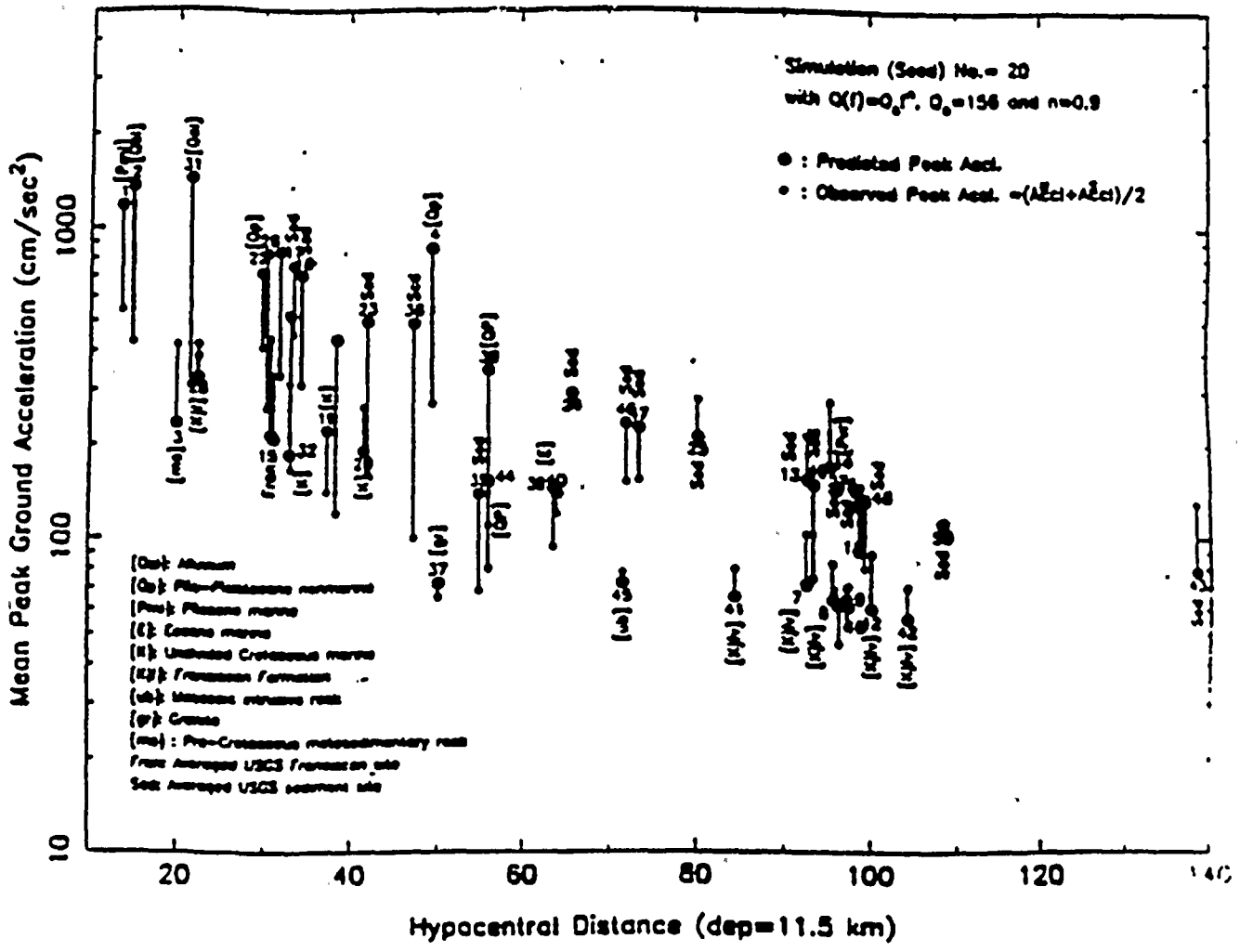


FIGURE 10. Comparison of peak acceleration (small open circle) observed during the Loma Prieta earthquake and predicted one using the weak-motion amplification factor estimated for each site, reproduced from Chin and Aki (1991). At distances less than about 50 km, the prediction over-estimates considerably the observed at sediment sites.

h(=1/(2Q)). Sugito and Kameda (1990), on the other hand, simulated ground motion on the soil surface including the non-linear effect, and calculated the amplification factor for different levels of acceleration at the bedrock, which can be directly compared with the observed result on the Loma Prieta earthquake. They defined the conversion factor $\beta_a$ as the ratio of peak acceleration at the soil surface to that at bedrock, and estimated $\beta_a$ for typical soil conditions specified by geotechnical parameters $S_n$ and $d_p$ (see also Sugito, 1986). Their result is shown in Figure 11, where the flat part of $\beta_a$ value corresponds to

the linear response region and the decrease from the flat level indicates the non-linear region. The amount of decrease depends on the soil parameters ($S_n$, $d_p$) and acceleration at the rock surface (Ar). The parameter $d_p$ gives the depth to the bedrock where the shear velocity is 600-700 m/sec, and the parameter $S_n$ is calculated from the blow-count (N-value) profile obtained from the standard penetration test by the following formula.

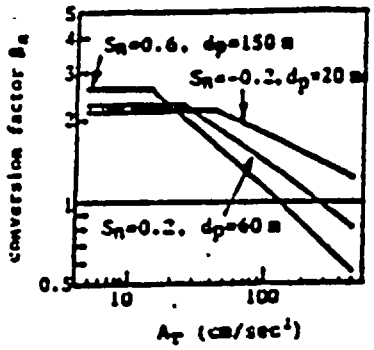


FIGURE 11. The ratio $\beta_a$ of acceleration at the surface of sedimentary layer to the bedrock surface acceleration calculated for various soil parameters as a function of bedrock acceleration $A_r$, reproduced from Sugito and Kameda (1990).

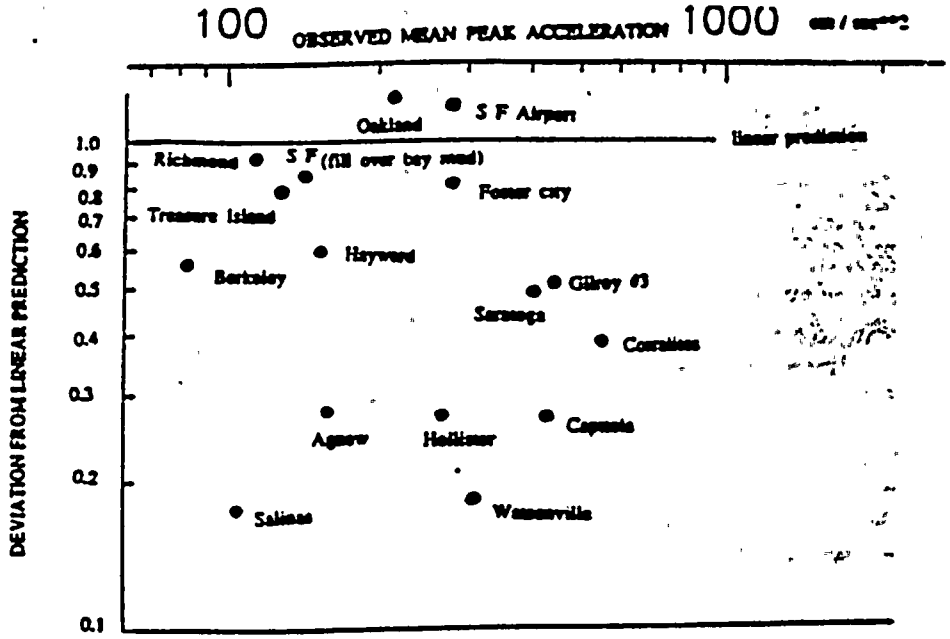


FIGURE 12. Observed deviation from the linear prediction for peak acceleration during the Loma Prieta earthquake of 1989 as a function of observed peak acceleration, reproduced from Chin and Aki (1991). This figure is directly comparable to the calculated one shown in Figure 11, except that the vertical axis is normalized to the weak-motion amplification factor at each site.

$$S_n=0.264\int_0^{d_s} \exp\{-0.04N(x)\}\exp\{-0.14x\}dx-0.885, \quad (4)$$

where N(x) is the blow count at depth x (in meters) and $d_s$ is the depth (in meters) of blow-count profile.

The corresponding observation from the Loma Prieta earthquake is shown in Figure 12, where the ratio of the observed peak acceleration to that predicted by Chin and Aki (1991) using the weak-motion amplification factor determined by Phillips and Aki (1986) and Su et al. (1990) is plotted against the observed peak acceleration. Figure 12 shows that the departure from the linear amplification effect is strong at stations within about 50km from the epicenter. All the stations located in the San Francisco Bay area show, within a factor of two, agreement with the linear prediction, consistent with the conclusion of Borcherdt (1990) with regard to the applicability of the weak-motion amplification factor to the Loma-Prieta data for the Bay area as mentioned earlier. Comparing Figures 11 with 12, we find that the geotechnical prediction by Sugito and Kameda and the observation during the Loma Prieta earthquake are comparable both in the magnitude of departure from the linear theory and in the threshold acceleration level beyond which the non-linearity effect begins. The values of parameters $S_n$ and $d_p$ used by Sugito and Kameda, however, may or may not be "typical" for the epicentral region of the Loma Prieta earthquake. Unfortunately, there are no geotechnical data available for the sites of the CDMG strong motion seismographs.

As mentioned earlier, the non-linearity of site effect during the Loma Prieta earthquake was manifested in the decrease in the difference in the amplification factor between rock and soil site with the increase in the acceleration level. Such a trend has been noticed by several researchers in the past. For example, Sadigh (1983) and Idriss (1985) found that the standard error of the empirical attenuation relations for peak acceleration decreased with increasing magnitude. Abrahamson (1988) confirmed this trend using the SMART-1 array data as shown in Figure 13. The extremely low standard error of Campbell's (1981) attenuation formula as compared to others may be another evidence for the above trend, because his data are restricted to the distance range less than 50 km, probably with higher accelerations than in others.

The apparently pervasive non-linearity in the amplification factor at sediment sites as discussed above is a serious challenge to seismologists, among whom the principle of linear elastic theory is widely accepted for strong motion prediction as exemplified in the so-called empirical Green's function method.

Clearly, the problem of local site effect on strong ground motion is much more complex than most seismologists have considered. The non-linearity certainly will not allow us to simply apply the weak-motion amplification factor to strong motion prediction. This does not mean the diminished value of the weak-motion amplification factor. On the contrary, it has become more important to measure accurately the site-specific weak motion amplification factors at all relevant frequencies at the site of a strong motion seismograph in order to characterize the in-situ non-linearity of the site effect, and relate it with the geotechnical parameters of the site.

Site-Specific Weak-Motion Amplification Factor and Intensity

Furthermore, the weak-motion amplification factor may be of some practical use even in the non-linear regime, because if the large weak-motion amplification factor is not

amplifying the strong motion linearly, it would be represented in the damage made to the site through the very non-linear effect. In fact, there have been several studies since Borcherdt (1970) that show a remarkable positive correlation between the weak-motion amplification factor and the site-dependent part of variation in the distribution of earthquake intensity which may be a more versatile seismic hazard parameter than the peak ground acceleration.

Borcherdt (1970) compared the intensities for the 1906 San Francisco earthquake with the amplification factors determined from the weak motion generated by underground explosions in the Nevada Test Site, and found without exception that an increase in intensity corresponds to an increase in amplification factor.

Borcherdt and Gibbs (1976) extended the measurement of NTS explosions to 99 sites in the San Francisco Bay region, and found that the site-dependent part of the intensity variation $\delta I$ in San Francisco for the 1906 earthquake can be related with a high correlation coefficient of 0.95 to the average horizontal spectral amplitude (AHSA) in the frequency 0.25 to 3.0 Hz as follows:

$$\delta I = 0.27 + 2.70 \log (AHSA), \qquad (5)$$

where the intensity is measured in the 1906 San Francisco scale. According to Borcherdt and Gibbs, use of the San Francisco scale reduces uncertainties in the predictions. Approximate conversions from the San Francisco scale to the Rossi-Forel and Modified Mercalli scales are summarized by Borcherdt et al. (1975). They also calculated the mean

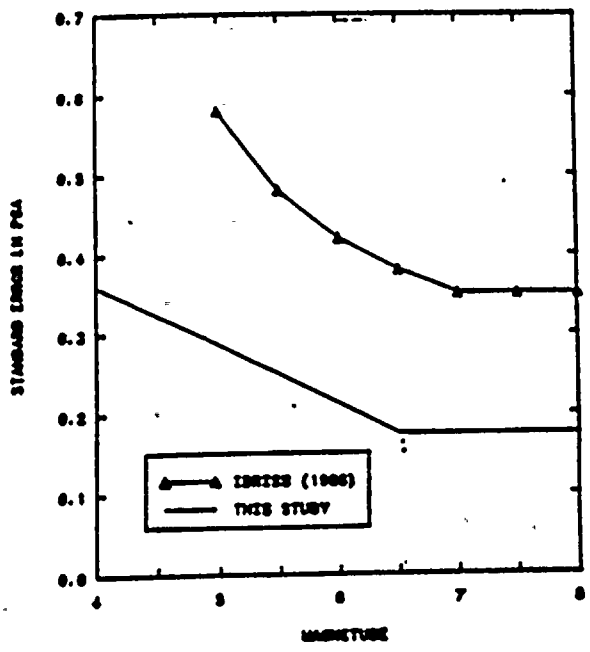


FIGURE 13. Magnitude dependence of the lognormal standard error for peak ground acceleration reproduced from Abrahamson (1988). The curve marked as "this study" is for the SMART-1 array data, and the Idriss curve is for the data from broadly distributed stations.

and standard deviation for both AHSA and δI for the various geological units as shown below.

TABLE 1.

| | AHSA | | δI | |
|---|---|---|---|---|
| Geological Unit | Mean | Standard Error | Mean | Standard Error |
| Granite | 0.63 | 0.11 | -0.29 | 0.21 |
| Franciscan Formation | 1.00 | 0.38 | 0.19 | 0.47 |
| Great Valley Sequence | 1.42 | 0.45 | 0.64 | 0.34 |
| Santa Clara Formation | 1.70 | 0.64 | 0.82 | 0.49 |
| Alluvium | 2.44 | 1.08 | 1.34 | 0.58 |
| Bay Mud | 7.08 | 3.78 | 2.43 | 0.58 |

The above range of AHSA variation according to geology is quite similar to that of the coda amplification factors at 1.5 and 3 Hz, although precise comparison is difficult because of the different sites selected for the NTS explosion recording and for the USGS permanent network stations.

More recently, King et al. (1990) recorded ground motion induced by blasts at an open-pit coal mine at many sites in Olympia (33 to 40 km from the mine) that reported Modified Mercalli (MM) intensities from the Puget Sound earthquake of 29 April 1965. They calculated the ratio of Fourier spectral amplitudes at an alluvium site to spectral

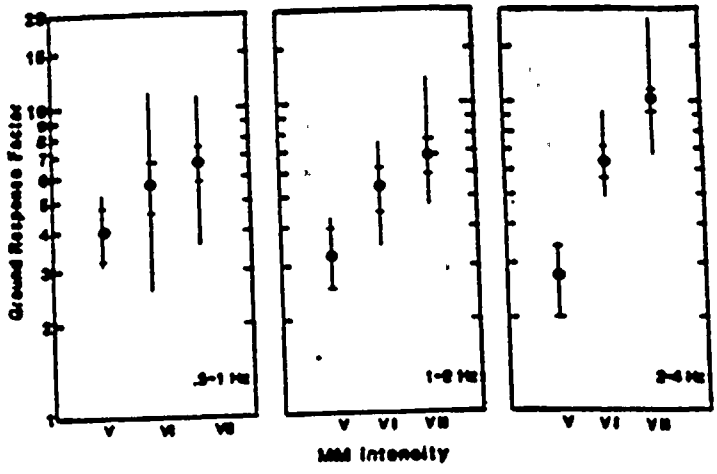


FIGURE 14. Relation between MM intensity and weak-motion amplification factor (Ground Response Factor) at three frequency bands (.5 to 1, 1 to 2, and 2 to 4 Hz) in Olympia, reproduced from King et al. (1990). The MM intensity is observed during the Puget Sound earthquake of 1965.

amplitudes on hard rock, called GRF (ground response function), in three frequency bands (0.5 to 1.0 Hz, 1.0 to 2.0 Hz, and 2.0 to 4.0 Hz). Figure 14 shows the comparison of

GRF with observed MM intensities separately for the three bands. The 2.0 to 4.0 Hz band shows the strongest correlation between GRF and intensity. The coefficient relating GRF increment with intensity increment for this band is comparable to the one relating AHSA with $\delta I$ found by Borcherdt and Gibbs (1976) for San Francisco.

The maximum range of intensity variation due to site effect is 2.7 between granite and Bay mud according to the Borcherdt-Gibbs table. Evernden et al. (1981) used the table as the basis for their intensity prediction using the surface geology. The seismic zonation based on predicted intensity has been applied to various parts of U.S., including the Los Angeles Basin (Evernden and Thomson, 1985). More recently, Toppozada et al. (1988) used a similar intensity prediction for drawing a planning scenario for a major earthquake on the Newport-Inglewood fault zone. Unlike Evernden and Thomson (1985), the latter assumed that shaking intensity does not depend on depth to water table (in Japan, the water table is considered for the amplification of vertical motion through its effect on P-wave velocity profile, but not for the horizontal) and the maximum range of intensity variation due to site effect in the Los Angeles Basin is 2.0 between rock sites and Holocene deposits as shown below.

TABLE 2.

| Geologic Unit | Symbols | $\delta I$ |
|---|---|---|
| Plutonic and Metamorphic Rocks | $T_i$, $M_z$, $g_rM_z$, $g_rP_z$, $g_rC_z$, $g_b$, $M_{zv}$, gr-m, mv, m, pEc, pE, sch, J, gr | 0 |
| Volcanic Rocks | Qv, Qrv, Tv, Pv | 0.3 |
| Pre-Cretaceous Sedimentary Rocks | Pm, C | 0.4 |
| Upper Cretaceous Paleocene, and Eocene Marine Sediments | Ep, E, Ku | 1.2 |
| Tertiary Nonmarine Sediments | $T_c$ | 1.3 |
| Oligocene and Miocene Sediments | Mc, M, $O_c$ | 1.5 |
| Plio-Pleistocene and Pleistocene Sediments | $P_{ml}$, Pu, $Q_c$, $Q_m$, Qt, QP | 1.8 |
| Holocene Deposits | Qs, Qal | 2.0 |

How reliable are these intensity predictions based on surface geology? This is a key question for seismic zonation. We have seen successful cases in the 1906 San Francisco and the 1965 Puget Sound earthquake. Chavez-Garcia et al. (1990) also concluded that the intensity variation during the 1978 Tessaroniki earthquake correlates well with the site response for weak motion. Let us now consider an unsuccessful case of the Whittier Narrows earthquake of 1987 and examine why it did not work.

Figure 15 shows a topography and street map of downtown Whittier and Puente Hills (contour in feet) reproduces from Kawase and Aki (1990). The lines separating the area of MM intensities, VI, VII and VIII are adapted from the preliminary intensity map of the Whittier Narrows earthquake prepared by Leyendecker et al. (1988). The area of intensity VIII is supported by additional data, namely, solid circles representing the heavily damaged buildings and houses identified by a team of researchers from the University of Southern California, and open circles representing the water pipeline damage shown in Schiff (1988). The hypocenter of the earthquake is located at about 10 km to NNW at a depth of about 14 km.

The surface geology in this area does not correlate with the intensity distribution. For example, the north-eastern part of the intensity VIII area is on Tertiary sediment, while the part of intensity VI area to the north of Puente Hills is covered by Holocene deposits. The table shown above would predict 0.7 lower intensity at the former site as compared to the latter, making the discrepancy with the observed by as much as 2.7 intensity unit.

The above observed intensity pattern was explained quantitatively by Kawase and Aki (1990) as due to an unfortunate coincidence of the particular location of the area relative

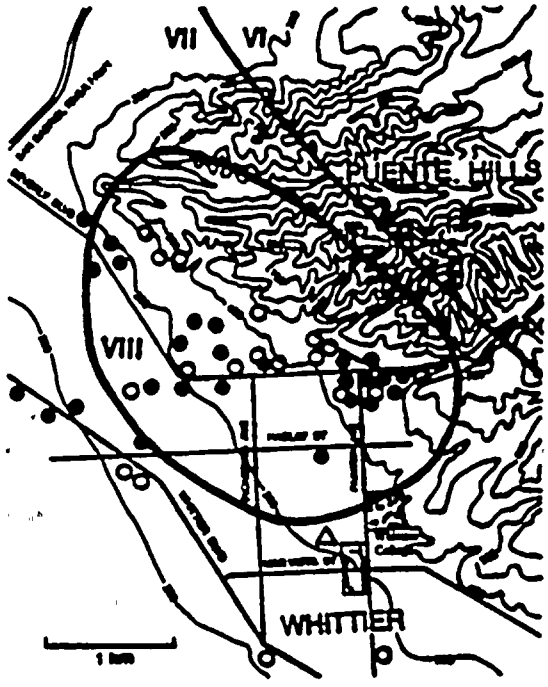


FIGURE 15. The distribution of MM intensity during the Whittier Narrows earthquake of 1987 by Leyendecker et al. (1988). The area of intensity VIII is supported by additional data, namely, solid circles representing the heavily damaged buildings identified by a team of USC researchers, and open circles representing the water pipeline damage shown in Schiff (1988). This figure is reproduced from Kawase and Aki (1990) who attribute the intensity distribution to a combined effect of the critically incident SV waves and the topography of Puente Hills.

to the earthquake hypocenter and the presence of a hill. The location of high intensity area corresponds to the place of arrival of SV waves at the critical angle from the hypocenter. (SV waves are vertically polarized S waves, and the critical angle $\theta$ of ray path from vertical is equal to $\sin\theta=\beta/\alpha$, where $\beta$ is the S wave velocity and $\alpha$ is the P wave velocity). Numerical simulations by Kawase and Aki (1990) demonstrated that critically incident SV waves will cause anomalous amplification at the slope of a hill on the other side of the hypocenter in agreement with the observed intensity pattern at Whittier.

Unusual ground fissures (tearing trees) discovered at a distance of 13 km from a M=4.2 Vonore, Tennessee earthquake of March 27, 1987 were also attributed to the same critically incident SV waves by Nava et al. (1989). Observations of dislocated boulders indicating vertical accelerations exceeding 1g by Umeda (1990) during the Loma Prieta earthquake of 1989 and the recent Philippine earthquake can also be explained by combined effects of topography and critically incident SV waves.

The above examples present challenging problems for seismologists engaged in the study of seismic zonation. There may be many other cases in which the combined effects of particular source, path and site conditions may generate anomalously strong ground shaking. The characterization of a site by the surface geology alone may miss the real cause of site amplification effect. Both Bard et al. (1988) and Kawase and Aki (1989), for example, concluded that the combined effect of deep sediment and shallow clay layer with different scales in their lateral variation was important in explaining the spatial variation in amplitude and duration of strong shaking in Mexico City during the Michoacan earthquake of 1985. Since anomalously strong and/or long shaking should be the subject of concern in strong motion seismology, a systematic exploration of such possibilities is needed. Once these effects are identified, the only practical way to include them in seismic zonation would be the probabilistic approach by assigning the probability of the occurrence of such earthquakes relative to a given site.

The above examples of the Whittier Narrows and Michoacan earthquakes demonstrates the importance of numerical simulation in order to advance the method of seismic zonation beyond the empirical prediction based on surface geology. The methods of numerical simulation for strong motion prediction have progressed considerably in the past two decades as reviewed in Sanchez-Sesma (1987) and Aki (1988). Here we shall briefly review more recent advances in this area.

## Recent Advances in Numerical Simulation

Numerical simulations have become a powerful tool for understanding the cause of local variations in strong ground motion in two particularly useful manners. One is to directly simulate the pattern of shaking during a particular target earthquake, and the other is to make parameter sensitivity studies for idealized models of irregular topography and basin structures. As concluded in a review by Aki (1988), adequate state-of-the-art methodologies are available for numerical simulation of local site effect as far as 2-D structures are concerned.

Current research in this area is, therefore, mainly aimed at the development of methodologies for studying 3-D structures. In the following, we shall make a brief survey of various approaches being taken toward this goal.

Since the 1970's, a variety of numerical methods have been developed to compute seismic response in irregularly layered structures. Following the classification by

Shinozaki (1988) with an addition by Horike et al. (1990), they are divided into seven groups: the wave function expansion method (Trifunac, 1971; Sanchez-Sesma, 1985; Lee, 1988), the finite element method (Lysmer and Drake, 1971; Zama, 1981), the finite difference method (Boore, 1972; Virieux, 1984), the discrete wavenumber method (Aki and Larner, 1970; Bouchon and Aki, 1977; Bard and Bouchon, 1980a,b, 1985), the boundary integral method (Wong and Jennings, 1975; Sanchez-Sesma and Esquival, 1979; Dravinski, 1983), discrete wavenumber boundary element method (Bouchon, 1985; Kawase, 1988), and ray and beam methods (Hong and Helmberger, 1978; Lee and Langston, 1983; Nowack and Aki, 1984). The above methods have their advantages and disadvantages, and, in general, those which can deal with more realistic models are less accurate, while those achieving higher accuracies are more time-consuming. Most of these methods are still actively being developed, because each has its own merit that effectively applies to a certain class of problems.

Let us start with studies attempting the simulation of observed shaking during actual earthquakes. The finite difference method for 2-D SH cases was used by Yamanaka et al. (1989) to simulate the ground motion in the period range from 3 to 10 sec observed in southwestern Kanto during the western Nagano earthquake of 1984. The simulation showed a good fit to observation in spite of the 2-D modeling. A similar 2-D finite difference method was used by Vidal and Helmberger (1988) to simulate both the P-SV and SH motions in the period range 2 to 10 sec observed in the Los Angeles basin during the San Fernando earthquake of 1971. They used the method of Helmberger and Vidal (1988) to define the appropriate line source for the 2-D simulation to mimic the radiation from a point shear-dislocation source, calculated ground motions for the basin structure inferred by Duke et al. (1971), and obtained results in an excellent agreement with observed ground motions as shown in Figure 16. A similar combination of 2-D structure and 3-D source has also been considered by Khair et al. (1989) using the hybrid method of boundary integral and finite element method.

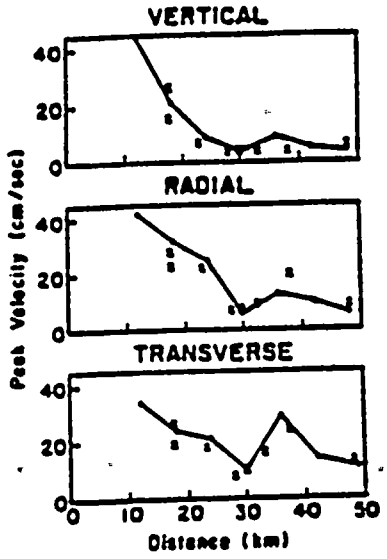


FIGURE 16. Peak velocity attenuation with distance for the San Fernando earthquake of 1971, reproduced from Vidale and Helmberger (1988). The crosses show the observed peak velocity, while the line shows the attenuation calculated by the finite difference method.

The 2-D Aki-Larner method was extended to the case of multiple interfaces and applied to simulate the seismic motion (around 1 Hz) observed in the Kyoto basin during the western Nagano earthquake of 1984 by Horike (1988). The predicted motion is not large enough to explain the observed, and the discrepancy led Horike et al. (1990) to extend the Aki-Larner method to the 3-D case. Their parameter sensitivity studies based on two-types of sedimentary basin (cosine-shape and trapezoidal interface) showed that the maximum amplification for the 3-D case is greater than that for the corresponding 2-D case by up to two.

The Aki-Larner method was extended to the 3-D case also by Ohori et al. (1990), who tested the validity of their method successfully against the result obtained by Jiang and Kuribayashi (1988) using the boundary element method applicable to an axisymmetric case. Ohori et al. (1990), then, made an extensive parameter sensitivity studies for a circular and elliptic sedimentary basin, and found that both the amplification factor and the frequency become higher as the dimension of the problem increases from 1-D to 3-D, as shown in Figure 17 for the case of an elliptic basin.

A similar comparison of 2-D and 3-D basin structures was made by Mossessian and Dravinski (1990) who used the boundary integral equation method, tested their method against the result of Sanchez-Sesma (1983) and found various discrepancies between the 3-D and approximate 2-D case of basin structure.

A 3-D ray method was applied by Ihnen and Hadley (1986) to simulate the ground motion in the Puget Sound region during the 1965 Seattle earthquake. They considered a six layer structure consisting of water, glacial alluvium, upper crust, lower crust, subducting Juan de Fuca plate and upper mantle, and included multiple reflections within the alluvium as long as they contributed significantly to the synthetic seismogram. The predicted peak ground acceleration was found to be consistent with the damage reports in the Seattle area.

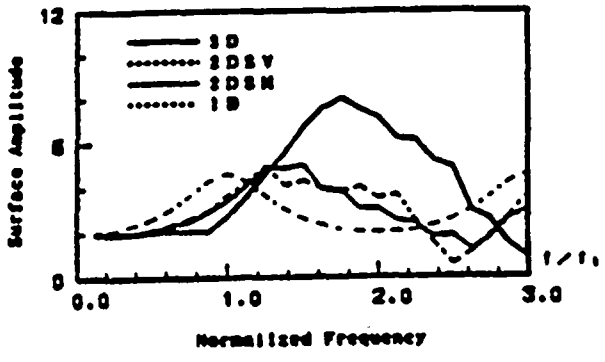


FIGURE 17. The amplification factor at a center of an elliptic basin for vertically incident S waves calculated by Ohori et al. (1990). The response calculated for the 3-D model is compared with the results obtained under 1-D and 2-D assumptions. The 1-D and 2-D assumptions tend to underestimate the true amplification factor.

In addition to these efforts toward the simulation for 3-D structures, the effect of inhomogeneity in the basin, such as the vertical velocity gradient was studied effectively by a combination of the boundary integral method and the Gaussian beam method (Benites and Aki, 1989; Benites, 1990). The above combination takes advantage of the strengths of the two methods, avoiding their weaknesses. The Gaussian beam method helps to reduce the number of unknowns needed by the boundary integral method, and the boundary integral method eliminates the need for calculating complex reflection and transmission coefficients for the beam by matching the boundary condition globally.

## B. DEVELOPING REGIONAL DATA BASE FOR GROUND MOTION ESTIMATION

Many important and urgent problems in strong ground motion estimation require the simultaneous acquisition of various geologic, seismic and geotechnical data at common sites. For example, the in-situ determination of non-linear site effect requires both weak motion and strong motion amplification factor at the same site. The dependence of ground motion response on geological and geotechnical conditions of site can be accurately evaluated only when these data are obtained at the same sites. The data base for the macroseismic information such as intensity and building damage factor are also desirable at the same sites where geologic, seismic and geotechnical measurements are made.

The site-specific weak-motion amplification factor can be most effectively determined by the coda method using local small earthquakes as demonstrated by Phillips and Aki (1986) and Su et al. (1990). In areas where local small earthquakes are not available, artificial sources at some distances can be used (Borcherdt, 1970; Rogers et al., 1985; King et al., 1990), although the available frequency band may be limited to frequencies lower than a few Hz. On the other hand, the amplification factor for relatively long-period (3 to 6 sec) may be most effectively estimated by the use of ambient microseisms from distant sources (Kagami et al., 1982, 1986). In addition to the strong motion records of past major earthquakes in the region, the data base should also include detailed survey of intensity (Ohta et al., 1979), and some quantitative building damage factor (e.g., Iglesias, 1989).

Conventional geologic maps are usually not adequate for the purpose of ground motion estimation, because they only crudely differentiate young unconsolidated deposits. For example, the differentiation of Quaternary sediments as shown in Table 3 was used by Tinsley and Fumal (1985) for the microzonation of Los Angeles basin, based on the work of Lajoie and Helley (1975) for the San Francisco Bay region. The map based on the above classification may be, for example, used for identifying the areas of liquefaction possibility by overlaying it with the map of water table elevation.

Well known formulas for calculating the shear wave velocity and density has been developed in Japan by Ohta and Goto (1978) based on geologic and geotechnical data. Geologic data used as an input to these formulas are the age of the sediment classified into Holocene (called Alluvium in Japan), Pleistocene (called Diluvium in Japan) and Tertiary and the texture of soil classified into clay, silt, sand or gravel.

The shear wave velocity is broadly recognized as the single most important parameter affecting the site amplification, and Fumal and Tinsley (1985) have developed a relation between shear wave velocity and geologic unit for the Los Angeles region as shown in the following table, following the work of Borcherdt et al. (1978) and Fumal (1978) for the San Francisco area based on mapping of Lajoie and Helley (1975).

TABLE 3.

| | | Shear Wave Velocity | |
|---|---|---|---|
| | Grain Size | Mean (in m/s) | Standard Error |
| Holocene | Fine | 200 | 20 |
| | Medium | 230 | 30 |
| | Coarse | 320 | 25 |
| | Very Coarse | 365 | 20 |
| Pleistocene | Fine | 305 | 50 |
| | Medium | 430 | 115 |
| | Coarse | 495 | 85 |
| | Very Coarse | 650 | 155 |

It is striking to compare the above table used as the basis for microzonation for Los Angeles with the one for Tokyo. The following table shows the classification of surface geology used for seismic zoning of Tokyo with the mesh size of 1 km x 1 km (Shima, 1978).

TABLE 4.

| Geology Units | Shear Wave Velocity (m/s) | Amplification Factor Relative to Loam |
|---|---|---|
| Peat | 80 | 1.9 |
| Humus | 90 | 1.7 |
| Clay | 100 | 1.5 |
| Loam | 150 | 1.0 |
| Sand | 170 | 0.9 |

Comparison of Table 3 and 4 shows that the best site in Tokyo is comparable to the worst site in Los Angeles as far as the shear wave velocity is concerned. In the San Francisco Bay area, however, we find areas comparable to Tokyo, namely, the bay mud with the shear wave velocity ranging from 55 to 115 m/s, and the man-placed fills from 159 to 222 m/s (Fumal, 1978). The worst known urban area is, of course, in the Mexico City where the shear wave velocity of the lake sediment is as low as 30 m/s (Figueroa, 1964).

With regard to the geotechnical data, Rogers et al. (1985) found, for both Los Angeles and San Francisco, that the most significant factor controlling site amplification is mean void ratio which strongly correlates (inversely) with shear wave velocity. The void ratio is related to the ratio of measured dry density to the solid without void. Rogers et al. studied several other geotechnical parameters, and found that in addition to the void ratio and shear wave velocity, the thickness of unconsolidated sediment and the depth to bedrock are also significant parameters controlling the amplification for periods 0.2-0.5 s. At periods longer than 0.5 s, depth to bedrock and the thickness of Quaternary sediments were found to be controlling factors. They found that the depth to water table is not a reliable predictor of site amplification.

Goto et al. (1982) showed that a geotechnical parameter calculated from blow-count (N-value) profiles from standard penetration test has a significant relation with the site amplification factor. The N-value has been used also in the Ohta-Goto (1978) formula as

well as in the prediction of non-linear site effect by Sugito and Kameda (1990) as mentioned earlier.

A typical geotechnical data set used for the prediction of site amplification effect (e.g. in the blind prediction experiment at Parkfield, California and at Ashigara, Japan) consists of borehole measurements on P-wave velocity, shear-wave velocity, density, and N-value. On the other hand, the damping or attenuation parameter such as h or Q (= 1/2h), is often inferred from the measured wave velocity.

A reliable measurement of seismic attenuation parameter Q (or h = 1/2Q) requires a vertical array of seismographs in a borehole. Several such studies, both in Japan and U.S. revealed that Q in general increases with frequency, approximately according to the power law $Q=Q_0 f^{\alpha}$, where $\alpha$ is between 0 and 1. For example, Sakai et al. (1989) determined Q from the borehole array records of local earthquakes with magnitude around 6. They found that at the Nakano site mainly consisting of find sand and clay, $Q = 7(0.8f)^{0.35}$, and at the Miyagino site mainly consisting of clay and gravel with clay, $Q = 4(0.4f)^{0.8}$, for the frequency range $0<f<10$ Hz. A similar study by Kobayashi et al (1989) using borehole arrays at Minamisuna and Narashino indicated that Q is proportional to frequency and can be expressed as $Q = \frac{V_s}{20} f$ for a silt-clay site, and $Q = \frac{V_s}{60} f$ for a sand-gravel site, where $V_s$ is shear-wave velocity in m/s. A similar result was obtained from deep borehole data in the Kanto area by Kinoshita (1983, 1986), who found Q = 4f and 5f for the Holocene sediment at Iwatsuki and Urayasu, respectively. He also found that Q = 50f in the range of $0.5<f<3.2$ Hz for the whole sedimentary layer of Quaternary and Tertiary.

Seale and Archuleta (1989), on the other hand, found from the records of local earthquakes (including M=5.8 and 6.4) at a 166 m borehole station in the Mammoth Lakes area that Q=10 independent of frequency up to 10 Hz for the surface layer composed of glacial till. Likewise, Joyner et al. (1976) using the records at a 186 m downhole array on the shore of the San Francisco Bay that Q = 16 for Bay mud, independent of frequency. The so called $\kappa$-effect found by Anderson and Hough (1984) also implies a frequency independent low Q layer near the surface. The frequency independent Q of 9-10 for filled land in Tokyo is reported by Shima et al. (1985). For higher frequencies, $30<f<90$ Hz, Kudo and Shima (1970) found the following frequency independent Q's at various soil sites Q = 8 (Pleistocene sand), Q = 20 (Holocene silt), Q = 6.5 (Tertiary mudstone), and Q = 5 (loam).

Finally, we repeat that it is crucially important to have all these geologic, seismic and geotechnical data at common sites as much as possible, in order to solve problems urgently requiring solutions as described earlier.

## C. PREDICTIVE GROUND MOTION MAPPING FOR SEISMIC ZONATION

So far in the present paper, we have described the state-of-the-art methods for characterizing the source, propagation path and local site effects on strong ground motion and the regional data base to be developed for ground motion estimation using these methods. Let us now describe how these ground motion estimates can be and should be synthesized into useful maps for seismic zonation.

Let us start with existing zoning maps for bedrock motion. The development of national maps for seismic zoning in the contiguous United States has been reviewed by

Algermissen (1983). There are two such national maps currently in use; one included in the Uniform Building Code (UBC, 1979), and the other in the Applied Technology Council report (ATC, 1978). The UBC map developed by Algermissen (1969) with later modifications, divide the contiguous United States into five zones numbered 0 through 4, based largely on the maximum Modified Mercalli intensity observed historically in each zone.

The ATC report, aiming the development of nationally applicable seismic design provisions, included maps of "effective peak acceleration" and "effective peak velocity", which can be used to calculate lateral force coefficients. These maps are based on the work of Algermissen and Perkins (1976) who estimated the expected maximum acceleration in rock in a 50-year period with a 10% chance of being exceeded throughout the contiguous United States. Algermissen et al. (1982) published similar maps for both ground acceleration and velocity for exposure times of 10, 50 and 250 years. Their method of estimating the exceedance probability is based on the assumption about source zone that the earthquake occurrence follows the Poission process in time and obeys the Gutenberg-Richter magnitude-frequency law, as well as an appropriate empirical attenuation relations. This type of seismic hazard analysis method is classified as Type III single model PSHA (probabilistic seismic hazard analysis) method in a report by the National Research Council (1988).

More sophisticated PSHA including the information on the characteristics of Quaternary faults, such as their location, segment length and slip rates has been described in the above NRC report as well as in the companion state-of-the-art paper by Coppersmith. Preliminary attempts for mapping peak ground acceleration and velocity based on such geologic data were made by Wesnousky (1986) for California.

Seismic zoning maps have a longer history in Japan than in U.S., starting with Kawasumi (1951). There are numerous maps published on the peak ground acceleration and velocity in Japan for various exposure times ranging from 50 to 200 years, but unfortunately almost all papers on the subject are written in Japanese. Most maps are based on the historic data going back up to the period of 1300 years interpreted by various statistical models of earthquake occurrence, but some attempts to include the data on active faults have also been carried out (Wesnousky et al., 1984).

In addition to the zonation map for bedrock motion as described above, in both U.S. and Japan, microzonation maps for selected areas have been developed in order to include the effect of local geology. Most existing maps are based on the relations among the site amplification factor, shear wave velocity, density, geologic age, texture of sediment, and other measurable geologic and geotechnical parameters discussed earlier. Maps in Japan are often divided into meshes of sizes 500 m x 500 m or 1 km x 1 km (e.g. Shima, 1978). Maps in the U.S. are often divided by continuous lines separating zones of different classifications of site effect (e.g. Fumal and Tinsley, 1985).

Earlier we presented a systematic dependence of weak-motion site amplification factor on the geologic age (Figure 8) and showed that the correlation is very significant on the average, but the standard error is large with regard to the individual measurement. The standard error for the individual measurement is about 0.5 in natural log, corresponding to a factor of about 1.6, nearly independent of frequency.

This large variability may be attributed to the detailed topography and subsurface structure of individual site in the 1-D, 2-D and 3-D configuration. For example, we

described earlier about a significant discrepancy between the observed intensity distribution of the Whittier Narrows earthquake and the one predicted on the basis of local geology, and explained the discrepancy in terms of the unfortunate coincidence of the particular location of the high intensity area relative to the hypocenter (critical SV incidence) and the presence of hill in the neighborhood.

This example points the way to go beyond the current practice for microzonation described above. Suppose that the damage in Whittier was due to the topography of Puente Hills and the hypocenter location in the direction of critical angle (about 30° from vertical) from Whittier. For a future earthquake like the Whittier Narrows earthquake, we should be able to predict a similar damage at a site with the similar topography located at the critical angle from the hypocenter. Since many such earthquakes are possible, it would be cumbersome to consider each possible case separately. On the other hand, we may assign the probability of occurrence to such individual earthquakes. Then, it would be straightforward to calculate the exceedance probability of ground motion for all possible earthquakes of this type at a given site, and then synthesize the result into a hazard map. The approach of PSHA is ideal for such cases.

There is, however, a difficulty with PSHA when we need to consider multiple ground motion parameters simultaneously. The currently available hazard map is restricted to a single ground motion parameter, such as the peak ground acceleration or velocity. Many users of the seismic hazard maps need more information, such as the duration of strong motion and response spectrum at various frequencies. One can construct a hazard map for each of these additional parameters in the same way as for the peak ground acceleration, but the problem is that the set of parameters thus obtained at a site for a given exceedance probability do not correspond to the set expected for a particular earthquake, and may not be useful for a certain design purpose. To remedy this, one needs numerous hazard maps for all combinations of different parameters, and the procedure becomes cumbersome.

One possible solution of the problem is to discard the traditional approach of constructing the omni-purpose zonation map. As we all know, different users of earthquake hazard information have different needs. We believe that the state-of-the-art of earthquake hazard science can now, or will in near future, meet these needs. But, the effective format of information transfer may not be by the omni-purpose zonation map.

We envision the seismic hazard analysis of the 21st century to be as a joint work participated by earth scientists and users through a computer. Earth scientists will identify potential earthquakes and assign probabilities to their occurrence. Their next job is to calculate a complete seismogram of ground motion at a given recording site due to each potential earthquake source. Depending on the frequency range of interest, the most effective synthesis technique among those described earlier will be selected for the calculation of time series. The user then decides what parameters of ground motion they want, and obtain the parameters from the calculated seismogram. The same calculation is repeated for all pairs of earthquake source and receiver site requested by the user. Finally, the exceedance probabilities will be evaluated for each combination of wanted parameters.

Maps delineating potentially vulnerable zones, such as intensity maps, maps for landslide and liquefaction potentials, etc. will always be useful for planning purposes. These maps permit definition of zones in which special studies for specific hazards should be undertaken for desired type of development.

## D. PREDICTIVE EARTHQUAKE INTENSITY MAPPING FOR SEISMIC ZONATION

The broader usefulness of earthquake intensity than peak ground acceleration or velocity has been recognized by some researchers and used as a basis for developing scenarios of earthquake damage for emergency-response planning. For example, Davis et al. (1982 a,b) describe anticipated damage of highways, airports, railroads, marine facilities, communication, water supply and waste disposal, electric power, natural gas, and petroleum fuels for a magnitude 8.3 earthquake on the San Andreas fault in the San Francisco Bay area and southern California. They used the intensity map constructed by Evernden's method mentioned earlier. A similar study on a magnitude 7 earthquake on the Newport Inglewood fault was done by Toppozada et al. (1988), who modified Evernden's method by excluding the effect of shallow water table as mentioned earlier. Similar studies have been done also in Japan for a potential magnitude 8 earthquake in the Tokai region and others. Japanese approaches include those based entirely on empirical intensity data due to Ohta et al. (1979).

There have not been enough cases for comparing predicted and observed intensities to enable a general evaluation of the accuracy of these predicted intensity maps. Earlier, we pointed out an example of discrepancy between the predicted and observed relative intensities by almost three units in the case of the Whittier Narrows earthquake, and attributed it to a combination of a particular source-receiver direction and a topography effect. A similar comparison can be made for the Loma Prieta earthquake between the observed preliminary intensity map shown in Figure 18 (Plafker and Galloway, 1989) and

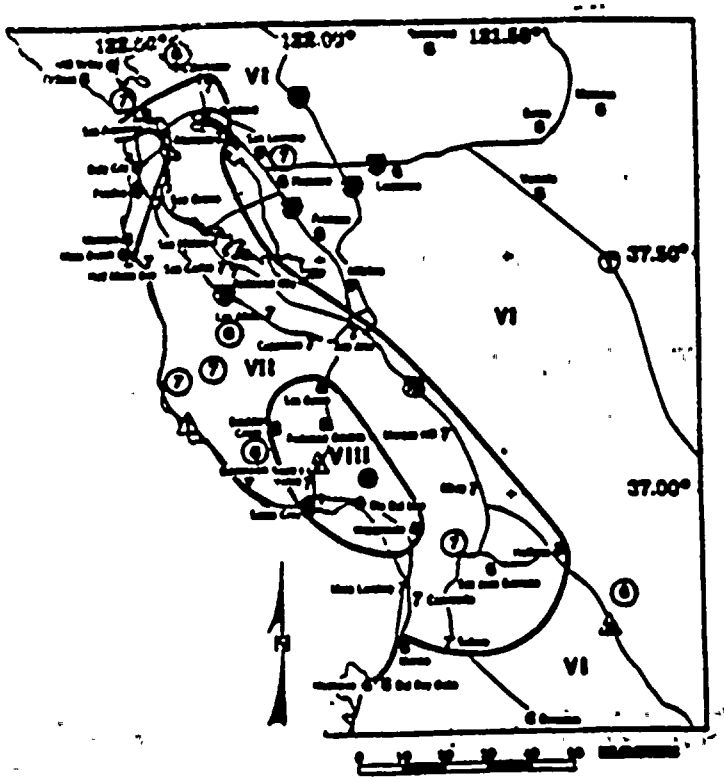


FIGURE 18. Preliminary intensity distribution for the Loma Prieta earthquake of 1989, reproduced from Plafker and Galloway (1989).

the site dependent intensity variation δI listed in Tables 1 and 2. The observed and predicted intensities seem to agree in the northern part of the mapped area, but not in the southern part, where the observed intensity does not seem to distinguish rock site and soil site. This is similar to what Chin and Aki (1991) observed for peak ground acceleration. They found that the site effect on peak acceleration was conspicuous outside the epicentral area but disappeared within 50 km from the epicenter. They attributed this to the non-linear amplification at sediment sites as discussed earlier.

In addition to the non-linear site effect, the source effect such as the directivity of rupture propagation and the propagation path effect such as the focused reflection from the crustal discontinuities contribute to further complexity of our problem. The intensity, however, can probably be estimated from the predicted acceleration time history. Thus, the predicted map of intensity in the future will be produced as a subset of the predicted maps of ground motion described in the preceding section.

## E. FUTURE RESEARCH NEEDS TO IMPROVE SEISMIC ZONATION FOR MITIGATING EARTHQUAKE SHAKING HAZARDS

The most urgent need to improve seismic zonation is the clear understanding of the non-linear amplification effect at soil sites which may be more pervasive than most seismologists thought earlier, as supported by three new pieces of seismological evidence described in the present report. The first is the systematic difference in frequency dependent site effect between the weak motion and the strong motion. On the average, weak motion amplification factor is greater at soil sites than rock sites at all frequencies at least up to 12 Hz. On the other hand, the strong motion amplification factor is greater at soil sites than rock sites only for frequencies lower than 5 Hz, and the relation is reversed for higher frequencies on the average. This frequency dependence is reflected in the generally observed independence of strong motion peak ground acceleration on the broad classification of site condition.

The second evidence for non-linearity is the systematic decrease in variability of peak ground acceleration with the increasing earthquake magnitude, and the third is the recent results from the Loma Prieta earthquake showing that the peak ground acceleration is site-independent in the epicentral region, and become site-dependent at epicentral distances beyond about 50 km. All these observations seem to support a pervasive non-linear amplification effect at soil sites, which have been predicted by geotechnical studies but has escaped the detection in the past seismological studies.

In order to establish the above evidence more firmly with a clear understanding of physical mechanism, it is essential to make simultaneous measurements on (1) site-specific strong motion amplification factor, (2) site-specific weak motion amplification factor, and (3) geologic, geotechnical and seismological characterization of the site condition at many common sites. Both strong and weak motion amplification factors need to be measured at all relevant frequencies. One of the reasons for the past inconclusiveness with regard to the non-linear effect was because each of these different measurements were done independently at different sites, and it was difficult to develop exact relationships among them.

Projects for such simultaneous measurements have been underway by a cooperative effort of international researchers at few test areas, such as Turkey Flat in the vicinity of Parkfield, California (Cramer and Real, 1990), and Ashigara, Japan. We need many more sites of simultaneous measurements, in order to establish in-situ phenomenology of the

non-linear effect, and to understand its physics in terms of soil properties. This research will require much closer cooperative work than that currently existing among geologists, seismologists and geotechnical engineers. Most seismologists will be reluctant to accept the importance of non-linearity in the local site effect because it would mean the inadequacy of standard seismological approach based on linear elasticity for strong motion prediction, at least, at soil sites. On the other hand, it will open up a new challenge for seismologists of studying non-linear site effects in 2-D and 3-D irregular structures, leading them to a fascinating research subject in non-linear physics.

Another important area of urgent needs for research is the improvement in the relation with the community of users of the earth science information. The user community is diverse, and the ground motion parameters required are also diverse. It is impractical to prepare common omni-purpose zoning maps meeting all of their needs. We envision the following procedure as the future seismic zoning.

Since any ground motion parameter can be extracted from the acceleration time series, we shall compute the time series for a given source-receiver pair using the state-of-the-art method on the basis of our current knowledge on the earthquake source, propagation path and recording site condition. We then extract the ground motion parameter requested by a customer, and attach the probability of the occurrence of the particular earthquake to the parameter. We repeat the same procedure for all relevant source-receiver pairs, and synthesize the results into a site-specific, or a map view of the parameter for a given probability of exceedance in the usual manner of probabilistic seismic hazard analysis. Such a custom made zoning map will be possible in the future with the improved capability of computer.

A quick evaluation of ground shaking in the form of intensity map immediately following a damaging earthquake to help the officials in charge of emergency-response may also be a possibility in the future. This area of research needs more extensive cooperative work than that currently existing among policy makers, engineers, physical and social scientists.

## ACKNOWLEDGEMENT

The authors are grateful to R. Borcherdt and W. B. Joyner for their comments on the first draft of the present paper. We thank also Drs. M. Ordaz and S. K. Singh for their permission to use their figure before publication. During the 1-year period of preparing this paper the first author (K.A.) was supported by the National Science Foundation under grant BCS-8819988, involved in the Kajima-CUREe project, visited the Disaster Prevention Research Institute of Kyoto University as a fellow of the Japan Society for Promotion of Science, and started to participate in the activities of the Southern California Earthquake Center, a newly established center of the Science-Technology center program of the National Science Foundation, jointly funded by the U.S. Geological Survey. All of the above activities contributed to the collection of material and generation and exchange of ideas for the writing of the present review paper, and the support of above institutions and agencies are gratefully acknowledged.

## REFERENCES

Abdel-Ghaffer, A. M. and R. F. Scott, Shear moduli and sampling factors of earth dam., Jour. GED. ASCE.105, 1405-1426, 1979.Abrahamson, N. A., Statistical properties of peak ground accelerations recorded by the SMART-1 array, Bull. Seis. Soc. Am., 78, 26-41, 1979.

Abrahamson, N. A., Statistical properties of peak ground acceleration recorded by the SMART 1 array, Bull. Seism. Soc. Am., 78, 26-41, 1988.

Aki, K., Scaling law of seismic spectrum, J. Geophys. Res., 72, 1217-1231, 1967.

Aki, K., and K. L. Larner, Surface motion of a layered medium having an irregular interface due to incident plane SH waves, J. Geophys. Res., 75, 933-954, 1970.

Aki, K., Attenuation and scattering of short-period seismic waves in the lithosphere, Proceedings of the Nato Advanced Institute, Aug. 1980, Oslo, Norway, 1981.

Aki, K., Scattering and attenuation of shear waves in the lithosphere, J. Geophys. Res., 85, 6946-6504, 1980.

Aki, K., and P. G. Richards, Quantitative Seismology: Theory and Methods, W. H. Freeman and Co., New York, 1980.

Aki, K., Attenuation and site effects at high frequency in the Strong Ground Motion Simulation and Earthquake Engineering Applications, EERI, 85-02, 23-1, 1985.

Aki, K., Local site effect on ground motion, in *Earthquake Engineering and Soil Dynamics*. II: Recent Advances in Ground-Motion Evaluation, J. Lawrence Von Thun (Editor), Am. Soc. Civil Eng./ Geotechnical Special Publication, 20, 103-155, 1988.

Aki, K. and A. S. Papageorgiou, Separation of source and site effects in acceleration power spectral of major California earthquakes, Proceedings of 9WCEE, 8, 163-167, 1989.

Algermissen, S. T., Seismic risk studies in the United States, Proc. 4th World Conf. on Earthquake Engineering, Santiago, Chile, vol. 1, 14-27, 1969.

Algermissen, S. T., and D. M. Perkins, A probabilistic estimate of maximum acceleration in rock in the continuous United States, U.S. Geological Survey Open-File Report 76-416, 1976.

Algermissen, S. T., D. M. Perkins, P. C. Thenhaus, S. L. Hanson, and B. L. Bender, Probabilistic estimates of maximum acceleration and velocity in rock in the contiguous United States, U.S. Geological Survey Open-File Report 82-1033, 1982.

Algermissen, S. T., An introduction to the seismicity of the United States, Earthquake Engineering Research Inst., 148p, 1983.

Anderson, J. G., and S. E. Hough, A model for the shape of the Fourier amplitude spectrum of acceleration at high frequencies, Bull. Seis. Soc. Am., 74, 1969-1994, 1984.

Anderson, J. G., P. Bodin, J. N. Brune, J. Prince, S. K. Singh, R. Quass, and M. Onate, Strong ground motion from the Michoacan, Mexico, earthquake, Science, 233, 1043-1049, 1986.

Applied Technology Council, Tentative provisions for the development of seismic regulations for buildings, ATC3-06, NBS Spec. Pub. 510, NSF Pub. 78-8, 1978.

Archuleta, R. J., A faulting model for the 1979 Imperial Valley earthquake, J. Geophys. Res., 89, 4459-4585, 1984.

Atkinson, G. M., and D. M. Boore, Recent trends in ground motion and spectral response relations for North America, Earthquake Spectra, 6, 15-36, 1990.

Bard, P. Y., and M. Bouchon, The seismic response of sediment-filled valleys, Part I. The case of incident SH waves, Bull. Seis. Soc. Am., 70, 1263-1286, 1980a.

Bard, P. Y., and M. Bouchon, The seismic response of sediment-filled valleys, Part II. The case of incident SH waves, Bull. Seis. Soc. Am., 70, 1921-1941, 1980b.

Bard, P. Y., and M. Bouchon, The two-dimensional resonance of sediment-filled valleys, Bull. Seis. Soc. Am., 75, 519-541, 1985.

Bard, P. Y., M. Campillo, F. J. Chavez-Garcia and F. Sanchez-Sesma, The Mexico earthquake of September 19, 1985 - A theoretical investigation of large- and small-scale amplification effects in the Mexico City Valley, Earthquake Spectra, 4, 609-633, 1988.

Benites, R., and K. Aki, Boundary integral-Gaussian beam method for seismic wave scattering: SH in two-dimensional media, J. Acoust. Soc. Am., 86, 375-386, 1989.

Benites, R., Seismological applications of boundary integral and Gaussian beam methods, Ph.D. thesis, Massachusetts Institute of Technology, 1990.

Beroza, G. C., and P. Spudich, Linearized inversion for fault rupture behavior: application to the 1984, Morgan Hill, California earthquake, J. Geophys. Res., 93, 6275-6196, 1988.

Boatwright, J. and D. M. Boore, Analysis of the ground accelerations radiated by the 1980 Livermore Valley earthquakes for directivity and dynamic source characteristics, Bull. Seism. Soc. Am., 72, 1843-1865, 1982.

Boatwright, J., The seismic radiation from composite models of faulting, Bull. Seism. Soc. Am., 78, 489-508, 1988.

Boore, D. M., A note on the effect of simple topography on seismic SH waves, Bull. Seis. Soc. Am., 62, 275-284, 1972.

Boore, D. M. and W. B. Joyner, The influence of rupture incoherences on seismic directivity, Bull. Seis. Soc. Am., 68, 283-300, 1978.

Boore, D. M., W. B. Joyner, A. A. Oliver, III, and R. A. Page, Peak acceleration, velocity, and displacement from strong motion records, Bull. Seis. Soc. Am., 70, 305-321, 1980.

Boore, D. M., Stochastic simulation of high-frequency ground motions based on seismological models of the radiated spectra, Bull. Seism. Soc. Am., 73, 1865-1894, 1983.

Boore, D. M., Short-period P- and S-waves radiation from large earthquakes: implications for spectral scaling relations, Bull. Seism. Soc. Am., 76, 43-64, 1986.

Boore, D. M., and G. M. Atkinson, Stochastic prediction of ground motion and spectral response parameters at hard-rock sites in eastern North America, Bull. Seis. Soc. Am., 77, 440-467, 1987.

Boore, D. M., L. Seekins, and W. B. Joyner, Peak acceleration from the 17 October 1989 Loma Prieta earthquake, Seism. Res. Letters, 60, 151-166, 1989.

Boore, D. M., and G. M. Atkinson, Spectral scaling of the 1985 to 1988 Nahanni, Northwest Territories, earthquakes, Bull. Seism. Soc. Am., 79, 1736-1761, 1989.

Boore, D. M., and W. B. Joyner, The effect of directivity on the stress parameter determined from ground motion observations, Bull. Seis. Soc. Am., 79, 1984-1988, 1989.

Borcherdt, R. D., Effects of local geology on ground motion near San Francisco Bay, Bull. Seis. Soc. Am., 60, 29-61, 1970.

Borcherdt, R. D., J. F. Gibbs, and K. R. Lajoie, Prediction of maximum earthquake intensities in the San Francisco Bay region for large earthquakes on the San Andreas and Hayward faults, U. S. Geol. Surv., Misc. Field Studies Map, 709, 1975.

Borcherdt, R. D., and J. F. Gibbs, Effects of local geological conditions in the San Francisco Bay region on ground motions and the intensities of the 1906 earthquake, Bull. Seis. Soc. Am., 66, 467-500, 1976.

Borcherdt, R. D., J. F. Gibbs, and T. E. Fumal, Progress on ground motion predictions for the San Francisco Bay region, California, Proc. 2nd Int'l. Conf. on Microzonation for Safer Constr. Res. Appl., 1, 241-251, 1978.

Borcherdt, R. D., Influence of local geology in the San Francisco Bay region, California, on ground motion generated by the Loma Prieta earthquake of October 17, 1989, Proc. Int'l Symposium on Safety and Urban Life and Facilities, Tokyo Inst. Tech., Tokyo, Japan, 1990.

Bouchon, M., and K. Aki, Discrete wavenumber representation of seismic source wavefield, Bull. Seis. Soc. Am., 67, 259-277, 1977.

Bouchon, M., A simple, complete numerical solution to the problem of diffraction of SH waves by an irregular surface, J. Acoust. Soc. Am., 77, 1-5, 1985.

Brune, J. N., Tectonic stress and the spectra of seismic shear waves from earthquakes, J. Geophys. Res., 75, 44997-5009, 1970.

Brune, J. N., Corrections, J. Geophys. Res., 76, 5002, 1971.

Campbell, K. W., Near-source attenuation of peak horizontal acceleration, Bull. Seis. Soc. Am., 71, 2039-2070, 1981.

Campbell, K. W., Predicting strong ground motion in Utah, in Evaluation of Regional and Urban Earthquake Hazards and Risk in Utah, W. W. Hays and P. L. Gori, Editors, U. S. Geol. Surv. Open-file Rep. 87-585, L1-L10, 1987.

Campillo, M., M. Bouchon and B. Massinon, Theoretical study of the excitation, spectral characteristic, and geometrical attenuation of regional seismic phases, Bull. Seism. Soc. Am., 74, 79-90, 1984.

Chael, E., Spectral scaling of earthquakes in the Miramichi region of New Brunswick, Bull. Seis. Soc. Am., 77, 347-365.

Chavez-Garcia, F. J., G. Pedotti, D. Hatzfeld, and P. Y. Bard, An experimental study of site effects near Thessaloniki (Northern Greece), Bull. Seis. Soc. Am., 80, 784-806, 1990.

Chin, Byau-Heng and K. Aki, Simultaneous determination of source, path and recording site effects on strong ground motion during the Loma Prieta earthquake - a preliminary result on pervasive non-linear site effect, submitted to Bull. Seism. Soc. Am., 1991.

Chun, K., R. Kokoski, and G. West, Source spectral characteristics of Miramichi earthquake: Results from 115 P-wave observations, Bull. Seis. Soc. Am., 79, 15-30, 1989.

Cramer, C. H. and C. R. Reed, Turkey Flat, USA site effects test area, Technical Report No. 90-2, Calif. Dept. of Conservation, Division of Mines and Geology, 1990.

Das, S., and K. Aki, Fault plane with barriers: a versatile earthquake model, J. Geophys. Res., 82, 5648-56, 1977.

Davis, J. F., J. H. Bennett, G. A. Borcherdt, J. E. Kahle, S. J. Rice, and M. A. Silva, Earthquake planning scenario for a magnitude 8.3 earthquake on the San Andreas fault in the San Francisco Bay area, Calif. Dept. of Conservation, Division of Mines and Geology, 1982a.

Davis, J. F., J. H. Bennett, G. A. Borchardt, J. E. Kahle, S. J. Rice, and M. A. Silva, Earthquake planning scenario for a magnitude 8.3 earthquake on the San Andreas fault in Southern California, Calif. Dept. of Conservation, Division of Mines and Geology, 1982b.

Donovan, N. C. and A. E. Bornstein, Uncertainties in seismic risk procedures, Proc. Am. Soc. Civil Eng., J. Geotech. Eng. Div., 104, 869-887, 1978.

Dravinski, M., Amplification of P, SV and Rayleigh waves by two alluvial valleys, Soil Dynamics and Earthquake Eng., 2, 66-77, 1983.

Duke, C. M., J. A. Johnson, Y. Kharraz, K. W. Campbell, and N. A. Malpiede, Subsurface site conditions and geology in the San Fernando earthquake area, UCLA-ENG-7206, School of Engineering, UCLA, Los Angeles, CA, 1971.

Eaton, J., Determination of amplitude and duration magnitude and site residuals from short period seismographs in northern California, preprint, 1990.

E.E.R.I., Lessons learned from the Loma Prieta earthquake, Earthquake Spectra, supplement to volume 6, 1990.

Esteva, L., Microzoning: models and reality, Proc. of 6th WCEE, New Dehli, 1977.

Evernden, J. F., W. M. Kohler, and G. D. Clow, Seismic intensities of earthquakes of conterminous United States - Their prediction and interpretation: U.S. Geological Survey Professional Paper 1223, 50p., 1981.

Evernden, J. F., and J. M. Thomson, Predicting seismic intensities; in Ziony, J. I. editor, Evaluating earthquake hazards in the Los Angeles region, an earth-science perspective: U. S. Geological Survey Professional Paper, 1360, 151-202, 1985.

Fehler, M., M. Hoshiba, H. Sato, and K. Obara, Separation of scattering and intrinsic attenuation for the Kanto-Tokai region, Japan, using measurements of S wave energy vs. hypocentral distance, EOS, vol. 71, p. 1471, 1990.

Figueroa, J. A., Determination de la arcilladel valle de Mexico por prospection sismica, Bol. Soc. de Ing. Sismica, 2, 57-66, 1964.

Fukuyama, E. and K. Irikura, Heterogeneity of the 1980 Izu-Hanto-Toho-Oki earthquake rupture process, submitted to Geophys., J. R. Astr. Soc., 1988.

Fukuyama, E. and T. Tanaka, A new attenuation relation for peak horizontal acceleration of strong earthquake ground motion in Japan, Bull. Seism. Soc. Am., 80, 757-783.

Fumal, T. E., Correlations between seismic wave velocities and physical properties of geologic materials in the San Francisco Bay region, California, U.S. Geol. Surv. Open-File Report 78-1067, 114 pp, 1978.

Fumal, T. E., and J. C. Tinsley, Mapping shear-wave velocities of near-surface geologic materials, in Evaluating Earthquake Hazards in the Los Angeles region, ed. J. I. Ziony, U.S.G.S. Prof. Paper 1360, 127-149, 1985.

Gariel, J. C., K. Irikura and K. Kudo, Rupture process of the 1989 Ito-Oki earthquake, submitted to J. Physics of the Earth, 1991.

Goto, H., H. Kameda, and M. Sugito, Use of N-value profiles for estimation of site dependent earthquake motions (in Japanese), Collected Papers 317, Japanese Society of Civil Engineering, 69-78, 1982.

Gusev, A. A., Descriptive statistical model of earthquake source radiation and its application to an estimation of short-period strong motion, Geophys. J. Roy. Astr. Soc., 74, 787-808, 1983.

Gutenberg, B., Effects of ground on earthquake motion, Bull. Seism. Soc. Am., 47, 221-250, 1957.

Hanks, T. C. and R. K. McGuire, The character of high-frequency strong ground motion, Bull. Seism. Soc. Am., 71, 2071-2095, 1981.

Hanks, T. C., $f_{max}$ Bull. Seism. Soc. Am., 72, 1867-1879, 1982.

Hartzell, S. H., Earthquake aftershocks as Green's functions, Geophys. Res. Lett., 5, 104, 1978.

Hartzell, S. H. and T. Heaton, Teleseismic time functions for large, shallow subduction zone earthquakes, Bull. Seism. Soc. Am., 75, 965-1004, 1985.

Hartzell, S. H. and T. Heaton, Rupture history of the 1984 Morgan Hill, California, earthquake from the inversion of strong motion records, Bull. Seism. Soc. Am., 76, 649-674, 1986.

Hartzell, S. H. and M. Iida, Source complexity of the 1987 Whittier Narrows, California, earthquake from the inversion of strong motion records, J. Geophys. Res., 95B, 12475-12485, 1990.

Hayashi, S., H. Tsuchida, and E. Kurata, Average response spectra for various subsoil conditions, Third Joint Meeting, U.S.-Japan Panel on Wind and Seismic Effects, UJNR, Tokyo, May 10-12, 1971.

Helmberger, D. V., and J. E. Vidale, Modeling strong motions produced by earthquakes with two-dimensional numerical codes, Bull. Seis. Soc. Am., 78, 109-121, 1988.

Hong, T. L., and D. V. Helmberger, Glorified optics and wave propagation in non planar structures, Bull. Seis. Soc. Am., 68, 1313-1330, 1978.

Hori, M., K. Koketsu, and T. Minami, Seismic response analyses of sediment-filled valley due to incident plane waves by three-dimensional Aki-Larner method, Bull. Earthq. Res. Inst., 65, 433-462, 1990.

Horike, M., Analysis and simulation of seismic ground motion observed by an array in a sedimentary basin, J. Phys. Earth, 36, 135-154, 1988.

Horike, M., H. Uebayashi, and Y. Takeuchi, Seismic response in three-dimensional sedimentary basin due to plane S-wave incidence., J. Phys. Earth, 38, 261-284, 1990.

Houston, H. and H. Kanamori, Source spectra of great earthquakes: teleseismic constraints on rupture processes and strong motion, Bull. Seism. Soc. Am., 76, 19-42, 1986.

Hudson, D. E., Local distribution of strong earthquake ground motions, Bull. Seism. Soc. Am., 62, 1765-1786, 1972.

Idriss, I. M., Evaluating seismic risk in engineering practice, in Proc. Eleventh Intl. Conf. on Soil Mech. and Foundation Eng., San Francisco, California, 255-320, 1985.

Idriss, I. M., Earthquake ground motions, Lecture notes, Course on Strong Ground Motion, Earthquake Engin. Res. Inst., Pasadena, Calif., April 10-11, 1987.

Idriss, I. M., Response of soft soil sites during earthquakes, Proceedings of H. Bolton Seed Memorial Symposium, ed. J. M. Duncan, BiTech Publ., 273-290, 1990.

Ihnen, S. M., and D. M. Hadley, Prediction of strong ground motion in the Puget Sound Region: The 1965 Seattle earthquake, Bull. Seis. Soc. Am., 76, 905-922, 1986.

Iglesias, J., The Mexico earthquake of September 19, 1985 - Seismic zoning of Mexico City after the 1985 earthquake, Earthquake Spectra, 5, 257-271, 1989.

Irikura, K., Semi-empirical estimation of strong ground motions during large earthquakes, Bull. Disaster Prevention Res. Inst. (Kyoto Univ.), 32, 63-104, 1983.

Irikura, K. and T. Yokoi, Scaling law of seismic source spectra for the aftershocks of 1983 Japan-Sea earthquake, Abstracts of the Seismological Society of Japan, No. 1, 1984.

Irikura, K. and K. Aki, Scaling law of seismic source spectra and empirical Green's function for predicting strong ground motions, EOS, Trans. Am. Geophys. Union, 66, 967, 1985.

Irikura, K., Prediction of strong ground motions using empirical Green's function, Proceedings of the 7th Japan earthquake engineering symposium, 151-156, 1986.

Iwata, T. and K. Irikura, Tomographic imaging of heterogeneous rupture process of a fault plane, J. Seism. Soc. Jap., 42, 49-58, 1989.

Izutani, Y., A statistical model for prediction of quasi-realistic strong ground motion, J. Phys. Earth, 29, 537-557, 1981.

Jarpe, S. P., L. J. Hutchings, T. F. Hauk, and A. F. Shakal, Selected strong- and weak-motion data from the Loma Prieta earthquake sequence, Seis. Res. Letters, 60, 167-176, 1989.

Jarpe, S. P., C. H. Cramer, B. E. Tucker, and A. F. Shakal, A comparison of observations of ground response to weak and strong ground motion at Coalinga, California, Bull. Seis. Soc. Am., 78, 421-435, 1988.

Jiang, T., and E. Kuribayashi, The three-dimensional resonance of axisymmetric sediment-filled valleys, Soils and Foundations, 28, 130-146, 1988.

Jongmans, D., and M. Campillo, The 1983 Liege earthquake: damage distribution and site effects, Earthquake Spectra, 6, 713-738, 1990.

Joyner, W. B., R. E. Warrick, and A. A. Oliver, III, Analysis of seismograms from a downhole array in sediments near San Francisco Bay, Bull. Seis. Soc. Am., 66, 937-958, 1976.

Joyner, W. B., and D. M. Boore, Peak horizontal acceleration and velocity from strong motion recording including records from the 1979 Imperial Valley, California, earthquake, Bull. Seis. Soc. Am., 71, 2011-2038, 1981.

Joyner, W. and D. M. Boore, Prediction of earthquake response spectra, Proc. 51st Ann. Convention Structural Eng. Assoc. of Cal., also U.S. Geol. Surv. Open-File Report, 82-977, 16 p., 1982.

Joyner, W. and D. M. Boore, Measurement, characterization, and prediction of strong ground motion, Proceedings of Earthquake Engineering & Soil Dynamics, Park City, Utah, 27 to 30 June 1988, Am. Soc. Civil Engineers, 43-102, 1988.

Kagami, H., C. M. Duke, G. C. Liang, and Y. Ohta, Observation of 1- to 5-second microtremors and their application to earthquake engineering, Part 2: Evaluation of site effect upon seismic wave amplification due to extremely deep soil deposits, Bull. Seis. Soc. Am., 72, 987-998, 1982.

Kagami, H., S. Okada, K. Shiono, M. Oner, M. Dravinski, and A. K. Mal, Observation of 1- to 5-second microtremors and their application to earthquake engineering. Part 3:

A two-dimensional study of site effects in the San Fernando Valley, Bull. Seis. Soc. Am., 76, 1801-1812, 1986.

Kamiyama, M., Statistical identification for nonlinear amplification of strong-motion spectra due to surface layers, Proc. Nat. Symp. on Effects of Surface Geology on Seismic Motion, 43-48, 1989.

Kanai, K., R. Takahashi and H. Kawasumi, Seismic characteristics of ground, Proc. World Conf. Earthquake Engineering, E.E.R.I. 1-16, 1956.

Katayama, T., T. Iwasaki, and M. Saeki, Statistical analysis of earthquake acceleration response spectra, Collected Papers, 275, Japanese Society of Civil Engineering, 29-40, 1978.

Kawase, H., Time-domain response of a semicircular canyon for incident SV, P and Rayleigh waves calculated by the discrete wave number boundary element method, Bull. Seis. Soc. Am., 78, 1415-1437, 1988.

Kawase, H., and K. Aki, A study of the response of a soft basin for incident S, P and Rayleigh waves with special reference to the long duration observed in Mexico City, Bull. Seis. Soc. Am., 79, 1361-1382, 1989.

Kawase, H., and K. Aki, Topography effect at the critical SV-wave incidence: possible explanation of damage pattern by the Whittier Narrows, California, earthquake of 1 October 1987, Bull. Seis. Soc. Am., 80, 1-22, 1990.

Kawashima, K., K. Aizawa, and K. Takahashi, Attenuation of peak ground acceleration, velocity and displacement based on multiple regression analysis of Japanese strong motion records, Earthquake Engineering and Structural Dynamics, 14, 199-215, 1986.

Kawasumi, Measures of earthquake danger and expectancy of maximum intensity throughout Japan as inferred from the seismic activity in historical times, Bull. Earthq. Res. Inst., Tokyo University, 29, 469-82, 1951.

Khair, K. R., S. K. Datta and A. H. Shah, Amplification of obliquely incident seismic waves by cylindrical alluvial valleys of arbitrary P and SV waves, Bull. Seis. Soc. Am., 79, 610-630, 1989.

Kikuchi, M. and H. Kanamori, Inversion of complex body waves, Bull. Seism. Soc. Am., 72, 491-506, 1982.

Kikuchi, M. and Y. Fukao, Inversion of long-period P waves from great earthquakes along subduction zones, Tectonophysics, 144, 231-247, 1987.

King, K. W., A. C. Tarr, D. L. Carver, R. A. Williams, and D. M. Worley, Seismic ground-response studies in Olympia, Washington, and vicinity, Bull. Seis. Soc. Am., 80, 1057-1078, 1990.

Kinoshita, S., A study on sampling characteristics of surface layers, Proc. of JSCE, 330, 15-25 (in Japanese), 1983.

Kinoshita, S., Earthquake response characterization of a thick sedimentary layer estimated by means of a deep borehole observation, Rep. National Res. Ctr. Disast. Prev., 38, 25-245 (in Japanese), 1986.

Kinoshita, S., T. Mikoshiba, and T. Hoshino, Estimation of the average amplification characteristics of a sedimentary layer for short period S-waves, Zisin (Journ. Seis. Soc. Japan), Ser. 2, 39, 67-80, 1986.

Kinoshita, S., Frequency dependent attenuation of shear waves in the crust of the Kanto area, Japan and source-controlled $f_{max}$ submitted to Bull. Seism. Soc. Am., 1990.

Kinoshita, S., personal communication, 1991.

Kobayashi, K., Y. Abe, and F. Amaike, Frequency dependence and modeling of Q values in soil deposits, Proc. Nat. Symp. on Effects of Surface Geology on Seismic Motion, 49-54, 1989.

Kobayashi, H., and S. Midorikawa, Study of site effects in Mexico City using microtremors (in Japanese), Proc. of Japanese Symposium on Earthquake Engineering, 7, 355-360, 1986.

Kudo, K., and E. Shima, Attenuation of shear waves in soil, Bull. Earthq. Res. Inst., 48, 145-158, 1970.

Kuribayashi, E., T. Iwasaki, Y. Iida, and K. Tuji, Effects of seismic and subsoil conditions on earthquake response spectra, Proc. Int. Conf. on Microzonation, 499-512, 1972.

Lajoie, K. R., and Helley, E. J., Differentiation of sedimentary deposits for purposes of seismic zonation, in Borcherdt, R. D., ed., Studies for seismic zonation of the San Francisco Bay region: U.S.G.S. Prof. Paper 941-A, A39-A51, 1975.

Lay, T. and H. Kanamori, An asperity model for great earthquake sequences, in Earthquake Prediction - An International Review, Maurice Ewing Series 4, ed. D. W. Simpson and P. G. Richards, pp. 579-592, Am. Geophys. Union, Washington, D.C., 1981.

Lee, J.-J., and C. A. Langston, Three-dimensional ray tracing and the method of principal curvature for geometric spreading, Bull. Seis. Soc. Am., 73, 765-780, 1983.

Lee, V. W., Three-dimensional diffraction of elastic waves by a spherical cavity in an elastic half-space, I: closed form solutions, Soil. Dyn. and Earthq. Eng., 7, 149-161, 1988.

Leyendecker, E. V., L. M. Highland, M. Hopper, E. P. Arnold, P. Thenhaus, and P. Powers, The Whittier Narrows, California, earthquake of October 1, 1987: early results of isoseismal studies and damage surveys, Earthquake Spectra, 4, 339-366, 1988.

Lysmer, J., and L. A. Drake, The propagation of Love waves across nonhorizontally layered structures, Bull. Seis. Soc. Am., 61, 1233-1252, 1971.

McNally, K. C., T. Lay, M. Protti-Quesada, G. Valensise, D. Orange, and R. S. Anderson, Santa Cruz Mountains (Loma Prieta) earthquake, EOS, 70, No. 5, 1463, 1989.

Mohraz, B., A study of earthquake response spectra for different geological conditions, Bull. Seis. Soc. Am., 66, 915-935, 1976.

Mossessian, T. K., and M. Dravinski, Amplification of elastic waves by a three-dimensional valley, Part 1: steady state response, Earthq. Eng. and Struct. Dyn. 19, 667-680, 1990a, Part 2: transient response, 681-691, 1990b.

Nava, S. J., J. W. Munsey and A. C. Johnson, First fault plane identification in the southern Appalachians: the M4.2 Vonoro, Tennessee earthquake of March 27, 1987, Seis. Res. Letters, 60, 119-129, 1989.

National Research Council, Probabilistic seismic hazard analysis, 97p., National Academy Press, 1988.

Nowack, R., and K. Aki, The two-dimensional Gaussian beam synthetic method; testing and applications, J. Geophys. Res., 89, 7797-7819, 1984.

Nuttli, O., Similarities and differences between western and eastern United States earthquakes and their consequences for Earthquake Engineering, Beaver, J. E. (Editor), in Earthquakes, 25-51, 1981.

Nuttli, O., Average seismic source-parameter relations for mid-plate earthquakes, Bull. Seis. Soc. Am., 73, 519-535, 1983.

Nuttli, O., D. Bowling, J. Lawson, and R. Wheeler, Some aspects of seismic scaling and the strong ground motion of the eastern Missouri earthquake of January 12, 1984, Seis. Res. L., 58, 53-58, 1987.

Ohta, Y. and N. Goto, Empirical shear wave velocity equations in terms of characteristic soil indexes, Earthquake Engineering and Structural Dynamics, 6, 167-187, 1978.

Ohta, Y., N. Goto and H. Ohashi, A questionnaire survey for estimating seismic intensities, Bull. Faculty of Engineering, Hokkaido Univ., No. 92, 241-250, 1979.

Ohori, M., K. Koketsu and T. Minami, Seismic Response analyses of sediment-filled valley due to incident plane waves by three-dimensional Aki-Larner method, Bull. Earthq. Res. Inst., Tokyo Univ., 65, 433-463, 1990.

Ordaz, M. and S. K. Singh, Source spectra and spectral attenuation of seismic waves from Mexican earthquakes, and evidence of amplification in the hill zone of Mexico City, submitted to Bull. Seism. Soc. Am., 1991.

Papageorgiou, A. S. and K. Aki, A specific barrier model for the quantitative description of inhomogeneous faulting and the prediction of strong motion, Part I description of the model, Bull. Seism. Soc. Am., 73, 693-722, 1983a.

Papageorgiou, A. S. and K. Aki, A specific barrier model for the quantitative description of inhomogeneous faulting and the prediction of strong motion, Part II applications of the model, Bull. Seism. Soc. Am., 73, 953-978, 1983b.

Papageorgiou, A. S. and K. Aki, Scaling law of far field spectral based on observed parameters of the specific barrier model, PAGEOPH, 123, 353-374, 1985.

Papageorgiou, A. S., On two characteristic frequencies of acceleration spectra: patch corner frequency and $f_{max}$, Bull. Seis. Soc. Am., 509-529, 1988.

Phillips, W. S., and K. Aki, Site amplification of coda waves from local earthquakes in central California, Bull. Seis. Soc. Am., 76, 627-648, 1986.

Plafker, G., and J. Galloway, Lessons learned from the Loma Prieta earthquake of October 17, 1989, U.S. Geol. Survey Circular 1045, 1989.

Rogers, A. M., R. D. Borcherdt, P. A. Covington, and D. M. Perkins, A comparative ground response study near Los Angeles using recordings of Nevada nuclear tests and the 1971 San Fernando earthquake, Bull. Seis. Soc. Am., 74, 1925-1949, 1984.

Rogers, A. M., J. C. Tinsley, and R. D. Borcherdt, Predicting relative ground response, in Evaluating Earthquake Hazards in the Los Angeles region, ed. J. I. Ziony, U.S.G.S. Prof. Paper 1360, 221-248, 1985.

Ruff, L. and H. Kanamori, The rupture process and asperity distribution of three great earthquakes from long-period diffracted P waves, Phys. Earth Planet Interiors, 31, 202-230, 1983.

Sabetta, F. and A. Pugliese, Attenuation of peak horizontal acceleration and velocity from Italian strong-motion records, Bull. Seism. Soc. Am., 77, 1491-1513, 1987.

Sadigh, K., Considerations in the development of site-specific spectra, in Proc. Conf. XXII, A workshop on site effects of soil and rock on ground motion and their implications for earthquake resistant design, Santa Fe, New Mexico, 1983, U. S. Geol. Surv., Open-File Rept., 83-845, 423-458, 1983.

Sakai, S., M. Ichikawa, and N. Yoshimura, Evaluation of amplification characteristics of body wave in ground surface layers, Proc. Nat. Symp. on Effects of Surface Geology on Seismic Motion, 19-24, 1989.

Sanchez-Sesma, F. J., and J. A. Esquivel, Ground motion on alluvial valleys under incident plane SH waves, Bull. Seis. Soc. Am., 69, 1107-1120, 1979.

Sanchez-Sesma, F. J., Diffraction of elastic waves by three-dimensional surface irregularities, Bull. Seis. Soc. Am., 73, 1621-1636, 1983.

Sanchez-Sesma, F. J., Diffraction of elastic SH waves by wedges, Bull. Seis. Soc. Am., 75, 1435-1446, 1985.

Sanchez-Sesma, F. J., Site effects in strong ground motion, Soil Dyn. Earthq. Eng., 6, 124-132, 1987.

Sanchez-Sesma, F. J., F. J. Chavez-Garcia, and M. A. Bravo, Seismic response of a class of alluvial valleys for incident SH waves, Bull. Seis. Soc. Am., 78, 83-95, 1988.

Saragoni, G. R. and G. C. Hart, Simulation of artificial earthquakes, Earthquake Eng. Structured Dyn., 2, 249-267, 1974.

Schiff, A. J., The Whittier Narrows California earthquake of October 1, 1987: response of lifelines and their effect on emergency response, Earthquake Spectra, 4, 339-366, 1988.

Seale, S. H., and R. J. Archuleta, Site amplification and attenuation of strong ground motion, Bull. Seis. Soc. Am., 79, 1673-1695, 1989.

Seed, H. B., C. Ugas, and J. Lysmer, Site-dependent spectra for earthquake-resistant design, Bull. Seis. Soc. Am., 66, 221-243, 1976.

Shakal, A., M. Huang, M. Reichle, C. Ventura, T. Cao, R. Sherbourne, M. Savage, R. Darragh, and C. Petersen, CSMIP strong-motion records from the Santa Cruz Mountains (Loma Prieta), California earthquake of 17 October 1989, California Strong Motion Instrumentation Program Report No. OSMS 89-06, 195 pp., 1989.

Shima, E., Seismic micro-zoning map of Tokyo, 2nd International Conference on Micro-Zonation, 433-443, 1978.

Shima, E., M. Yanagisawa, K. Kohketsu, S. Zama and T. Hoshino, Behavior of seismic waves in the newly developed cut-down and fill-in grounds, Bull. Earthq. Res. Inst., Tokyo Univ., 60, 179-199, 1985.

Shinozaki, Y., High frequency response of a sediment-filled valley for incident plane SH waves, Proc. of second workshop of IASPEI/IAEE joint working group on effects of surface geology on seismic motion, v1- v8, 1988.

Singh, S. K., E. Mena, and R. Castro, Some aspects of source characteristics of the 19 September 1985 Michoacan earthquake and ground motion amplification in and near Mexico City from strong motion data, Bull. Seis. Soc. Am., 78, 451-477, 1988.

Singh, S. K., E. Mena, J. G. Anderson, J. Lermo and R. Quaas, Source spectra and RMS acceleration of Mexican subduction zone earthquake, PAGEOPH, in press, 1990.

Sommerville, P. G., J. P. McLaren, L. V. LeFeuve, R. W. Burger, and D. V. Helmberger, Comparison of source scaling relations of eastern and western North American earthquakes, Bull. Seis. Soc. Am., 77, 322-346.

Sommerville, P. G., and J. Yoshimura, The influence of critical Moho reflections on strong ground motions recorded in San Francisco and Oakland during the 1989 Loma Prieta earthquake, Geophys. Res. Letters, 17, 1203-1206, 1990.

Su, F., S. Koyanagi, Y. Zeng, K. Mayeda, T. Teng, and K. Aki, A recursive stochastic inversion of site effect using coda waves, EOS, Trans. Am. Geophys. Union, 71, 1475, 1990.

Sugito, M., and H. Kameda, Non-linear soil amplification model with verification by vertical strong motion array records, 4th U.S. NCEE, 1-10, 1990.

Sugito, M., Earthquake motion prediction, microzonation, and buried pipe response for urban seismic damage assessment, Ph.D. thesis, School of Civil Engineering, Kyoto University, 1986.

Takahashi, R., and K. Hirano, Seismic vibrations of soft ground, Bull. Earthq. Res. Inst., Tokyo University, 19, 534-543, 1941.

Takemura, M. and T. Ikeura, A semi-empirical method using a hybrid of stochastic and deterministic fault models: simulation of strong ground motions during large earthquakes, J. Phys. Earth, 36, 89-106, 1988.

Takeo, M., An inversion method to analyze the rupture processes of earthquakes using near-field seismograms, Bull. Seism. Soc. Am., 77, 490-513, 1987.

Tinsley, J. C., and T. E. Fumal, Mapping quaternary sedimentary deposits for area variations in shaking response, in Evaluating Earthquake Hazards in the Los Angeles region, ed. J. I. Ziony, U.S.G.S. Prof. Paper 1360, 101-149, 1985.

Tokimatsu, K., and S. Midorikawa, Nonlinear soil properties estimated from strong motion accelerograms, International Conference on recent advances in geotechnical engineering and soil dynamics, St. Louis, USA, 117-122, 1981.

Toppozada, T. R., J. H. Bennett, G. Borchardt, R. Saul, and J. F. Davis, Planning scenario for a major earthquake on the Newport-Inglewood fault zone, Calif. Div. Mines and Geology, 1988.

Trifunac, M. D., Surface motion of a semi-cylindrical alluvial valley for incident plane SH waves, Bull. Seis. Soc. Am., 61, 1755-1770, 1971.

Trifunac, M. D., Preliminary empirical model for scaling Fourier amplitude spectra of strong ground acceleration in terms of earthquake magnitude, source-to-station distance and recording site condition, Bull. Seis. Soc. Am., 66, 1343-1373, 1976a.

Trifunac, M. D., Preliminary analysis of the peaks of strong earthquake ground motion-dependence of peaks on earthquake magnitude, epicentral distance and recording site conditions, Bull. Seis. Soc. Am., 66, 189-219, 1976b.

Tsujiura, M., Spectral analysis of the coda waves from local earthquakes, Bull. Earthq. Res. Inst., Tokyo Univ., 53, 1-48, 1978.

Tucker, B. E., and J. L. King, dependence of sediment-filled valley response on the input amplitude and the valley properties, Bull. Seis. Soc. Am., 74, 153-165, 1984.

Umeda, Y., An earthquake source model with a ripple generating core, J. Phys. Earth, 29, 341-370, 1981.

Umeda, Y., Y. Lio, A. Kuroiso, K. Ito and H. Murakami, Scaling of observed seismic spectra, Zisin, Ser. 1, 37, 559-567, 1984.

Umeda, Y., The bright spot of an earthquake, submitted to the Proc. Intl. Symp. Earthq. Source Physics and Earthquake Precursors, 19-22 November 1990, Tokyo, 1990.

Uniform Building Code, International Conference of Building Officials, Whittier, CA, 1979.

Vidale, J. E., and D. V. Helmberger, Elastic finite difference modeling of the 1971 San Fernando, California, earthquake, Bull. Seis. Soc. Am., 78, 122-141, 1988.

Virieux, J., Wave propagation in heterogeneous media: velocity-stress finite-difference method, Geophysics, 49, 1933-1957, 1984.

Wesnousky, S. G., C. H. Scholz, K. Shimazaki, and T. Matsuda, Integration of geological and seismological data for the analysis of seismic hazard: A case study of Japan, Bull. Seis. Soc. Am., 74, 687-708, 1984.

Wesnousky, S. G., Earthquakes, quaternary faults and seismic hazards in California, J. Geophys. Res., 91, 12,587-12,631, 1986.

Wong, H. L., and P. C. Jennings, Effect of canyon topography on strong ground motion, Bull. Seis. Soc. Am., 65, 1239-1257, 1975.

Yamanaka, H., K. Seo, and T. Samano, Effects of sedimentary layers on surface-wave propagation, Bull. Seis. Soc. Am., 79, 631-644, 1989.

Zama, S., Behavior of the elastic waves propagating through the irregular structure, Bull. Earthq. Res. Inst., Tokyo Univ., 56, 741-777, 1981.